

A CARBON AND NITROGEN FLUX MODEL IN A COASTAL UPWELLING  
REGION

by

Debby C. Ianson

M.Sc. Physics, University of British Columbia, 1994

B.Sc.E. Hons., Physics, Queens University, 1991

A THESIS SUBMITTED IN PARTIAL FULFILLMENT OF  
THE REQUIREMENTS FOR THE DEGREE OF  
DOCTOR OF PHILOSOPHY

in

THE FACULTY OF GRADUATE STUDIES  
DEPARTMENT OF EARTH AND OCEAN SCIENCES, OCEANOGRAPHY

We accept this thesis as conforming  
to the required standard

THE UNIVERSITY OF BRITISH COLUMBIA

January 2001

© Debby C. Ianson, 2001

In presenting this thesis in partial fulfilment of the requirements for an advanced degree at the University of British Columbia, I agree that the Library shall make it freely available for reference and study. I further agree that permission for extensive copying of this thesis for scholarly purposes may be granted by the head of my department or by his or her representatives. It is understood that copying or publication of this thesis for financial gain shall not be allowed without my written permission.

Department of Oceanography - EOS

The University of British Columbia  
Vancouver, Canada

Date February 7, 2001

## Abstract

An improved understanding of oceanic biogeochemical cycles is critical for predicting global climate. In coastal upwelling regions fluxes of both carbon and nitrogen are disproportionately large relative to the global ocean. This is especially true of the downward flux of organic matter that transports carbon away from the ocean surface layer causing absorption of atmospheric carbon dioxide (i.e. the 'biological pump'). In addition to biologically limiting nutrients, upwelling brings inorganic carbon to the surface, potentially providing a source of carbon to the atmosphere. However, global models seldom resolve the complex, non-homogeneous coastal ocean. I have developed a carbon and nitrogen flux model for coastal upwelling regions that considers all important processes both within and below the euphotic zone over time scales of days to decades. Physical circulation is represented by six boxes, an upper and lower box for three horizontal regions: the continental shelf, slope and open ocean. Dissolved inorganic, dissolved organic and particulate organic forms of both carbon and nitrogen as well as salinity are modelled. The model is parameterized and physically forced to apply to the west coast of Vancouver Island, Canada. In addition, a field study during July 1998 was undertaken to complement and constrain the model. The model predicts annual primary production, net air-sea CO<sub>2</sub> gas exchange and net export fluxes between the open ocean and the model system under different physical forcing scenarios (including El Niño-Southern Oscillation Events). Model results suggest that coastal upwelling regions do not contribute to the oceanic sequestration of CO<sub>2</sub>; rather, they provide a conduit for subsurface inorganic carbon to the surface ocean. There is net annual air-sea CO<sub>2</sub> gas influx over the shelf and slope, but it is small. In winter, subsurface waters enriched in inorganic carbon and nitrogen are

mixed into the surface, causing gas evasion that almost balances the summer invasion. On the other hand, there is a large flux of inorganic carbon from the lower ocean to the surface ocean via the model system, probably leading to CO<sub>2</sub> outgassing offshore of the shelf. Meanwhile, fluxes of organic carbon from the model system to the open ocean are small (compared with the inorganic carbon flux), especially in the lower layer. Thus, temperate coastal upwelling regions do not operate as strong biological pumps.

## Table of Contents

<b>Abstract</b>	<b>ii</b>
<b>List of Tables</b>	<b>viii</b>
<b>List of Figures</b>	<b>ix</b>
<b>Preface</b>	<b>xi</b>
<b>Acknowledgements</b>	<b>xii</b>
<b>1 Introduction</b>	<b>1</b>
1.1 Motivation . . . . .	1
1.2 Goals . . . . .	3
1.3 Coastal upwelling regions . . . . .	3
1.3.1 Physical . . . . .	4
1.3.2 Biological . . . . .	5
1.3.3 Chemical . . . . .	6
1.3.4 The west coast of Vancouver Island . . . . .	7
1.4 Model review . . . . .	10
1.4.1 Physical models of coastal upwelling regions . . . . .	10
1.4.2 Ecological nitrogen-based models . . . . .	11
1.4.3 Carbon models . . . . .	14
1.4.4 Coastal Processes in Global Models . . . . .	16
1.5 Data from coastal regions . . . . .	17

1.6	My model . . . . .	18
<b>2</b>	<b>A Field Study of the Inorganic Carbon System</b>	<b>20</b>
2.1	Introduction . . . . .	20
2.2	Materials and Methods . . . . .	24
2.2.1	Analysis of seawater . . . . .	25
2.2.2	Data analysis and calculations . . . . .	25
2.3	Results and Discussion . . . . .	28
2.3.1	Physical data . . . . .	28
2.3.2	Inorganic carbon data . . . . .	32
2.3.3	Organic carbon data . . . . .	37
2.3.4	Variations in inorganic carbon and nitrogen . . . . .	40
2.3.5	DIC and $\text{NO}_3^-$ budgets . . . . .	46
2.4	Conclusions . . . . .	49
<b>3</b>	<b>Model Development and Major Results</b>	<b>51</b>
3.1	Introduction . . . . .	51
3.2	Model . . . . .	53
3.2.1	Currencies . . . . .	55
3.2.2	State Variables . . . . .	55
3.2.3	Physical Circulation . . . . .	56
3.2.4	Biological Model . . . . .	59
3.2.5	Gas Flux . . . . .	66
3.3	Physical Forcing . . . . .	67
3.3.1	Upwelling and Downwelling . . . . .	67
3.3.2	Light, Wind, Temperature and Salinity . . . . .	67
3.3.3	Buoyancy flux . . . . .	69

3.3.4	Mixed Layer Depth . . . . .	71
3.3.5	Open Ocean . . . . .	71
3.3.6	Parameter Choice . . . . .	71
3.4	Results . . . . .	73
3.4.1	Primary Production . . . . .	73
3.4.2	Gas Flux . . . . .	80
3.4.3	Net Annual Exchange Fluxes between the Model and the Open Ocean . . . . .	83
3.5	Discussion and Conclusions . . . . .	85
<b>4</b>	<b>State Variable Results and Comparison with Data</b>	<b>88</b>
4.1	Salinity and Dissolved Inorganic Nitrogen . . . . .	88
4.1.1	Tuning the physical model . . . . .	91
4.2	Dissolved Inorganic Carbon . . . . .	94
4.3	Particulate Organic Matter . . . . .	97
4.4	Dissolved Organic Matter . . . . .	98
4.5	Comparison of Model Fluxes with Data . . . . .	102
4.6	Conclusions . . . . .	105
<b>5</b>	<b>Modelling the character of organic matter in a coastal upwelling region</b>	<b>106</b>
5.1	Introduction . . . . .	106
5.2	Model . . . . .	108
5.3	Results . . . . .	109
5.4	Discussion and Conclusions . . . . .	114
<b>6</b>	<b>Conclusions and Suggestions for Future Research</b>	<b>119</b>
6.1	Model development . . . . .	119

6.2	Conclusions . . . . .	120
6.3	Future Research . . . . .	124
	<b>Bibliography</b>	<b>127</b>
	<b>Appendix A Organic Carbon Burial and Denitrification</b>	<b>138</b>
A.1	Burial of organic matter . . . . .	138
A.2	Denitrification . . . . .	139
	<b>Appendix B Ordinary Differential Equations for Salinity</b>	<b>140</b>
	<b>Appendix C Buoyancy Fluxes</b>	<b>142</b>
	<b>Appendix D Annual Mixed Layer Depth</b>	<b>144</b>
	<b>Appendix E Open Ocean State Variable Concentrations</b>	<b>146</b>
	<b>Appendix F Steady State Solutions</b>	<b>148</b>
F.1	Steady State Equations . . . . .	148
F.2	Values for Pools and Parameters . . . . .	149
F.3	Quasi-Steady Solutions . . . . .	153
F.4	Summary . . . . .	156
	<b>Appendix G Sensitivity Analysis</b>	<b>157</b>
G.1	Summary . . . . .	162
	<b>Appendix H Organic Matter Data from the Oregon Coast</b>	<b>166</b>

## List of Tables

2.1	Measured $p\text{CO}_2$ . . . . .	38
2.2	Measured POC, primary production and chlorophyll $a$ . . . . .	39
2.3	Daily DIC and $\text{NO}_3^-$ budgets . . . . .	48
3.1	Model state variables for each currency . . . . .	56
3.2	Physical model parameters . . . . .	57
3.3	Biological model parameters . . . . .	63
3.4	Modelled gas flux sensitivity . . . . .	82
3.5	Net annual exchange flux between the open ocean and the model system	84
4.1	Integrated DIC data . . . . .	96
4.2	Integrated PON, POC and $pp$ in the upper layer . . . . .	98
C.1	Values of inner-shelf state variables . . . . .	143
E.1	Values of open ocean state variables . . . . .	146
F.1	Summer steady state solution parameter and pool values . . . . .	150
F.2	Winter steady state solution parameter and pool values . . . . .	152
G.1	Sensitivity analysis . . . . .	163

## List of Figures

1.1	Map of the Vancouver Island continental shelf . . . . .	8
2.1	Map of stations sampled in the field study . . . . .	22
2.2	Surface Currents on the coast of British Columbia . . . . .	23
2.3	DIC budget . . . . .	27
2.4	T-S curves on the C transect . . . . .	30
2.5	T-S curves on the G transect . . . . .	31
2.6	DIC profiles on transects A, C, D and G . . . . .	33
2.7	DIC vs. salinity . . . . .	35
2.8	Total alkalinity vs. salinity . . . . .	36
2.9	Contours of chl $a$ , NO $_3^-$ and DIC along transect C . . . . .	41
2.10	Contours of chl $a$ , NO $_3^-$ and DIC along transect G . . . . .	42
2.11	Measured $\Delta$ DIC: $\Delta$ DIN on transects A, C, D and G . . . . .	45
3.1	The physical model . . . . .	54
3.2	Vertical structure of model state variable concentrations . . . . .	60
3.3	The biological model . . . . .	61
3.4	Upwelling and downwelling forcing . . . . .	68
3.5	Buoyancy fluxes . . . . .	70
3.6	Shelf primary production and DIN . . . . .	74
3.7	Slope primary production and DIN . . . . .	75
3.8	Shelf DIN during and following an ENSO year . . . . .	79
3.9	Model gas flux and $p$ CO $_2$ for the shelf and slope . . . . .	81

4.1	The annual salinity cycle for a typical model run. . . . .	90
4.2	The annual DIN cycle for a typical model run. . . . .	91
4.3	The annual DIC cycle for a typical model run. . . . .	95
4.4	The annual PON cycle for a typical model run. . . . .	99
4.5	The annual POC cycle for a typical model run. . . . .	100
4.6	The annual DON cycle for a typical model run. . . . .	102
4.7	The annual DOC cycle for a typical model run. . . . .	103
5.1	DOC, DON, POC and DIN during two upwelling events over the shelf. . .	111
5.2	DOC, DON, POC and DIN during two upwelling events over the slope. . .	112
5.3	TOC and DIN during two upwelling events over the shelf and slope. . . .	113
5.4	Modelled total organic carbon . . . . .	115
5.5	Modelled total organic nitrogen . . . . .	116
D.1	Seasonal variation in mixed layer depth ( $h_u$ ) for shelf and slope. . . . .	145
F.1	Summer steady state solution . . . . .	154
F.2	Winter steady state solution . . . . .	155
G.1	The annual upper layer POC and <i>pp</i> cycle for zooplankton grazing model run. . . . .	161
H.1	An annual cycle of chl $a$ , TOC, POC and DOC in the Oregon upwelling region . . . . .	168
H.2	An annual cycle of DIN, TON, PON and DON in the Oregon upwelling region . . . . .	169
H.3	Integrated TOC, DOC and POC from the Oregon upwelling region . . . .	170
H.4	Integrated model TOC, POC, and DOC . . . . .	171

## Preface

The analysis of the data acquired in this thesis is presented in Chapter 2, which will be submitted to *Deep Sea Research I*. The model development and major results, presented in Chapter 3, have been submitted to *Global Biogeochemical Cycles* under the title 'A two-dimensional nitrogen and carbon flux model in a coastal upwelling region' with minor changes to the text. Parts of this Chapter have also been presented at the PICES Ninth Annual Meeting, October 2000, Hakodate, Japan, in a paper titled *Carbon gas exchange and export flux from the west coast of Vancouver Island, Canada: Results of 2-D model simulations*. The remainder of the model results are presented in Chapters 4 and 5. Chapter 4 focuses on a comparison of the data (Chapter 2) with the model results and the physical tuning of the model. In Chapter 5, the characterization of marine organic matter in coastal upwelling regions is discussed and model results are compared with data from a coastal upwelling region south of the study area. Remaining model details are presented in the Appendices.

## Acknowledgements

I am very thankful for the helpful input from all of my committee members, Susan Allen, Kristin Orians, Ken Denman, Steve Calvert, Paul Harrison and C. S. Wong during the model development and the writing. I am especially grateful to Susan Allen for her support on many levels and to Ken Denman and Steve Calvert during the final push for their prompt and thorough comments on the thesis. I thank Kristin Orians for taking care of the administrative details of the defense. I am grateful for the excellent help that I received from Roger Pieters, Joseph Tam and Denis Laplante with computer and systems challenges. I thank William Hsieh and his group for allowing me to run my model on bowhead. There are many people who helped me in the collection and analysis of the field data and I thank Shannon Harris, Susan Allen, Diana Varela, Keith Johnson, Marty Davelaar, Doug Yelland, Ken Hall, Hugh McLean, Maureen Soon and the crew of the *CSS John P. Tully*. Rick Thomson, Robin Brown and Frank Whitney provided useful data and insight into the natural system I have modelled. Rich Pawlowicz has given excellent help with Matlab and I am thankful to Susan Allen for her help with the subtleties of Latex software. I appreciate the helpful comments on the written thesis from Nicole Marshall, Ted Tedford and Ramzi Mirshak and the stimulating modelling conversations with Nicole.

On a personal level I am eternally grateful to my son William for his patience and understanding throughout my degree and in particular during the final push. It is with a good deal of emotion that I thank all of my friends who became an invaluable part of our family and community during our time in Vancouver. I thank my mother and father for all of the tools that they provided me that helped shape my work.

## Chapter 1

### Introduction

In this thesis, I investigate the factors that control carbon and nitrogen fluxes and the magnitudes of these fluxes in coastal upwelling regions. My approach is the development of a general integrated biogeochemical-physical model for coastal upwelling regions over time scales of days to decades. The model was parameterized for the continental shelf off southwestern Vancouver Island, Canada. Additionally, carbon data were collected in the study area to complement and constrain the model. Following a presentation of the motivation for this study, I discuss the goals, some useful background information and I review previous models and field studies pertinent to this research. Chapters 2, 3, 4 and 5 deal with the data study, the model itself, comparison between the model and the data, and the characterization of marine organic matter, respectively.

#### 1.1 Motivation

Recent studies suggest that the large input of anthropogenic carbon dioxide ( $\text{CO}_2$ ) to the atmosphere over the last century is affecting global climate (Crowley, 2000). The ocean plays a very important role in the global carbon cycle (Denman et al., 1996). It holds the largest reservoir of active carbon on Earth (Siegenthaler and Sarmiento, 1993) and ultimately sets the atmospheric  $\text{CO}_2$  concentration (Najjar, 1992). Thus, accurate and well-tested models of the ocean are necessary to understand and predict the global carbon balance.

Oceanic circulation and biological production have large impacts on the ocean's capacity for absorbing carbon (Volk and Hoffert, 1985; Shaffer, 1993). At high latitudes, where deepwater formation occurs, cold water enriched in inorganic carbon (because solubility increases with decreasing temperature) sinks, thereby transporting carbon into the deep ocean. This water circulates through the deep ocean basins where it remains out of contact with the atmosphere. Carbon is released back to the atmosphere by upwelling in warm lower latitudes (where solubility is lower). Thus, the physical circulation sets a carbon balance between the atmosphere and the ocean, termed the 'solubility pump' (Volk and Hoffert, 1985). The marine biota takes up inorganic carbon in the surface ocean, transforming it into organic carbon, and drawing down the surface ocean partial pressure of CO<sub>2</sub> ( $p\text{CO}_2$ ). The eventual fate of the organic carbon is remineralization back to inorganic forms. Some of the remineralization occurs in the surface (raising  $p\text{CO}_2$ ). However a fraction of the organic matter sinks and is remineralized away from the surface, increasing carbon concentrations below the euphotic zone. This vertical transport of organic carbon away from the surface increases the ocean's carbon storage. It has been named the 'biological pump' (Volk and Hoffert, 1985).

A disproportionate amount of primary production occurs in coastal regions and much of it is exported to depth (Eppley and Peterson, 1979). Coastal regions may therefore form an important part of the biological pump. However, these regions are seldom included in global carbon models because resolution is not high enough to deal with the small spatial scales and inherent inhomogeneity. It is one of the major weaknesses of these models (Doney, 1999). Furthermore, previous data studies tend to concentrate on either the coastal or the open ocean as disconnected systems. Thus, little is known about the extent of mass exchange between the two systems (Falkowski et al., 1994).

Vertical export of organic matter associated with high production (i.e. the biological

pump) is extremely large in coastal upwelling regions. Coastal upwelling brings subsurface (100 – 250 m), nutrient-rich water to the surface to fuel this high primary production. Upwelling occurs in pulses or events, supporting a plankton community in which a large fraction sinks out of the euphotic zone (Hutchings et. al, 1994; Harrison et al., 1987). Upwelled water is also rich in inorganic carbon and so could be a source of carbon to the atmosphere (a part of the solubility pump that is often neglected) (Christensen, 1994). Thus, coastal upwelling regions are exceptionally dynamic and have large carbon and nitrogen fluxes that are expected to be important on a global scale.

## 1.2 Goals

My primary goal was to develop a model for carbon and nitrogen fluxes in a coastal upwelling region that is as simple as possible while producing reasonable (compared to data where possible) seasonal cycles. To accomplish this task, all major fluxes, both within and below the euphotic zone, over daily to decadal time scales, are modelled. The model is used to investigate the response of the system to changes in physical forcing and to determine what quantities are most important in the system and therefore what measurements need to be made to better understand it. Specifically, the model is used to investigate the impact of coastal upwelling regions on the global carbon budget. To this end, net annual air-sea CO<sub>2</sub> exchange within the system and net annual exchange fluxes between the open ocean and the model system are predicted.

## 1.3 Coastal upwelling regions

It is useful at the outset to separate the system into its physical, biological and chemical components. Processes that are not important over the timescales of this model, such as the burial flux of organic matter and denitrification, are discussed separately in

## Appendix A.

**1.3.1 Physical**

The interaction between friction, due to the wind stress at the surface, and the Coriolis force is responsible for upwelling and downwelling circulation. This interaction causes the surface currents to flow  $20^\circ - 40^\circ$  to the right (to the left in the southern hemisphere) of the wind direction. Friction between vertical layers of water causes an Ekman spiral (Ekman, 1905) in which flow is always to the right of the overlying layer. When this spiral is vertically integrated, net mass transport is perpendicular to the wind direction and to the right (left in the southern hemisphere). Along the western coasts of continents, this net transport is directed offshore when the wind stress is equatorward and onshore when winds are poleward (true in both hemispheres). A divergence at the coast causes subsurface water to be brought to the surface (upwelling). If winds are poleward, convergence of surface water at the coast results in a depression of the pycnocline (downwelling).

Wind-forcing is intermittent, so that upwelling occurs in pulses or events. Using current-meter data from coastal upwelling regions, Lentz (1992) found that upwelling occurs inside the shelf break and that the offshore mass transport in the surface layer is consistent with that predicted from the wind (e.g. Gargett, 1991). Over the broad shallow northwest African shelf, upwelling occurs closer to the shelf break (Barton et al., 1977) than it does over the narrower shelves off California, Oregon and Peru (Lentz, 1992). The nature of the sub-surface onshore compensatory flow is not as well understood as the offshore transport, but it occurs at intermediate depths (100 – 250 m) (Smith, 1994). A front develops between the nutrient-rich upwelled water and the nutrient-depleted open ocean water (Sverdrup, 1937). The extent of advective exchange through this front is not well known (Smith, 1994; Mackas and Yelland, 1999).

On the other hand, coastal downwelling has not been well studied (Huthnance, 1995).

### 1.3.2 Biological

Large fluxes of new nutrients are delivered intermittently (due to forcing by pulsed wind events) in coastal upwelling regions. Diatoms are the dominant phytoplankton in these conditions (Cochlan et al, 1991; Hutchings et al., 1994), forming the base of the classical food chain (diatoms – copepods and euphysiids – fish) (Cushing, 1989). Diatoms have high specific growth rates, using nutrients rapidly and developing large populations. New nutrients are depleted in a matter of days, depending on seed populations and light availability (Hutchings et al., 1994). When nutrients are exhausted, diatoms sink quickly out of the euphotic zone, often becoming sticky and physically aggregating (Hansen et al., 1995). Mesozooplankton exert little grazing control on diatom blooms associated with upwelling events (Hutchings et al., 1994). Thus, variability in phytoplankton biomass is extreme during the upwelling season. Furthermore the system is characterized by high  $f$ -ratios (Dugdale and Goering, 1967) which can exceed 0.5 (Hutchings et al., 1994), leading to high sinking fluxes of organic matter.<sup>1</sup>

Nitrogen is usually the limiting nutrient in coastal upwelling regions (Hutchings et al., 1994). However, Dugdale et al. (1995) have suggested that silicic acid is sometimes limiting in the Peruvian upwelling system, and iron was observed to be limiting off some regions of the Californian coast during an El Niño year (Hutchins and Bruland, 1998).

Resting spores are often formed by diatoms in coastal upwelling regions and they may be an important part of their evolutionary strategy (Smetacek, 1985; Hansen et al., 1995). The upwelling circulation provides an excellent means to reintroduce resting spores back into the euphotic zone and indeed intact spores have been observed in upwelled water (Pitcher, 1990).

---

<sup>1</sup>The  $f$ -ratio is defined as nitrate uptake divided by the total nitrogen uptake (nitrate and ammonium). This ratio represents the amount of production that is exported from the euphotic zone under steady state.

### 1.3.3 Chemical

Upwelling brings subsurface water that is enriched in dissolved inorganic carbon (DIC) and total alkalinity (TA) to the surface. Surface waters have lower DIC concentrations and TA because of dilution (by freshening). The deep water is enriched in metabolic  $\text{CO}_2$  by the biological pump (for DIC) and TA is depleted in surface waters by calcium carbonate ( $\text{CaCO}_3$ ) formation. These chemical effects are complex.

DIC comprises bicarbonate ( $\text{HCO}_3^-$ ), carbonate ( $\text{CO}_3^{2-}$ ) and  $\text{CO}_2$  (and  $\text{H}_2\text{CO}_3$  which cannot be distinguished from  $\text{CO}_2$ ). Their ratios are determined by the DIC concentration and TA. In the ocean,  $\text{HCO}_3^-:\text{CO}_3^{2-}:\text{CO}_2$  occurs in a ratio of roughly 150:15:1. To determine the carbonate system, two of the following four observables are required: DIC, pH,  $p\text{CO}_2$  or alkalinity (TA) (Dickson and Goyet (1994); Skirrow, 1975). Temperature, salinity and pressure are also needed to estimate the solubility and the dissociation constants in the carbon system (*ibid.*). Alkalinity is a quantity set by the charge balance in the ocean. It is defined as the difference between the excess of positive charges associated with cations (e.g. calcium,  $\text{Ca}^{2+}$ ) and negative charges associated with anions of strong acids in a given water sample (*ibid.*). This difference is made up by negative charges from the anions of weak acids, the sum of which is the total alkalinity.<sup>2</sup> In the ocean (under oxic conditions), alkalinity is primarily made up of  $\text{HCO}_3^-$  and  $\text{CO}_3^{2-}$  and to a lesser extent boron species:

$$\text{TA} = [\text{HCO}_3^-] + 2[\text{CO}_3^{2-}] + [\text{B}(\text{OH})_4^-] + \dots \quad (1.1)$$

Surface alkalinity is affected by precipitation (and evaporation), and by the formation of calcium carbonate ( $\text{CaCO}_3$ ) tests or 'hard parts' by certain organisms. The effect of alkalinity changes on  $p\text{CO}_2$  is not intuitive. In the first case, dilution of the salts (by

---

<sup>2</sup>equivalently TA is defined as the number of equivalents of  $\text{H}^+$  needed to convert all anions of weak acids to their respective acids.

buoyancy fluxes) causes alkalinity to decrease (and vice versa). In the second ( $\text{CaCO}_3$  formation), the removal of the  $\text{Ca}^{2+}$  ion also causes TA to decrease. To maintain charge balance there is a shift from  $\text{CO}_3^{2-}$  (two negative charges) to  $\text{HCO}_3^-$  (one negative charge). This shift causes  $p\text{CO}_2$  to increase even though the total dissolved inorganic carbon has decreased (in the first case by dilution, in the second by the removal of the carbonate ion from solution). In many coastal regions, including the study area, fresh water dilution of TA is important, but biological  $\text{CaCO}_3$  production is small. It is not well known why  $\text{CaCO}_3$  formation occurs in some places and not others (Shaffer, 1993); however historically it has not been observed off of the west coast of Vancouver Island (with the exception of one observation in the summer of 1997 during El Niño conditions (S. Harris, pers. com.)). Thus, I model buoyancy fluxes (dilution) but not  $\text{CaCO}_3$  formation.

Sinking, dissolution and burial of  $\text{CaCO}_3$  tests form the remainder of the  $\text{CaCO}_3$  cycle. These processes are an integral part of the global carbon cycle, affecting oceanic carbon capacity over large time scales (10 kyr) (eg. Boyle, 1988; Archer and Maier-Reimer, 1994). However, this thesis does not address such long time-scales and so does not model the lower layer processes in the cycle.

#### 1.3.4 The west coast of Vancouver Island

The model study area was chosen to be the southern section of the Vancouver Island shelf and slope (Figure 1.1, Lines A through G). Extensive physical and biological data are available in this region. The physical circulation is dynamic, there is a productive fishery and this region is more easily accessible relative to areas farther north. This area conforms to the broad description of coastal upwelling regions discussed previously, with the addition of some local features.

The west coast of Vancouver Island is at the northern limit of where winds are upwelling favourable (Freeland and Denman, 1982). Winds switch direction during the

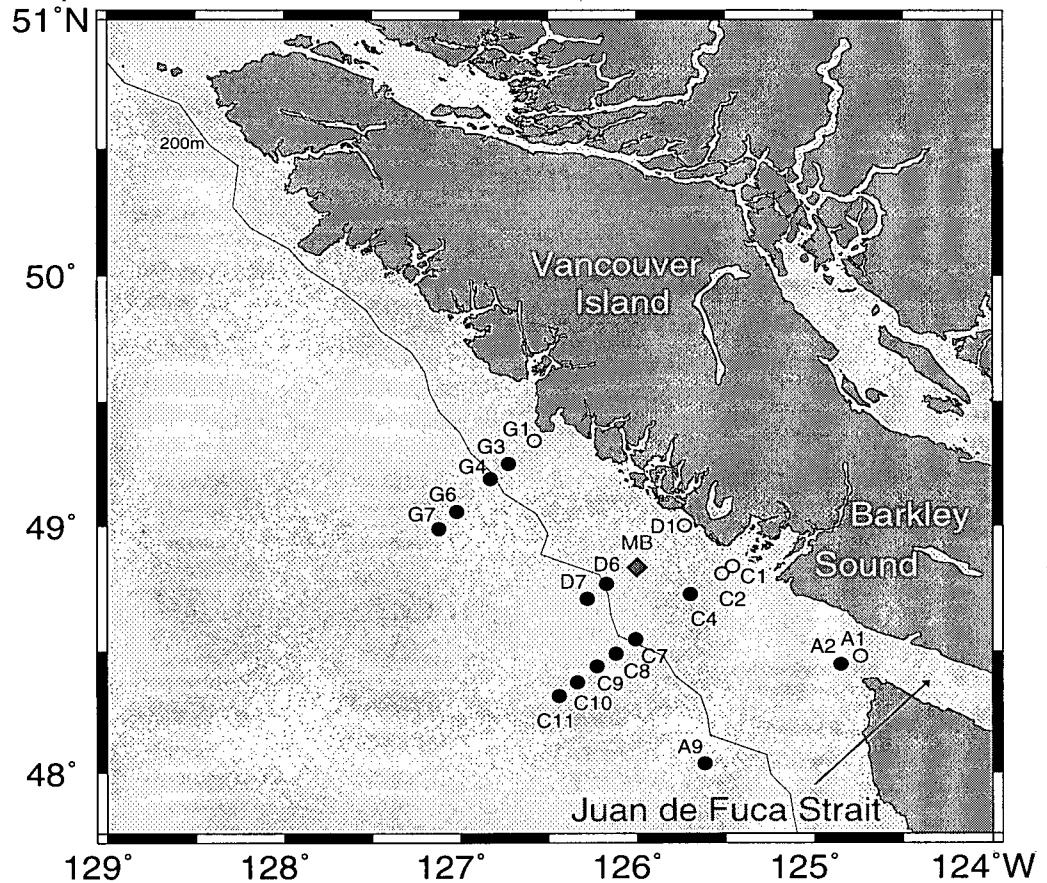


Figure 1.1: The west coast of Vancouver Island. Stations sampled in the data study are marked (open circles are expected to be in the coastal buoyancy current; closed circles in the outer-shelf current (equatorward in summer)). Note, stations A2, C4 and G3 may be within the buoyancy current and their water properties may be affected by this current. MB marks the location of the meteorological buoy. The Juan de Fuca Strait is the source of the Vancouver Island Coastal Current VICC. The 200 m depth contour runs approximately along the shelf break.

winter producing a distinct, although short, downwelling season (Thomson and Ware, 1996). The along-shore surface currents (associated with the pressure gradient due to the divergence or convergence at the coast) are strong, flowing poleward in the winter ( $30 - 40 \text{ cm s}^{-1}$ ), switching to equatorward in the spring ( $15 - 20 \text{ cm s}^{-1}$ ), becoming the northern extension of the California current system (Freeland et al., 1984). A surface buoyancy current (called the Vancouver Island Coastal Current, VICC) flows from the Juan de Fuca Strait northward over the inner shelf throughout the year (due to mainly to snow melt in the interior of British Columbia in the summer and local run-off due to heavy rainfall in the winter) hugging the coast and counter to the equatorward wind-forced current during the summer (Hickey et al., 1991). Below about 300 m there is a slow poleward undercurrent, presumably the northern extension of the California Undercurrent (Freeland and Denman, 1982). Section 3.3 includes an additional description of circulation in the area.

The phytoplankton population is dominated by diatoms (Cochlan et al., 1991; Harris, 2000) with primary production generally high and variable during the summer (Harris, 2000). Large pulses of sinking phytodetritus have been observed over the Vancouver Island continental shelf to the north of the study area (Peña et al., 1996). During the fall and winter, light availability limits primary production so that nutrients are able to build up to high concentrations in the surface, resulting in a strong spring bloom. The zooplankton population over the shelf is generally low despite the high primary production (Mackas, 1992). Over the slope, zooplankton concentrations increase throughout the summer while they decrease over the shelf probably because they are advected offshore by the Ekman transport (Mackas, 1992). The nutrients that allow high summer production come from upwelling and also from the near-shore buoyancy current (Freeland and Denman, 1982; Crawford and Dewey, 1989). (The buoyancy current is rich in nutrients as a result of intense mixing prior to entering the Juan de Fuca Strait.) In addition, upwelling is locally

enhanced by topography, i.e., underwater canyons (Freeland and Denman, 1982; Allen et al., 2000).

This region has been well studied during the summer months, but less so in the winter, mainly because it is a biologically unproductive time and also because winter weather makes it less accessible. Although there are reasonably large biological and physical data sets, no inorganic carbon data over the shelf have previously been reported (as is the case in many coastal regions). As part of this research, samples of DIC and TA were collected in conjunction with a comprehensive biological and physical study (sponsored by Global Ocean Ecosystem Dynamics Study (GLOBEC) Canada) during the summer of 1998 (Chapter 2).

#### **1.4 Model review**

My research integrates three types of models: a physical model of coastal upwelling circulation; a nitrogen-based ecological model; and a carbon cycle model. No previous research has integrated these three components.

##### **1.4.1 Physical models of coastal upwelling regions**

A detailed two-dimensional physical model of coastal upwelling has been developed for the upwelling region off the Oregon coast (Allen et al., 1995; Federiuk and Allen, 1995). This model focuses on modelling flow response to wind forcing at the surface during upwelling over short time-scales. Downwelling circulation has been modelled in the same area over similar time scales (Allen and Newberger, 1996). Results show the depression of the pycnocline over the shelf and the development of a downwelling front. Foreman and Thomson (1997) have developed a diagnostic three-dimensional finite element model of the physical circulation in our study area which shows the physical interactions that create large

diurnal tides. A higher resolution extension of this model was applied to the summer and winter season separately over time scales of several days (Foreman et al., 2000). Neither of the above models incorporate ecological models (although both principal investigators are interested in doing so (J. Allen, pers. com.; M. Foreman, pers. com.)). Wroblewski (1977) developed one of the earliest nitrogen-based ecological models and coupled it with a two-dimensional physical model of coastal upwelling (for the Oregon coast) over time scales of an upwelling event. He showed that offshore advection of phytoplankton and detritus is important and exerts the strongest influence on their distributions. Similarly, Batchelder et al. (2000) have integrated a nitrogen-based ecological model with a detailed two-dimensional physical model of coastal upwelling (also over the timescale of an upwelling event). Their model focuses on zooplankton behaviour and success in the system.

#### 1.4.2 Ecological nitrogen-based models

There are many oceanographic ecological nitrogen-based models, of varying complexity. In general, the initial bulk models (eg. Evans and Parslow, 1985 (North Atlantic and Northeast Pacific); Frost, 1987 (Northeast Pacific, Stn P); Fasham et al., 1990 (Atlantic, Stn S)) of the upper mixed-layer have become the standard building blocks for more recent modelling studies. The main goal of these models was to reproduce annual nitrogen cycles in the upper mixed layer, which they did with some success. They focus on a limited number of processes. For example, Evans and Parslow (1985) demonstrated how spring phytoplankton blooms can be caused and that they do not necessarily require shoaling of the mixed layer. Frost (1987) showed that zooplankton could successfully limit primary production at Stn P. Fasham et al. (1990) modelled nitrate and ammonium cycles and therefore  $f$ -ratios well. However, the models fall short of reproducing other ecological aspects (e.g. the Fasham et al., (1990) model does not follow observed chlorophyll (chl)

or primary production). Nonetheless, they have been important in developing basic mathematical relationships between compartments (or state variables). They also provide useful tools for ecosystem experiments where data are sparse and costly to collect. In particular, they show the effect of changes in model parameters (e.g. mixed layer depth (Evans and Parslow, 1985); microzooplankton grazing (Frost, 1987); detrital sinking rates (Fasham et al., 1990)) on seasonal cycles. The bulk models (often with some variation) have since been integrated in vertically resolved one-dimensional physical models (e.g. McGillicuddy et al., 1995; Doney et al., 1996; Denman and Peña, 1999) and also in three-dimensional circulation models (e.g. Sarmiento et al, 1993).

The major compartments in all of the bulk models are inorganic nitrogen (N), phytoplankton (P) and zooplankton (Z or H for herbivorous grazers) - hence the name NPZ (e.g. Evans and Parslow, 1985). Uptake of inorganic nitrogen by phytoplankton is usually limited by light or nutrients, but not both, following Liebig's law of the minimum. Saturation functions are used to determine uptake rates which often require parameters for the half-saturation coefficient and maximum growth rate (Michaelis-Menten kinetics) for nitrogen uptake. Light-limited growth rates can also be modelled by Michaelis-Menten kinetics; however, the exponential saturation function (e.g. Denman and Peña, 1999) is a better fit to observations. This function is also computationally more desirable. Zooplankton grazing is defined by a saturation function dependent on phytoplankton concentrations (e.g. Steele and Hendersen, 1992). Both zooplankton and phytoplankton have some form of decay flux back to inorganic nitrogen (i.e. mortality) which may be modelled as first order exponential decay (e.g. Evans and Parslow, 1985). More recent models recognize the importance of adding a detritus (non-living organic matter; D compartment i.e. NPZD models) (e.g. Doney et al., 1996; Denman and Peña, 1999). Detritus can sink out of the model system, which is important as the euphotic zone in natural systems is not closed. The detrital compartments are usually represented by one sinking

rate and one remineralization rate (e.g. Denman and Peña, 1999). Remineralization is modelled as first order exponential decay. Fasham et al. (1990) also model sinking detritus but they included a total of 7 compartments in their model, adding ammonium, dissolved organic nitrogen and bacteria. This complexity requires specifying many more parameters.

An innovative approach (Hurtt and Armstrong, 1996) based on the Fasham et al. (1990) model that seems more representative of natural ecosystems uses distributions for some of its compartments. First, the original model was simplified into only 4 state variables (NPD and ammonium). The phytoplankton compartment is a distribution of size classes (with variable growth and death rates) and the detrital (which they call recycling) compartment has different export rates. In addition, Hurtt and Armstrong (1996) incorporated a variable N:chl ratio that phytoplankton adjust to make light and nutrients more equally limiting. This addition improves modelled chl results relative to observations.

A major difficulty in all of these models is that most parameters are not well known and poorly measured. Single parameters can represent many processes. Several techniques have been used to optimize parameters to best reproduce observations. These include simulated annealing (Matear, 1995; Hurtt and Armstrong, 1996) and variational adjoint assimilation of observations (Spitz et al., 1998). The results show improvements (relative to the models on which they are based) but the models still do not reproduce certain features of the observations well. In the end, parameters are site specific and models cannot be easily applied to different areas, largely because many parameters are species specific and species composition varies between locations. Often the models are successful at producing certain processes (usually the ones that they were designed to investigate) and not others which limits their utility. Also, natural systems are simplified to such a degree that it is not surprising that single rates do not produce modelled fluxes

that are realistic. In addition, difficulties in reproducing observations could be at least partially a result of the simplified one-dimensional physical circulation used in most of these models.

### 1.4.3 Carbon models

Most carbon models require some biological component because, although carbon is not a biologically limiting nutrient, its uptake by the biota is a very important part of its cycle. Often the biological component is very basic. For example, some models calculate primary production from model predictions of surface values of a limiting nutrient (without biology) (e.g. Toggweiler, 1989; Najjar et al., 1992). They then restore nutrient concentrations to observed values and assume that the difference is used by the biota and carbon is taken up in accordance to the Redfield ratio (C:N:P of 106:16:1, Redfield et al., 1963). The restoration technique relies on observations, thus it cannot be used as a predictive tool. In fact, carbon models generally use units (or currencies) of either nitrogen or phosphate and (like the restoration technique) assume that carbon is taken up by the biota in the standard Redfield nutrient ratios. Regardless of how realistic the ecological model is, this assumption is restrictive. Variable uptake ratios (i.e. other than Redfield) in nature may have a significant effect on carbon cycling in the surface layer.

Simple global ocean bulk models have been used to show the importance of the biological pump and the solubility pump (i.e. thermohaline circulation) (e.g. Sarmiento and Toggweiler, 1984; Siegenthaler and Wenk, 1984; Knox and McElroy, 1984). These models (sometimes termed 'Harvardton Bear' models) use two-dimensional circulation, separating advection and diffusion and distinguishing between the surface ocean at high and low latitudes over 1000 yr time scales. Najjar (1992) uses a bulk model with three levels in the vertical to show that the depth of remineralization of organic carbon is important to the carbon capacity of the ocean. While these simple models cannot be

used to accurately predict climate change and atmospheric CO<sub>2</sub>, they are valuable in identifying important processes. They divide the ocean into the minimum of physical regions (boxes) necessary to model physical circulation and important differences between regions (e.g. the differing carbon capacity of the high and low latitude oceans in the Harvardton Bear models). Their simplicity allows results to be easily interpreted, which is not always the case in the more complicated models.

Global circulation models (GCMs) have embedded carbon models using basic ecological models (previous section) (e.g. Bacastow and Maier-Reimer, 1990; Bacastow and Maier-Reimer, 1991). There are also nitrogen and phosphate based GCMs (some with ecological models embedded) that have goals of understanding the carbon system but that do not model carbon explicitly (e.g. Najjar et al., 1992; Sarmiento et al., 1993). Results depend heavily on parameterization and the ability of the GCM to reproduce physical circulation, but they also identify significant processes. In particular, it has been clearly shown that characterization of the non-living organic matter is important. This characterization can be done by partitioning the non-living organic matter (termed detritus in the ecological models) into dissolved and particulate pools (or compartments) and parameterizing recycling of the particulate fraction by a decay length (equivalent to a sinking rate and a decay rate). The dissolved fraction is modelled as non-sinking and parameterized by a decay rate that is usually relatively low so that only new production (as defined by Dugdale and Goering, 1967) is modelled (e.g. Bacastow and Maier-Reimer (1991) use 50 yrs as the turnover time for their DOC pool). A more detailed discussion of the remineralization scales of non-living organic matter is given in the introduction to Chapter 5.

There are also regional upper layer carbon models that employ one-dimensional vertically resolved physical models (e.g. Garçon et al., 1992; Archer et al., 1993). These models

are not predictive (nor do they incorporate ecological models); rather they require comprehensive data (e.g. dissolved oxygen and carbon dioxide) to provide important insight into the sizes of carbon fluxes in the surface.

#### 1.4.4 Coastal Processes in Global Models

There are few models that have considered the coastal ocean in a global context. Christensen (1994) used the model of Sarmiento and Toggweiler (1984), with the addition of two boxes, one for the coastal shelf and the other for coastal sediments using nitrogen rather than phosphorus as a limiting nutrient. He investigated the effect on atmospheric  $p\text{CO}_2$  of carbon export (due to high production) from the shelf to the deep sea and changing the fraction of global denitrification occurring over the shelf versus in the deep sea. (Denitrification produces  $\text{N}_2$ , which is largely biologically inert and thus a loss of nitrogen to the biological system.) Results show that while carbon export affected conditions on the shelf, it did not affect global  $p\text{CO}_2$ . However, increasing the proportion of denitrification over the shelf produced an increase in  $p\text{CO}_2$  over 1000 yr time scales. Smith and Hollibaugh (1993) constructed an annual global carbon budget based on data. They suggested that respiration of organic matter may exceed primary production (i.e. net heterotrophy) in coastal waters due to terrestrial inputs of organic matter and that this imbalance is globally significant. Mackenzie et al. (1998) used a global model (with terrestrial as well as oceanic and ocean sediment boxes) to investigate the balance between coastal respiration and production over the last three centuries. They showed that increased anthropogenic inputs of organic matter in the coastal ocean have caused net heterotrophy over continental margins. This heterotrophy impacts the global budget (in agreement with Smith and Hollibaugh, 1993) by making coastal zones carbon sources to the atmosphere. In contrast, Tsunogai et al. (1999) propose that continental shelves are net sinks for atmospheric carbon, coining the term 'continental shelf pump'. Based on

inorganic carbon data from the East China Sea, they suggest that the shallow shelf water becomes cooler and thus more dense relative to the neighbouring ocean water. This water sinks along isopycnals, transporting water rich in DIC (due to high coastal production and subsequent remineralization of organic matter) into the ocean interior.

These studies show that despite their small surface area, coastal regions impact the global ocean. However, the models focus on large time scales and homogenize all coastal regions into one physical compartment. Coastal regions are highly diverse and it is likely that productive upwelling regions do not fit well into these models (Mackenzie et al., 1998). The processes investigated by different researchers often contradict one another when they are extrapolated to a global scale. This contradiction is not surprising because the regions studied are so heterogeneous. There is a need for different coastal regions to be investigated separately before drawing net conclusions about the entire coastal ocean.

### 1.5 Data from coastal regions

There are many observational studies from coastal regions, but few that have reported inorganic carbon data and only one of those during the winter season. Studies in coastal upwelling regions show that during summer, biological  $p\text{CO}_2$  drawdown is intense (e.g. Simpson and Zirino, 1980; Simpson, 1986; Friederich et al., 1994), leading Friederich et al. (1994) to suggest that coastal upwelling regions are major sinks for atmospheric carbon dioxide. Codispoti et al. (1982) also observed intense biological drawdown of  $p\text{CO}_2$  in the Bering Sea during the spring and summer. In the North Sea, Kempe and Pegler (1991) collected a large inorganic carbon data set over the summer and determined that the North Sea was a net sink for atmospheric carbon during that period, again due to biological drawdown. The only winter measurements of coastal DIC were made in the East China Sea during two winter (and two fall) cruises (Tsunogai et al., 1999). In this

basin  $p\text{CO}_2$  was primarily controlled by temperature and salinity variations, with the exception of the late fall when turbulent mixing caused surface nutrient and inorganic carbon concentrations to rise. As a result, measured  $p\text{CO}_2$  was the lowest during the winter when temperature and thus solubility was highest. Based on these data, Tsunogai et al. (1999) suggested that the East China Sea is a net annual sink for atmospheric  $\text{CO}_2$ .

## 1.6 My model

I chose not to use any of the previous models, but to develop my own model to accomplish the goals of this research. Many processes are involved, so in an effort to understand them, the model was kept as simple as possible. Complexity was added when it was necessary to obtain reasonable results relative to available data, always focusing on the mechanisms that were being modelled. The physical model must run throughout the year and repeat annual cycles. For this purpose, a bulk physical model was developed with two-layers in the vertical, the minimum resolution needed to accommodate a biological model and represent seasonal cycles. The two-layer structure was slightly modified (described in Chapter 3) to make vertical fluxes more realistic. Horizontally, the model consists of three regions, again the minimum necessary to describe the important aspects of the physical circulation. The biological model was developed to have the fewest possible state variables, three for each currency (carbon and nitrogen). It is specific to diatom-dominated ecosystems, so that the high sinking rate associated with the particulate organic flux is an integral part of the model. The model also takes advantage of the fact that trophic structure is less complex relative to many other ecosystems so primary producers are represented by only one pool (and there is no zooplankton compartment). Modelled carbon and nitrogen uptake are not always coupled in accordance with a fixed Redfield ratio, so that the model is able to reproduce observations.

The thesis is divided into five remaining chapters as follows. The data that were gathered as part of this modelling study are presented in Chapter 2. The field study investigated carbon and nitrogen fluxes within the study area following summer upwelling and summer downwelling over both the shelf and slope, and within the VICC. The model development and the most significant results are presented in Chapter 3. These results include primary production, the response to El Niño Southern-Oscillation Events, net annual air-sea CO<sub>2</sub> exchange and net annual exchange fluxes between the model system and the open ocean. Model results for all of the state variables, the tuning of the model parameters and a comparison of the model results with the data (from Chapter 2) are discussed in Chapter 4. Chapter 5 focuses on modelling the character of organic matter and includes a comparison of model results with data from the upwelling region off the Oregon coast. Finally, Chapter 6 presents collated conclusions and suggestions for future research.

## Chapter 2

### A Field Study of the Inorganic Carbon System

#### 2.1 Introduction

Fluxes of organic carbon are disproportionately large over continental margins relative to the open ocean (Eppley and Peterson, 1979; Harrison et al., 1987). Despite the small surface area of these regions, they are dynamic and likely to be important to the global carbon budget. However, few inorganic carbon data have been collected in the coastal ocean.

Coastal upwelling brings intermediate depth water to the surface (Smith, 1994). Thus coastal upwelling regions have the potential to ventilate inorganic carbon and could be a source of carbon dioxide to the atmosphere (Christensen, 1994). However, biologically limiting nutrients (such as nitrogen) are also brought to the surface during upwelling and they allow high, diatom-based, primary production (*pp*) (Hutchings et al., 1994). The drawdown of inorganic carbon associated with this high production has been shown to cause low surface partial pressures of carbon dioxide ( $p\text{CO}_2$ ) off the coasts of Peru and California (Friederich et al., 1994; Simpson, 1986; Simpson and Zirino, 1980). This drawdown has led some to suggest that coastal upwelling regions may be a significant sink of atmospheric  $\text{CO}_2$ .

Other studies have suggested that some non-upwelling coastal systems may also absorb  $\text{CO}_2$  from the atmosphere due to biological drawdown in the surface ocean. For example, Codispoti et al. (1986) observed intense spring drawdown of  $p\text{CO}_2$  in the Bering

Sea. The North Sea was also shown to be a net sink of atmospheric CO<sub>2</sub> during the summer (Kempe and Pegler, 1991). Data reported from the China Sea by Tsunogai et al. (1999) suggest that coastal areas are a net sink of atmospheric CO<sub>2</sub> even during the winter.

Elevated carbon uptake (with respect to nitrogen) has been observed in the North Atlantic, over Georges Bank (Sambrotto et al., 1993) and in the Bering Sea (Codispoti et al., 1986). If phytoplankton take up dissolved inorganic carbon (DIC) in excess relative to limiting nutrients, the effects of biological  $p\text{CO}_2$  drawdown could be significantly enhanced.

I report inorganic carbon data from the coastal upwelling region west of southern Vancouver Island following an upwelling event and during a period of summer downwelling conditions. Although not as shallow, the continental shelf in this region is generally wider than off the Oregon, Californian and Peruvian coasts (20 – 30 km on lines D and G) and almost as broad as the Northwest African shelf in some areas (40 – 50 km on lines A and C) (Figure 2.1). Upwelling off Vancouver Island is driven both by local wind forcing and by wind forcing further south along the Oregon and Californian coasts, connected to this region via shelf waves (Freeland and Denman, 1982). In addition, a buoyancy current (the Vancouver Island Coastal Current, VICC) flows northward throughout the year (due to local run-off in the winter and snow melt in the interior of British Columbia in the summer) over the inner-shelf hugging the southern coast of Vancouver Island (Freeland et al., 1984; Hickey et al., 1991) (Figure 2.2). This current runs counter to the equatorward surface current that flows over the mid- and outer-shelf in the summer (Figure 2.2, lower panel). The equatorward current is part of the classical upwelling circulation (Smith, 1994). The VICC, is also an important source of nutrients (due to intense mixing in Haro Strait, the source of this current) and supports significant  $pp$  in the area (Mackas et al., 1980; Crawford and Dewey, 1989).

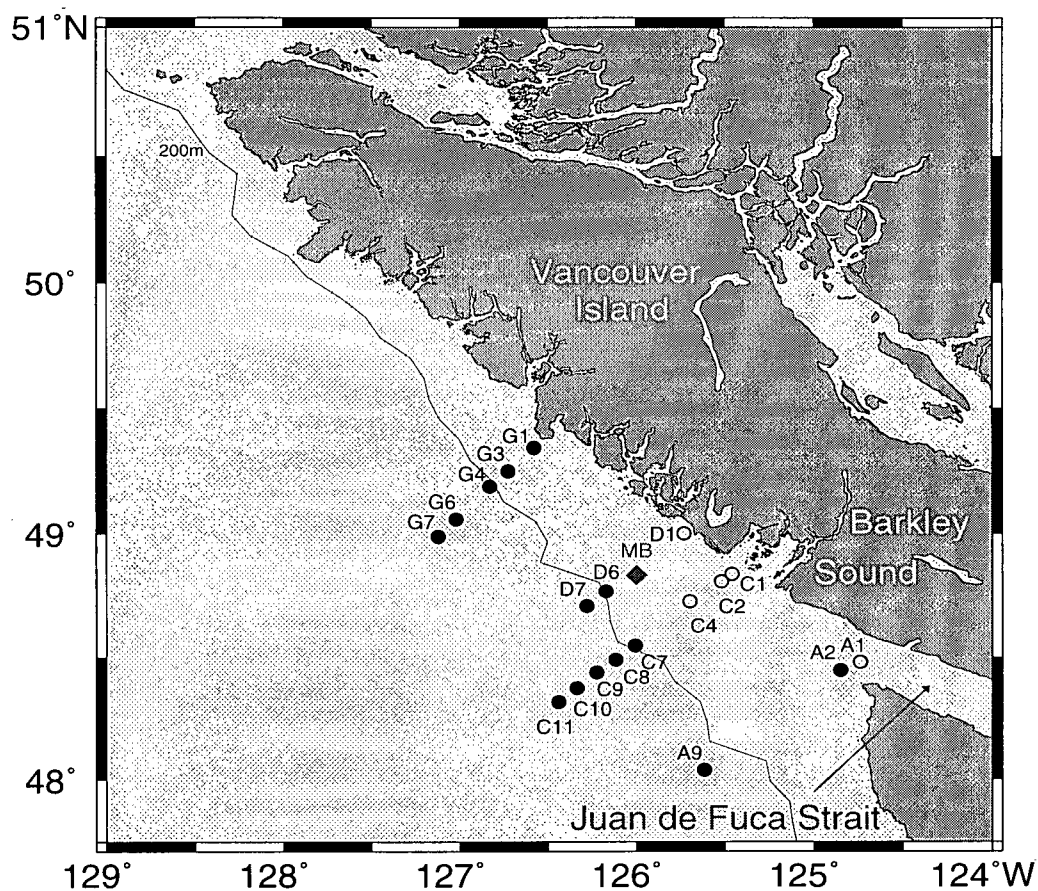


Figure 2.1: A map of all stations sampled. Stations marked with open circles were clearly influenced by the Vancouver Island Coastal Current during this study (July 1998). MB marks the location of the meteorological buoy. The Juan de Fuca Strait is the source of the VICC. The 200 m depth contour runs approximately along the shelf break.

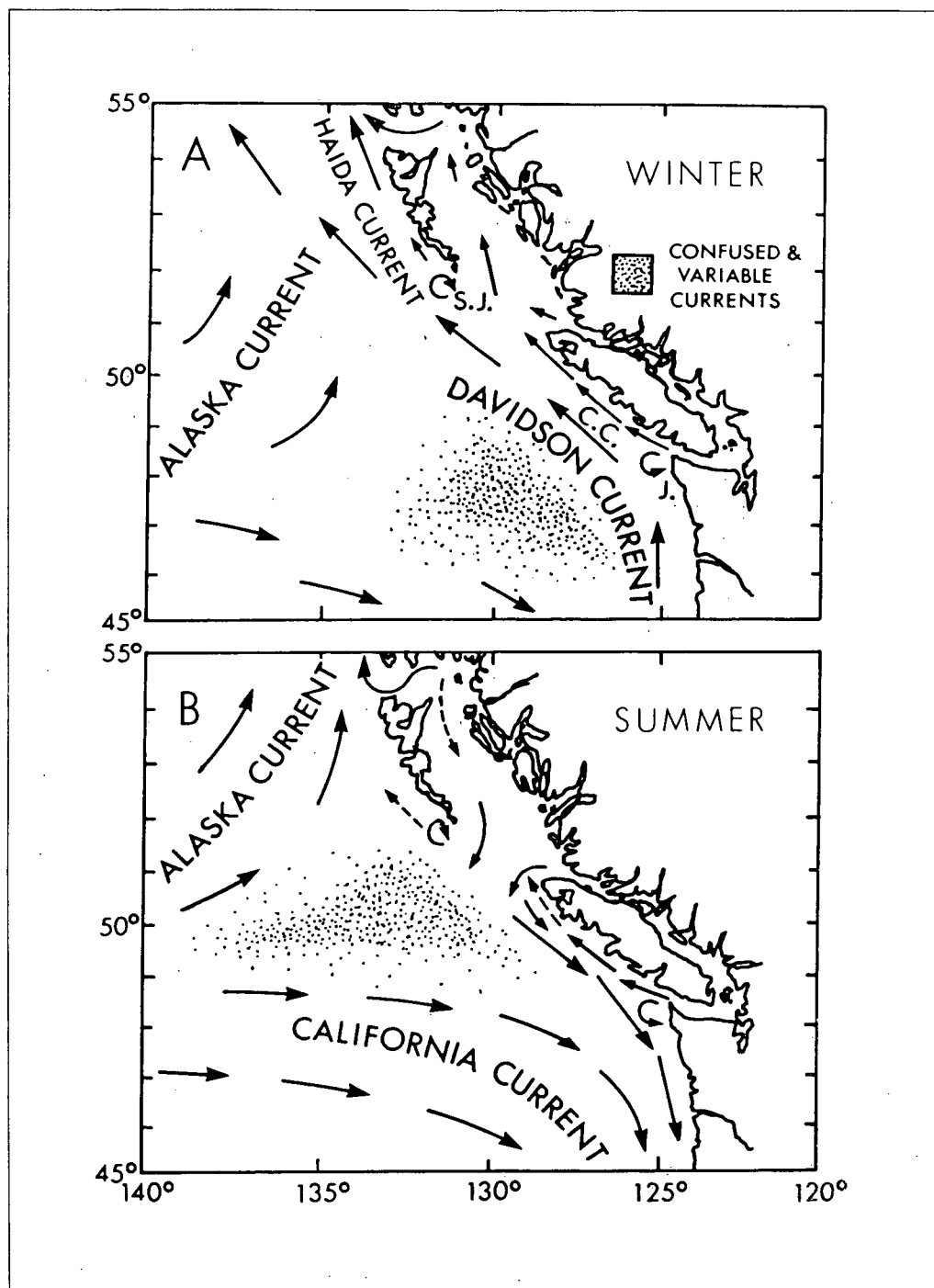


Figure 2.2: The surface circulation patterns off the British Columbian coast during winter (a) and summer (b). Here the VICC is labeled as 'C.C.' This figure has been reprinted from Thomson et al. (1989) with the permission of R. Thomson.

I describe the inorganic carbon system for each physical regime: the VICC, the outer-shelf and the slope, during downwelling and after upwelling. Biological uptake of carbon relative to nitrogen is compared for each of these regimes. Finally, daily carbon and nitrogen budgets are constructed and the dominance of large phytoplankton cells are contrasted for each regime.

## 2.2 Materials and Methods

Data were gathered as part of the Canadian Global Ocean Ecosystem Dynamics program (GLOBEC) during July 1998 from the *CSS John P. Tully* along transects A (July 14), C (July 15), D (July 19) and G (July 23) (Figure 2.1). Profiles of dissolved inorganic carbon (DIC), total alkalinity (TA), nitrate ( $\text{NO}_3^-$ ) and chlorophyll *a* (*chl**a*) were collected at each station (except DIC and TA were not sampled at G3 and G7, and  $\text{NO}_3^-$  and *chl**a* were not sampled at A9). Conductivity, temperature, depth (CTD) (Seabird Model SBE 911+ CTD) casts were made concurrently at each station and  $\sigma_T$  calculated from temperature (T) and salinity (S) using the equations of Millero and Poisson (1981). At C4, C9, G3 and G7 total and size-fractionated primary production (*pp*), particulate organic carbon (POC) and particulate organic nitrogen (PON) were measured. Depths for these measurements were chosen by light levels (100, 50, 30, 10, 3 and 1% of surface photosynthetically available radiation (PAR) for *pp* and 100, 50, 10 and 1% for POC and PON) that were determined by a Biospherical QSP -200 L4S 4495 PAR sensor (Harris, 2000). A total of 114 DIC and 49 TA samples were collected. Additional samples for  $\text{NO}_3^-$ , *chl**a*, as well as ammonium, phosphate, silicic acid and samples for nitrogen uptake experiments were also gathered in the study area as part of the GLOBEC project (Harris, 2000; Varela, in prep.).

### 2.2.1 Analysis of seawater

Seawater samples were collected using acid-cleaned 10-L PVC Niskin bottles equipped with Teflon coated springs and fittings and silicon tubing mounted on an instrumented rosette sampler. DIC and TA samples were drawn from the bottles using the collection methods of Dickson and Goyet (1994), and samples for  $\text{NO}_3^-$ , chl $a$ ,  $pp$  (triplicate) and POC-PON (duplicate) were drawn using the methods of Parsons et al. (1984). DIC was then determined coulometrically (Johnson et al., 1985; Johnson et al., 1987) and TA samples were determined by potentiometric titration (Millero et al., 1993).  $\text{NO}_3^-$  plus nitrite ( $\text{NO}_2^-$ ) was measured on filtered (with combusted GFF 0.7  $\mu\text{m}$  filters) samples using a Technicon<sup>TM</sup> Autoanalyzer II (Wood et al., 1967) and the total reported as  $\text{NO}_3^-$  (since  $\text{NO}_2^-$  represents  $\leq 5\%$  of the total  $\text{NO}_3^- + \text{NO}_2^-$ ). Chl $a$  (0.7  $\mu\text{m}$  filter) was determined by in vitro fluorometry (Parsons et al., 1984). Rates of primary production were estimated using the  $^{14}\text{C}$  technique (*ibid.*). Primary production samples (70 ml) were inoculated with 100  $\mu\text{Ci}$  of  $^{14}\text{C}$  and incubated for 6 h under natural light conditions using neutral density screening, and size fractionation (0.7  $\mu\text{m}$  and 5.0  $\mu\text{m}$ ) was done by gravity filtration at the end of the incubation (Harris, 2000). POC and PON samples were filtered (0.7  $\mu\text{m}$ ), dried and analyzed with a Carlo Erba Elemental Analyzer (Verardo et al., 1990). This analysis measures all particulate carbon (C) and nitrogen (N) present; thus it is assumed any inorganic forms of N and C are negligible relative to the organic forms.

### 2.2.2 Data analysis and calculations

The partial pressure of carbon dioxide ( $p\text{CO}_2$ ) was calculated from TA and DIC measurements using the relations of Skirrow (1975). Gas flux ( $G$ ) was then estimated from the

uppermost  $p\text{CO}_2$  ( $p\text{CO}_{2w}$ ) at each station (usually  $\leq 2$  m) using the standard equation:

$$G = sol \cdot k (p\text{CO}_{2a} - p\text{CO}_{2w}) \quad (2.1)$$

where  $sol$  is the solubility of  $\text{CO}_2$  (estimated from T and S (*ibid.*)),  $k$  is the piston velocity and  $p\text{CO}_{2a}$  is the atmospheric  $p\text{CO}_2$  (380 ppm) extrapolated using seasonal and latitudinal dependencies from Manning (1993). The relationship of Wanninkhof (1992) for  $k$  based on long term averaged wind speed was used with averaged wind data from Meteorological Buoy 46206 (Figure 2.1).

I constructed instantaneous budgets for DIC and  $\text{NO}_3^-$  for spatial scales  $\leq 10$  km (approximately the Rossby radius which is the expected correlation length) on transects C and G over the mid-shelf and slope where  $pp$  was measured. The conservation equation for a scalar was used assuming that alongshore gradients were small enough to neglect. For DIC in the upper layer,

$$\frac{\partial \text{DIC}_u}{\partial t} = -u_E \frac{\partial \text{DIC}_u}{\partial x} - \frac{pp}{h_u} + \frac{M}{h_u} (\text{DIC}_{l1} - \text{DIC}_u) + \frac{G}{h_u} + r_d \text{DOC}_u \quad (2.2)$$

Terms on the right-hand side of the equation represent advection (Ekman transport), primary production, vertical mixing and entrainment, gas flux, and remineralization of DOC, respectively (Figure 2.3):  $t$  is time,  $x$  is the horizontal cross-shelf dimension increasing offshore,  $u_E$  is the Ekman velocity in the  $x$ -direction, subscript  $u$  denotes the upper mixed layer and  $h_u$  is the mixed layer depth.  $\text{DIC}_u$  is the average DIC concentration in the mixed layer,  $\text{DIC}_{l1}$  is the concentration 1 m below  $h_u$  and  $M$  is the mixing coefficient (units velocity). DOC is the average concentration of the semi-labile dissolved organic carbon in the upper mixed layer and  $r_d$  is its remineralization rate. These terms were estimated from data (described below) and the time rate of change (left-hand side of the equation) was calculated from their sum. The  $\text{NO}_3^-$  equation is identical except that there is no gas flux.

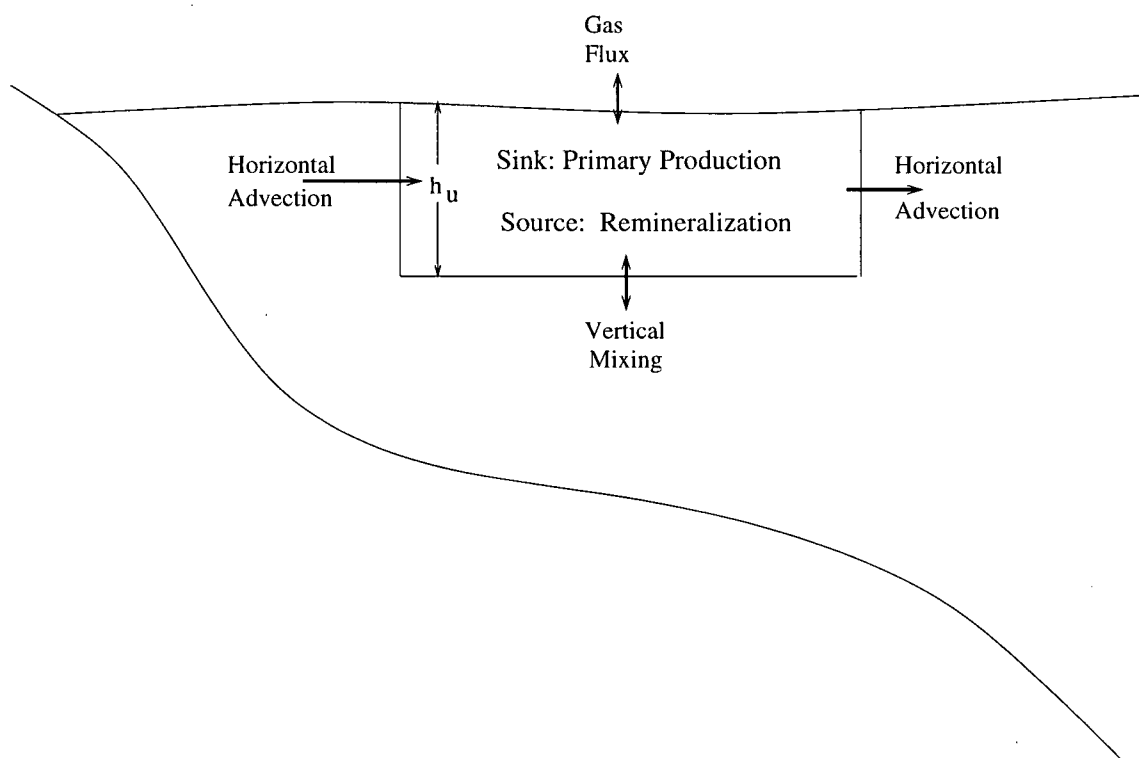


Figure 2.3: The fluxes in the DIC budget (Equation 2.2). The time rate of change within the box (depth,  $h_u$ ) is a sum of the physical transfer (shown by arrows) and the source and sink terms within the box. Fluxes in the  $\text{NO}_3^-$  budget are identical except there is no gas flux.

The velocity  $u_E$  within the mixed layer was calculated from the standard equation for Ekman transport (e.g. Gargett, 1991) using the relationship between wind speed and wind stress from Large and Pond (1981) and assuming that half the transport occurs within the mixed layer (Lentz, 1992). Horizontal gradients were estimated using the upwind differencing method (Press et al., 1992). Vertical flux is difficult to approximate using estimates of vertical eddy diffusivity. Instead, I assume that the 2 m of fluid below the mixed layer is mixed or entrained into the upper layer each day (matched by mixing or detrainment of the same volume from the upper layer into the lower), based on daily fluctuations of mixed layer depths in the area (Thomson and Fine, 2000). Thus  $M$  is 2 m d<sup>-1</sup>.

Unfortunately, the DOC samples that I collected were contaminated so the remineralization term was based on DOC data from the Oregon upwelling region (Hill, 1999) assuming that the semi-labile fraction of the DOC is about 0.3 of the total (Carlson and Ducklow, 1995; Carlson et al., 1994) and the rate  $r_d$  is 0.005 d<sup>-1</sup>, based on model values (Appendix F). I estimate the remineralized flux of DON using the same data (again assuming that one-third of the bulk is semi-labile) and  $r_d$  of 0.0065 d<sup>-1</sup> (Appendix F).

## 2.3 Results and Discussion

### 2.3.1 Physical data

I used temperature-salinity (T-S) data to identify water masses (VICC, inner-shelf, outer-shelf and slope) and wind and current data to show the physical state (upwelling, downwelling or relaxation) of each transect at the time of sampling.

T-S characteristics are in good agreement with the patterns described by Freeland et al. (1984). The VICC is shown clearly as colder (as much as 4°C colder above 50 m, A1

upper left portion of Figure 2.4), fresher (0.5 in salinity compared with the slope above 50 m) water over the inner-shelf along transects A, C (Figure 2.4) and D. Further north (transect G) there was little evidence of the VICC. If it was present, significant mixing had occurred between it and the equatorward current (Figure 2.5, T-S are similar over the entire shelf and are warmer and fresher in the surface (upper left portion) than the VICC (shown by A1)). Along Line C there was a fresh estuarine wedge originating from Barkley Sound outflow shoreward of C2 (note the depths of the T-S point (T = 9.81, S = 31.87) decrease moving offshore, Figure 2.4), and VICC water was found beneath this wedge from C1 seaward to the shelf-break, including C4 and influencing C7, further offshore than expected. This wedge was likely enhanced by a strong storm with heavy rainfall several days prior to sampling the C line. A similar offshore deflection of the VICC due to an outflow event from Barkley Sound was observed during July 1984 (Hickey et al., 1991). Surface T-S data from stations over the slope were all saltier (as much as 1) and slightly warmer ( $< 1^{\circ}\text{C}$ ) than those from the outer-shelf, but at depths below roughly 40 – 50 m T-S were similar at all stations. There is little evidence of upwelling (or downwelling) in the T-S data (note the depths of the T-S point (T = 8.85, S = 32.7) Figures 2.4 and Figure 2.5) (although there is a bulge in salinity at G4 25 – 29 m below the surface, indicated by the 'X' in Figure 2.5, that may have been caused by upwelling). However, upwelling only occurred towards the end of the study.

Between July 11–18 (peaking in a rare summer storm on July 14) winds were downwelling favourable and the equatorward surface current reversed direction (S. Allen, pers. com.). Much of my data were collected during and at the end of this period. Line A was sampled right after the storm (July 15) and Line C just after the transition back to normal upwelling favourable winds (July 18). On July 21 local winds increased and an upwelling event occurred (*ibid.*). Data from the D line were collected before this event (July 19) and from the G line two days later (July 23). Thus I consider transects A

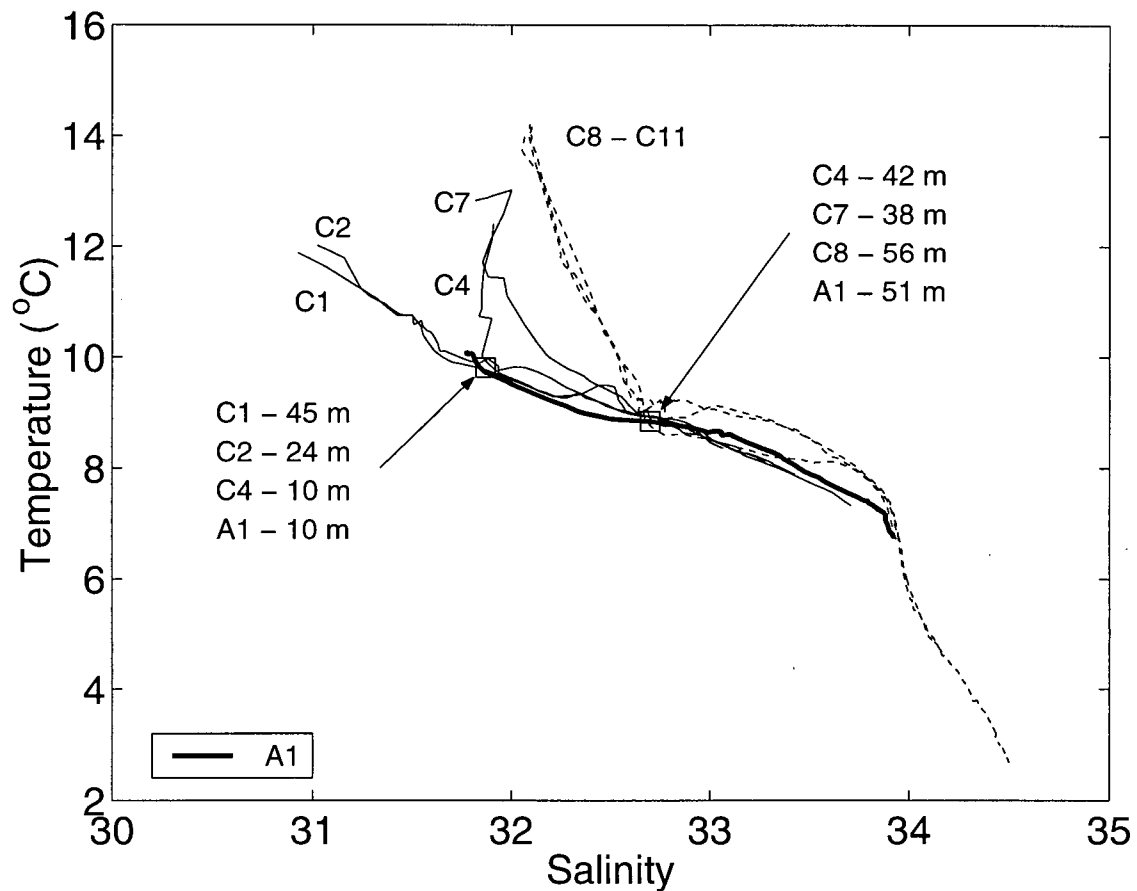


Figure 2.4: T-S curves for the C transect (over the shelf, solid line —; over the slope, dashed line, - -). The VICC is indicated by the T-S from A1 (thick solid line). The depths for all stations passing through two T-S points, ( $T = 9.81$ ,  $S = 31.87$ ) and ( $T = 8.85$ ,  $S = 32.7$ ), marked by open squares are indicated for comparison. Note that below  $\sim 40 - 50$  m the water masses have overlapping T-S at all locations. The upper left portion of the plot contains the surface water from each station. The surface water of stations C1 and C2 is part of the fresh estuarine wedge originating from Barkley Sound. The surface water of stations C8-C11 is typical for the slope. The surface water of stations C4 and C7 is clearly influenced by the fresh wedge.

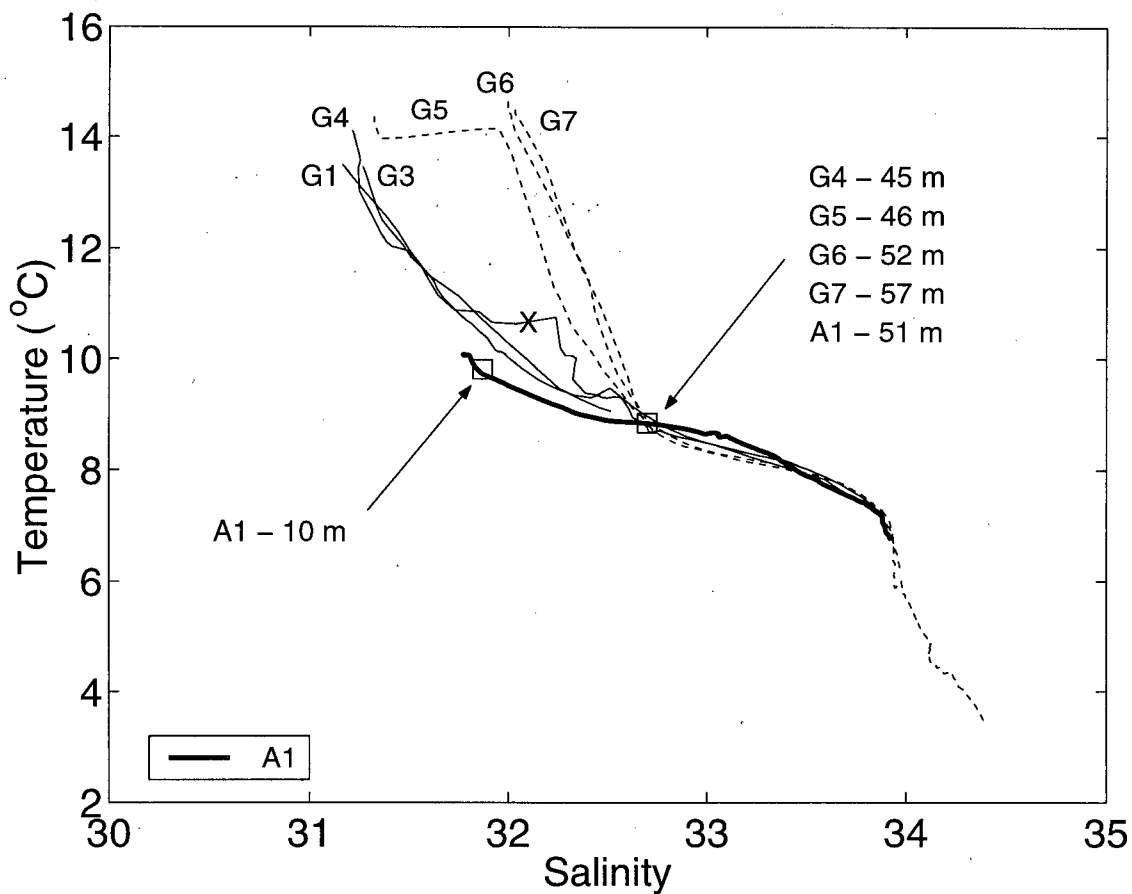


Figure 2.5: T-S curves for G transect (over the shelf, solid line —; over the slope, dashed line, - -). The VICC is indicated by the T-S from A1 (thick solid line). The depths for all stations passing through two T-S points, ( $T = 9.81$ ,  $S = 31.87$ ) and ( $T = 8.85$ ,  $S = 32.7$ ) (also shown in Figure 2.4), marked by open squares are indicated for comparison. Note that below  $\sim 50$  m the water masses have overlapping T-S at all locations. The X (in b) marks a bulge in G4 salinity at 26 – 29 m. The upper left portion of the plot contains the surface water from each station. The surface water of stations G5-G7 are typical for the slope. The surface water at G1, G3, G4 is only slightly fresher.

and C to be during summer downwelling, D during a relaxation period, and G after an upwelling event.

### 2.3.2 Inorganic carbon data

There are three distinctive features in the inorganic carbon system in the coastal upwelling region west of Vancouver Island. These features are shown in vertical DIC profiles normalized by salinity (to remove effects of fresh water runoff, precipitation and evaporation) (Figure 2.6). First, the VICC has high surface values at A1 and C2, which are diluted (and biologically drawn down) by the time the current reaches D1. Second, outside the VICC, biological drawdown of DIC is evident in the surface waters. This drawdown is strongest over the outer shelf relative to the slope (where sampled). Third, the deeper (> 50 m depth) water over the outer shelf is always higher in DIC than over the slope at the same depth. The bulge around 30 m at G4 (Figure 2.6) may be a result of recent upwelling (also seen in salinity, Figure 2.5 marked by an 'X'). On the other lines, however, there was no upwelling so the elevated DIC is likely due to remineralization of organic matter delivered from the productive surface waters over the shelf. The remineralized carbon is more concentrated over the shelf because the volume of the shelf water is limited by bathymetry.

The variation of the DIC and TA data with salinity is shown in Figures 2.7 and 2.8, respectively. Linear regressions of DIC below the mixed depth (Figure 2.7) and TA at all depths (Figure 2.8) with salinity (as an independent variable) are shown. Most surface DIC samples fall below the regression line due to biological drawdown; those in the VICC are all above the line because the VICC is rich in DIC. For comparison I show another regression of coastal summer DIC data in the North Sea (Kempe and Pegler, 1991) as well as an open ocean regression (Takahashi et al., 1991). Some surface data have been reported for fresher water (salinity 23 - 27) inshore of Vancouver Island (Johnson et

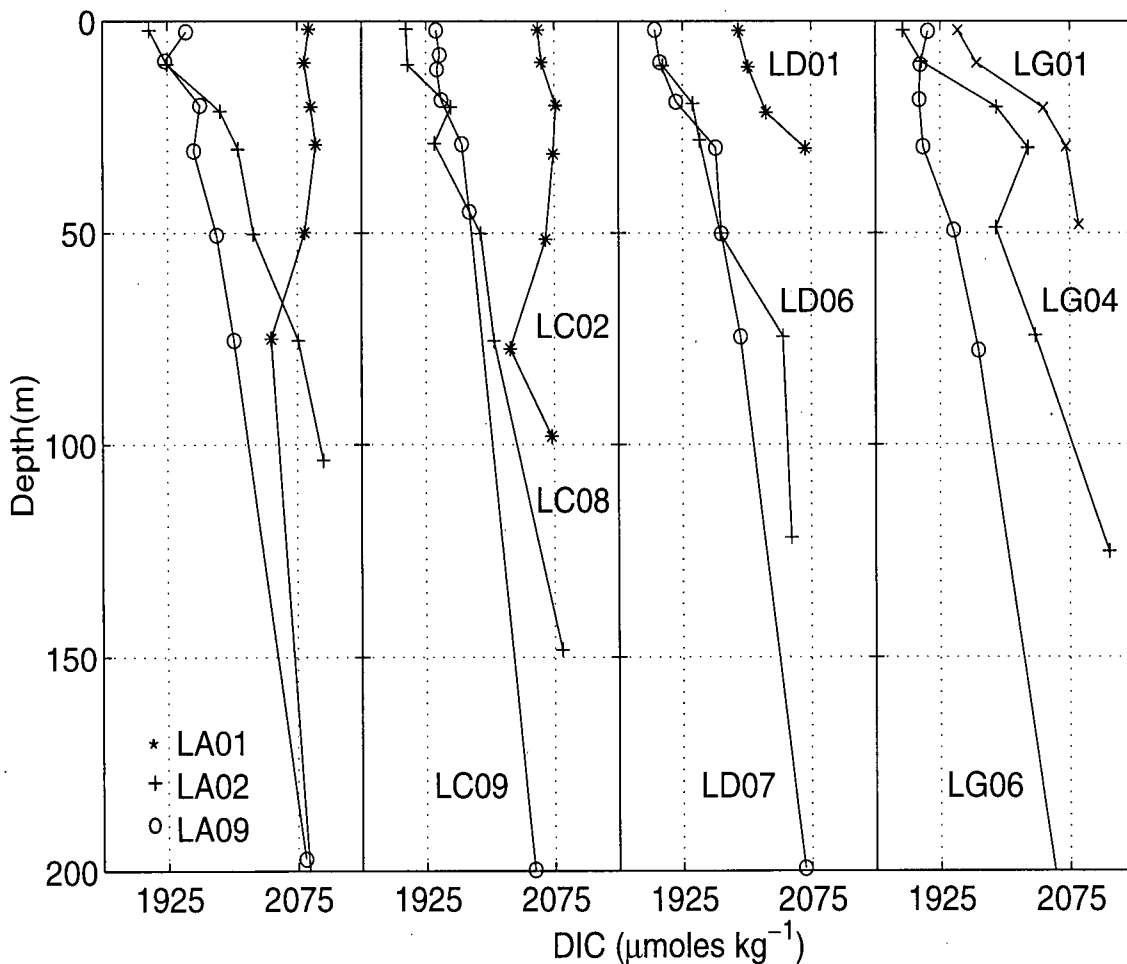


Figure 2.6: DIC profiles are shown from Line A, C, D, and G, in panels left to right, for outer slope stations (o), outer shelf stations (+), inner shelf stations north of the VICC (x) and in the VICC (\*). All data are normalized to a salinity of 32 (by multiplying by 32 and dividing by the salinity of the sample). Units are converted from  $\mu\text{M}$  to  $\mu\text{moles kg}^{-1}$  using the calculated density of the water.

al., 1979). These DIC data fall between predictions from my regression and the North Sea regression. The coastal data sets have much higher DIC per salinity than the open ocean data. This disparity is expected as water temperatures are higher in the open ocean data thereby reducing the carbon capacity. Carbon inventories may be higher in coastal waters than in the open ocean because remineralization of organic carbon from high coastal primary production is concentrated in a smaller water volume. This mechanism provides positive feedback, as high inventories of inorganic nutrients make for larger vertical fluxes of nutrients into the euphotic zone leading to higher primary production (Section 3.4.1 and Table G.1, run 3).

Unlike the North Sea DIC regression, my regression has a negative DIC intercept ( $-787 \mu\text{mole kg}^{-1}$ ). It is likely that particulate flux of organic matter to deeper waters during the summer makes for elevated deep water DIC (where salinity is higher) via remineralization (as seen over the outer shelf in Figure 2.6). Elevated values of DIC at higher salinities would tend to increase the slope of a DIC-S regression and could give rise to a negative intercept. The positive DIC intercept in the North Sea data would be expected to represent DIC concentrations in terrigenous fresh water sources there.

The regression of my TA data is close to the theoretical regression predicted by Skirrow (1975), but it has a positive intercept ( $472 \mu\text{eq kg}^{-1}$ ) possibly due to a small concentration of dissolved salts in the runoff from Vancouver Island. Data from the Bering Sea (Codispoti et al., 1986) fall well below my regression due to calcium carbonate production by coccolithophores (calcium carbonate formation was not observed during my study), while the North Sea data regression (Kempe and Pegler 1991) is much higher possibly due to a higher terrestrial input of  $\text{CaCO}_3$  into the North Sea.

The range in  $p\text{CO}_2$  of surface waters was extreme; from 117 ppm (at G4 after upwelling) to 1734 ppm (A1 near the source of the VICC) (Table 2.1). All estimates of  $p\text{CO}_2$  within the VICC are exceptionally high (mostly  $> 1000$  ppm), with the exception

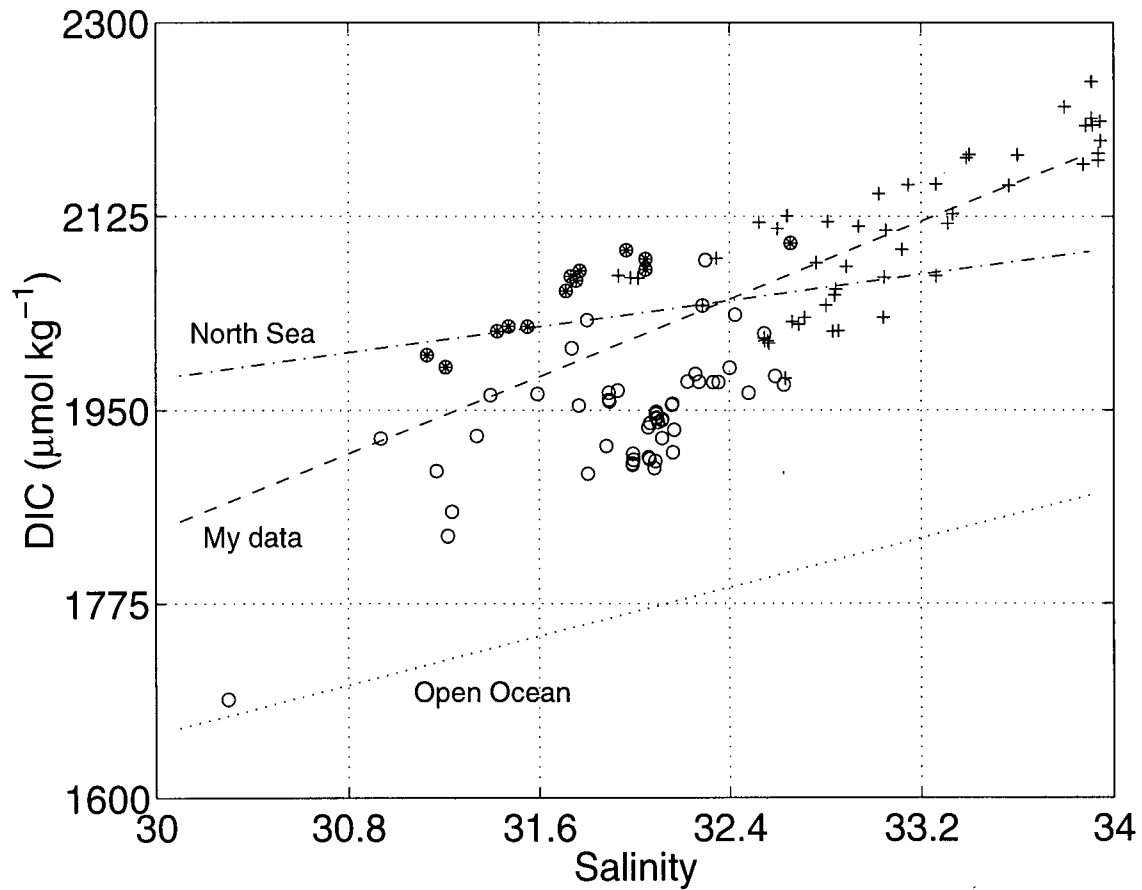


Figure 2.7: Upper layer (o) and lower layer (+) DIC data are plotted against salinity. The upper layer was defined as 20 m and above for stations over the shelf and 30 m and above further offshore. DIC samples from within VICC (all upper layer) are also marked with a \*. A linear regression (– dashed lines) of the lower layer DIC data is:  $\text{DIC} = 87.6 S - 787 \mu\text{mole kg}^{-1}$  ( $r^2 = 0.75$ ). A DIC regression from the North Sea (– · dash-dot lines) (Kempe and Pegler, 1991) and an open ocean regression (· · dotted line) from data in the equatorial Pacific (Takahashi et al., 1991) are shown.

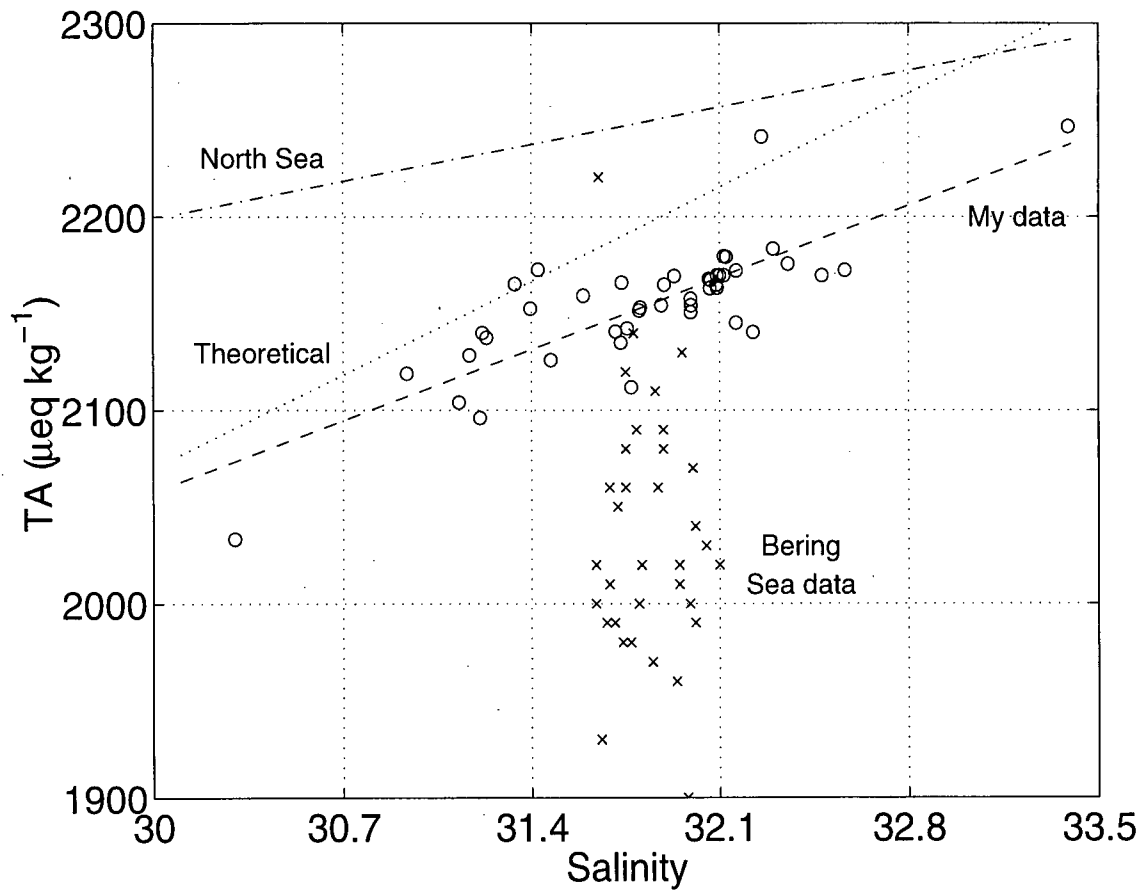


Figure 2.8: TA data from all depths (o) are plotted against salinity. TA data from the Bering Sea (Codispoti et al., 1986) where  $\text{CaCO}_3$  production occurred are also shown (x). A linear regression (— dashed lines) of my TA data is:  $\text{TA} = 52.85 S + 472 \mu\text{eq kg}^{-1}$  ( $r^2 = 0.80$ ). TA regressions from the North Sea data (— · dash-dot lines) (Kemp and Pegler, 1991) and from theory (· · dotted line) (Skirrow, 1975) are shown.

of the surface value at C1 which is significantly fresher ( $S < 31$ ) and has low DIC; presumably this sample contains some fresh water outflow from Barkley Sound with VICC water underneath. Given the high  $p\text{CO}_2$ , the predicted gas outflux from the VICC is high, particularly at A1 and C2. Outside the VICC, gas flux changes sign and is always into the ocean (with the exception of A9). The greatest influx occurs over the outer shelf where biological drawdown of DIC is strongest. This influx is highest after upwelling (G4). Over the slope,  $p\text{CO}_2$  is much closer to equilibrium (e.g. C9, C10 and C11).

### 2.3.3 Organic carbon data

POC,  $pp$  and  $chl_a$  (Table 2.2) were determined from samples along transects C and G at shelf stations (C4, G3) and slope stations (C9, G7). When sea water is filtered to make these measurements, non-living detritus and dormant cells are collected as well as living phytoplankton cells. I present values of POC,  $chl_a$  and  $pp$ , that were integrated over the euphotic zone and represent all the above forms of POC (Table 2.2a). In addition, the fraction of the total  $pp$  from the  $> 5.0 \mu\text{m}$  size class (representative of diatoms),  $C:chl_a$ , POC:PON ratios and average  $\text{NO}_3^-$  concentration ( $\overline{\text{NO}_3^-}$ ) are presented. To contrast with these data (particularly with the ratios) I include data from discrete depths (Table 2.2b) where  $pp$  and  $chl_a$  were high relative to other depths to represent samples with a larger fraction of viable phytoplankton.

Primary production was high over the shelf where the supply of nutrients was high due to the VICC at C4, and the recent upwelling event at G3 (though the largest upwelling response was centered at G4, discussed below) and lower over the slope (C9, G7). Large diatom cells dominated at all stations (Harris, 2000), but particularly where  $pp$  was higher due to the supply of new inorganic nutrients (Hutchings et al., 1994). POC:PON was relatively constant (range 5.6 to 6.4) between stations and close to the Redfield ratio (Redfield et al., 1963). Also this ratio was constant regardless of the fraction of

Table 2.1:  $p\text{CO}_2$  for all depths where both TA and DIC were measured on transects A, D and G (a) and C (b) (July, 1998). Air-sea gas flux is negative for gas evasion from the surface ocean to the atmosphere and positive for gas invasion.

	$p\text{CO}_2$ (ppm)			Gas flux ( $\text{mmol C m}^{-2}\text{d}^{-1}$ )
	2 m	10 m	20 m	
A1	1734	1384	2251	- 44
A2	244	292		3.3
A9	451		533	- 3.2
D1	406	441	556	- 1.8
D6		252	364	3.0
D7	242	241		3.3
G1	286	289	925	2.0
G4	117	207	419	5.4
G6	296	280	264	1.7

Table 2.1a

	$p\text{CO}_2$ (ppm)						Gas flux ( $\text{mmol C m}^{-2}\text{d}^{-1}$ )
	2 m	8 m	10 m	20 m	45 m	100 m	
C1	112		1033	687			7.6
C2	1087		1197	1279			- 24
C4			381				- 1.0
C7			409	1212		1738	- 1.9
C8	262		256	391			2.7
C9		346	352	265	535		0.1
C10			310				1.2
C11			331	325			0.6

Table 2.1b

Table 2.2: Particulate organic carbon (POC), chlorophylla (*chl**a*), primary production (*pp*), % of the total *pp* in the size class  $> 5.0 \mu\text{m}$  (mainly diatoms), C:*chl**a*, POC:PON and  $\text{NO}_3^-$  integrated over the euphotic zone (EZ) (6 depths for *pp* and 4 depths for POC) (a) and at discrete depths (*d*) (b) at stations C4, C9, G3 and G7 (July 1998). Discrete depths were chosen where *pp* and *chl**a* were high (relative to other depths) for comparison with integrated values (see text). At C9 (30 m) and G7 (6 m), POC and PON data were not available at these depths so another depth where all data were available was also included (19 m for C9 and 44 m for G7). Note that  $1 \text{ M} = 1 \text{ mole l}^{-1}$

Stn	EZ m	POC $\mu\text{mol m}^{-2}$	<i>chl</i> <i>a</i> $\text{mg m}^{-2}$	<i>pp</i> $\text{mgC m}^{-2}\text{h}^{-1}$	% <i>pp</i> $>5\mu\text{m}$	C: <i>chl</i> <i>a</i> g:g	POC:PON mol:mol	$\overline{\text{NO}_3^-}$ $\mu\text{M}$
C4	42	706.9	107.3	969.7	87	79	5.6	12.4
C9	45	490.7	66.9	243.6	62	88	6.4	1.2
G3	30	1134.2	242.3	649.5	84	56	5.9	8.2
G7	44	480.3	32.2	334.6	70	180	6.0	0.0

Table 2.2a

Stn	<i>d</i> m	POC $\mu\text{M}$	<i>chl</i> <i>a</i> $\text{mg m}^{-3}$	<i>pp</i> $\text{mgC m}^{-3}\text{h}^{-1}$	% <i>pp</i> $>5\mu\text{m}$	C: <i>chl</i> <i>a</i> g:g	POC:PON mol:mol	$\text{NO}_3^-$ $\mu\text{M}$
C4	0	46.31	9.0	154.1	94	62	5.5	4.4
C9	19	13.17	1.2	5.5	51	130	6.3	0.0
C9	30		2.8	5.9	85			0.3
G3	0	53.81	14.2	45.8	93	45	5.9	0.9
G7	6		0.4	42.79	84			0.0
G7	44	16.28	3.0	1.0	46	65	5.9	0.0

Table 2.2b

the particulate organic matter that was living (compare values from the discrete depths having a higher portion of viable phytoplankton with integrated values; i.e., Table 2.2a with 2.2b). Thus, there was no evidence of variable C:N incorporation by phytoplankton or of preferential remineralization of particulate carbon or nitrogen in the surface.

It is expected that non-living POC is low in *chl a* and my data are in agreement with this expectation. C:*chl a* varied considerably between integrated and discrete samples. The ratio was much lower (45 – 62) over the shelf at discrete depths (surface) in Table 2.2) that had a higher fraction of viable phytoplankton relative to the integrated data. Over the slope (C9 and G7) where this fraction was estimated to be highest, C:*chl a* could not be calculated because POC data were not available. In the integrated samples C:*chl a* was always higher (than at discrete depths where *pp* and *chl a* were high) and had a larger range (56 – 180). At G3 (after upwelling), the ratio had the smallest range, presumably because more of the integrated POC was living. At G7, the integrated C:*chl a* was very high, likely because  $\text{NO}_3^-$  was recently (over a period of days) exhausted and a bloom had just crashed. Phytoplankton may also reduce their cellular *chl a* when nitrogen is limiting and light is plentiful (Laws and Bannister, 1980; Taylor et al., 1997) which could add to the observed increase in the C:*chl a* ratio particularly at G7 following upwelling (note the high *pp* relative to low *chl a* at 6 m (Table 2.2b)).

#### 2.3.4 Variations in inorganic carbon and nitrogen

I use *chl a*,  $\text{NO}_3^-$  and DIC spatial patterns from line C and G to contrast summer downwelling with upwelling and the VICC (Figures 2.9 and 2.10). The data have not been smoothed. Where  $\text{NO}_3^-$  and DIC values do not increase with depth (instead there is a sign reversal in the vertical gradient; e.g.,  $\text{NO}_3^-$  at C10 is 4  $\mu\text{M}$  higher at 100 m than at 125 m) the contours have small sharp changes.

The VICC can clearly be seen in high *chl a* values in the upper 20 m (Figure 2.9,

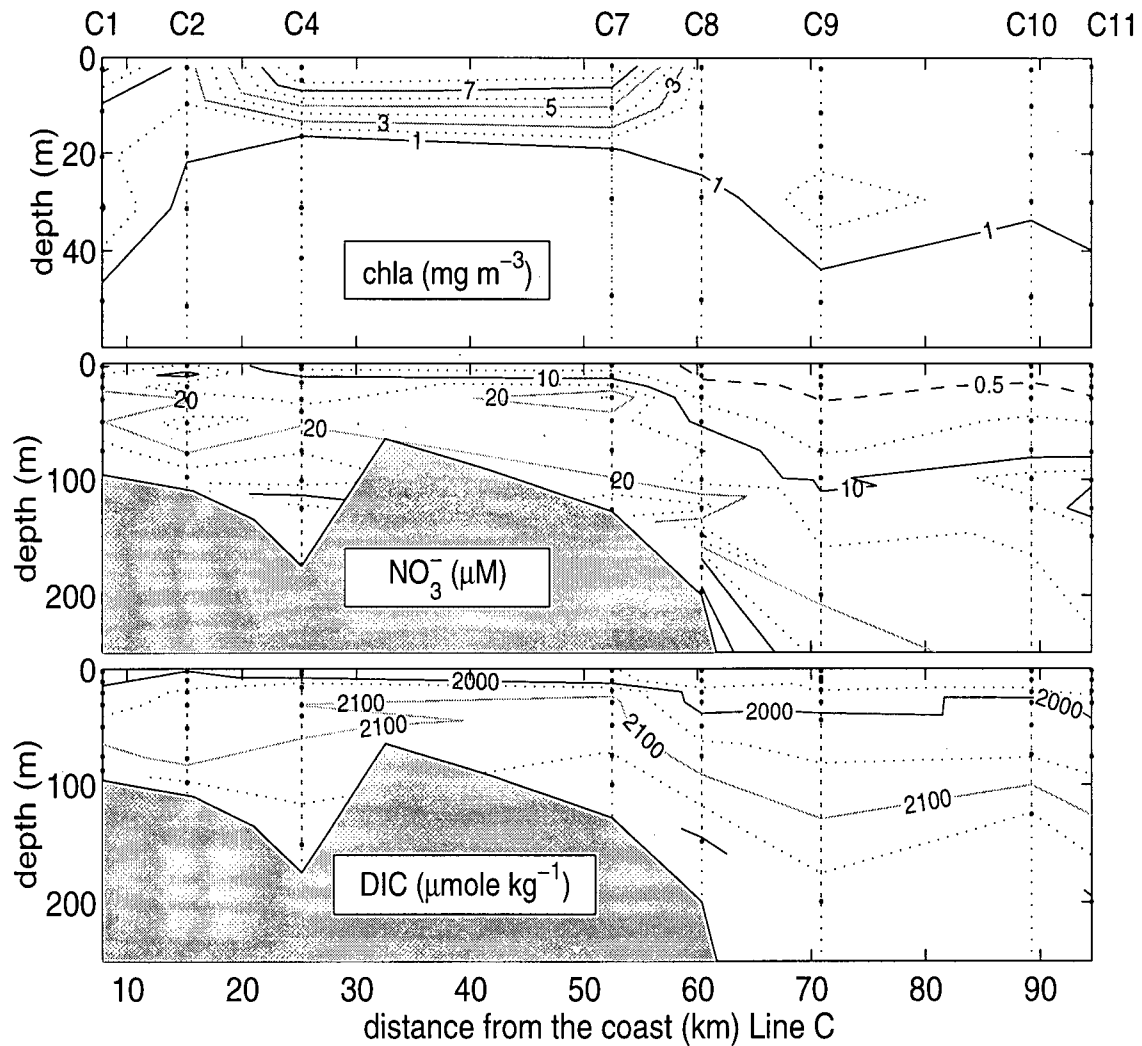


Figure 2.9: Contours of chl $a$ ,  $\text{NO}_3^-$  and DIC along line C. Note that the depth range is only 50 m for chl $a$  (where data were gathered) compared to 250 m for  $\text{NO}_3^-$  and DIC. Grey shading marks the bottom topography. Occasional sharp changes in contours reflect the data (which have not been smoothed) as discussed in the text.

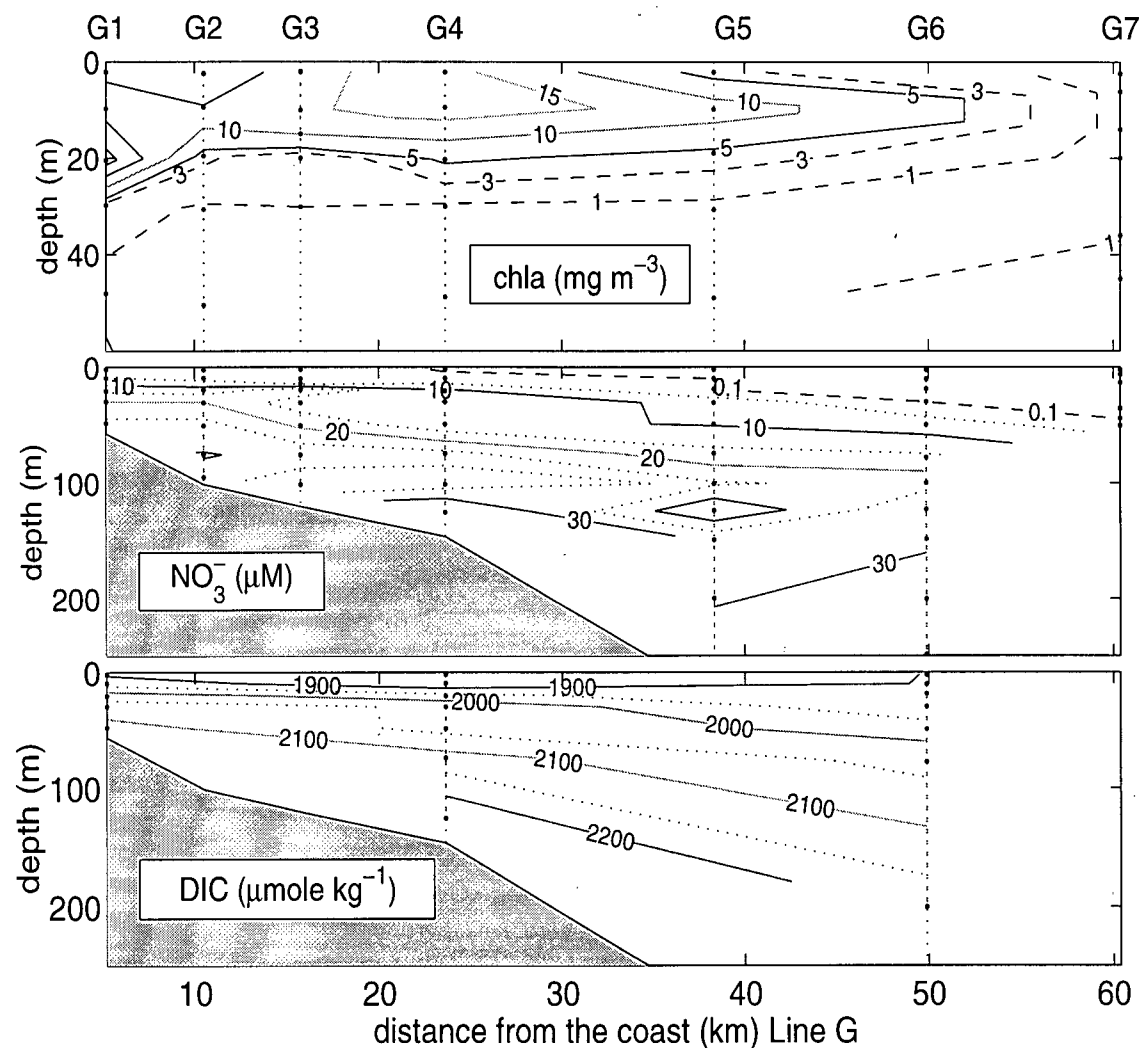


Figure 2.10: Contours of chl<sub>a</sub>,  $\text{NO}_3^-$  and DIC along line G (b). Note that the depth range is only 50 m for chl<sub>a</sub> (where data were gathered) compared to 250 m for  $\text{NO}_3^-$  and DIC. Grey shading marks the bottom topography. Occasional sharp changes in contours reflect the data (which have not been smoothed) as discussed in the text.

upper panel) extending from C2 to C7. (My T, S (Figure 2.4) and  $p\text{CO}_2$  (Table 2.1) data show the VICC at the time of sampling.) The VICC is not expected to extend as far seaward as C7, although it has been previously observed to do so (Hickey et al., 1991). In addition to high  $\text{chl}a$ , the VICC has high  $\text{NO}_3^-$  and high DIC (Figure 2.9, middle and lower panel, respectively). Seaward of the VICC (C8 – C11) summer downwelling conditions showed low concentrations of  $\text{chl}a$  at all depths and low  $\text{NO}_3^-$  above 100 m. DIC concentrations were moderate and depressed in the surface just beyond the VICC at C8 and C9. The most notable feature in the summer downwelling region was the low concentrations of inorganic nutrients (DIC and  $\text{NO}_3^-$ ) below the euphotic zone due to the deepening of the nutricline.

Transect G showed a strong response to upwelling in  $\text{chl}a$  (with values roughly twice as high as in the VICC) centered on G4 and extending seaward over the slope almost to G7 (Figure 2.10, upper panel). Surface (15 – 20 m over the shelf, 40 – 50 m over the slope) values of  $\text{NO}_3^-$  were very low (Figure 2.10, middle panel). Below 50 – 100 m, however,  $\text{NO}_3^-$  concentrations were very high. Here the contrast between upwelling (line G) and downwelling (C8 – C11) is evident as the 20  $\mu\text{M}$  contour was above 50 – 80 m after upwelling and between 150 – 250 m after downwelling. Contours were also smoother and more horizontal after upwelling. Biological drawdown of DIC after upwelling (and the absence of the VICC) caused much lower surface values (a depression of  $> 150 \mu\text{mol kg}^{-1}$  relative to line C) coincident with the high  $\text{chl}a$  patch (Figure 2.10, lower panel). DIC increased rapidly below the surface, however, and like  $\text{NO}_3^-$ , DIC contours occurred at shallower depths after upwelling than after downwelling.

DIC data were plotted against  $\text{NO}_3^-$  (Figure 2.11) to estimate C:N ratios of biological uptake and remineralization in my data. All data were normalized by salinity to account for effects of freshwater runoff, precipitation and evaporation. I chose to normalize to a salinity of 32, the average value for surface samples in which  $\text{NO}_3^-$  was undetectable. To

remove advective effects, data from each line were plotted separately. Because transects were sampled on different days and during different physical states, these effects were large. (Data are widely scattered when surface data are plotted together.)

The slope ( $\Delta\text{DIC}:\Delta\text{NO}_3$ ) represents a combination of biological uptake and remineralization of organic matter. The effects of air-sea  $\text{CO}_2$  gas exchange on the slope are expected to be small but would serve to decrease the measured  $\Delta\text{DIC}:\Delta\text{NO}_3$ . By dividing the data into surface (right column) and sub-surface (left column) plots I hope to separate biological uptake and remineralization, respectively. The theoretical Redfield C:N ratio (6.6) for these processes is included in each plot (dashed line) for comparison with my data. I do not have sufficient surface samples to make statistical regressions on my data.

On lines A, C and D (Figure 2.11 upper, second and third panel, left column) during downwelling and relaxation periods, biological uptake appears to exceed the Redfield ratio. The largest measured  $\Delta\text{DIC}:\Delta\text{NO}_3$  occurs during downwelling (Lines A and C) when surface  $\text{NO}_3^-$  was likely limiting (and for a longer period). After upwelling (Line G, Figure 2.11 lower panel) when a large quantity of  $\text{NO}_3^-$  has been recently supplied,  $\Delta\text{DIC}:\Delta\text{NO}_3$  is very close to the Redfield ratio. I could have also plotted lines with slopes of the measured POC:PON ratio (rather than the Redfield ratio) on transects C and G. However, the measured ratios are lower than 6.6, so this would only serve to decrease the slope making the excess carbon uptake larger. Others (Sambrotto et al, 1993; Codispoti et al., 1986) have observed excess uptake of DIC relative to  $\text{NO}_3^-$ . Evidently carbon is still processed by phytoplankton in the absence of nitrogen in response to light, although it is not incorporated into the particulate organic matter as the surface POC:PON ratio remains constant (Table 2.2) (although below the euphotic zone (at a depth of 200 m) the POC:PON ratio in sedimenting flux has been observed to be higher at times (ranging from 6 – 10) in the study area (Peña et al., 1999)). Measured DOC:DON ratios in the

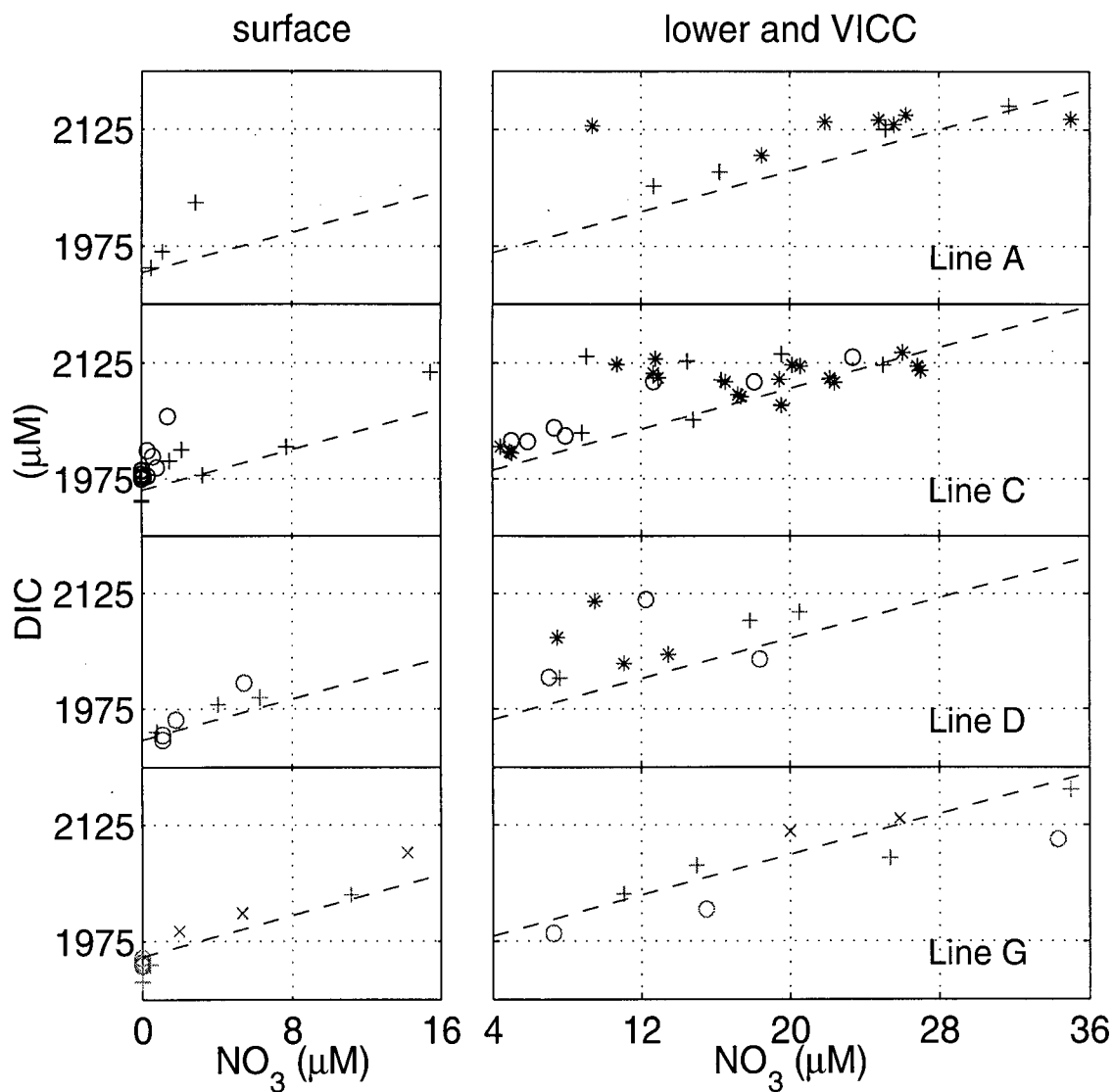


Figure 2.11: DIC ( $\mu\text{M}$ ) is plotted against  $\text{NO}_3^-$  ( $\mu\text{M}$ ) for surface values (left column) and sub-surface values (right column) to compare  $\Delta\text{DIC}:\Delta\text{DIN}$  for stations on transects A, C, D and G, respectively. All values are normalized to a salinity of 32. All values (surface and sub-surface) within the VICC (\*) are included with the sub-surface data. Outer shelf stations (+), inner shelf stations that are not part of the VICC (x) and slope-offshore stations (o) are separated into surface and sub-surface stations based on mixed layer depths ( $< 20$  m over the shelf and  $< 30$  m for the outer stations). The theoretical Redfield slope (C:N = 6.6) (- - dashed line) is plotted for each transect with different DIC intercepts (1940, 1960, 1935 and 1955  $\mu\text{M}$  for lines A, C, D and G, respectively) to correspond with the data.

slope region of my study area (C. S. Wong pers. com.) and in the Oregon upwelling region (Hill, 1999) are much higher ( $> 10$ ) than the Redfield ratio. A possible fate of excess carbon uptake is production of DOC.

Nutrients other than  $\text{NO}_3^-$  may be limiting in upwelling regions (e.g. silicic acid (Dugdale et al., 1995), iron (Hutchins and Bruland, 1998)). However, during my study  $\text{NO}_3^-$  was depleted before both phosphate and silicic acid and these nutrients were all highly correlated (Harris, 2000). Iron was not measured, although it is unlikely that it was limiting in my study area, close to a coastal region where terrigenous runoff is very high.

Measured  $\Delta\text{DIC}:\Delta\text{NO}_3$  below the surface mixed layer over the outer shelf and slope (Figure 2.11 right side) are close to the Redfield ratio (again shown as a dashed line), suggesting that remineralization of organic matter occurs in accordance to this ratio. However, the VICC samples (marked by an \*) appear to have lower  $\Delta\text{DIC}:\Delta\text{NO}_3$  (note that these data include surface values), perhaps because its source waters were not influenced by recent remineralization of organic matter and/or remineralization is not occurring in accordance to the Redfield ratio.

### 2.3.5 DIC and $\text{NO}_3^-$ budgets

Inorganic carbon and nitrogen budgets for the VICC (C4), after downwelling (C9) and after upwelling on the outer shelf (G4) and slope (G6) show the importance of each term in Equation 2.2 (Table 2.3). Physical transport and biological source and sink terms were estimated from data (see Section 2.2.2) and the rate of change was calculated from their sum. Uncertainties in this estimation are large and come from four different sources: measurement error (how well a quantity is estimated from a water sample), representativeness or patchiness (how well that water sample represents the homogenized physical box), neglected processes (such as along-shore advection) and unknown parameters or

quantities ( $r_d$ ,  $M$  and DOM). Uncertainties are estimated based on the largest source of error for each flux. All measurement errors are negligible compared with the other sources of error. The largest uncertainty in horizontal advection, biological uptake and gas flux comes from 'representativeness or patchiness', estimated from variations in measurements within the respective transects (C and G). Uncertainties in biological nitrogen uptake are large because it is estimated from carbon uptake using Redfield ratios, which are likely not followed (we estimate uncertainty as  $\pm 100\%$  (S. Harris, pers. com.)). In the vertical flux term uncertainty in the value of  $M$  (we estimate  $\pm 50\%$ ) is much greater than other quantities in this term (e.g. the uncertainty in average upper layer DIC is  $\sim 5\%$ ). The remineralization term is not based on measurements in my area (see Section 2.2.2) and subject to large uncertainties (I assume  $\pm 50\%$ ). However, its magnitude is small relative to the other terms and so its uncertainty only affects the slope budgets.

After downwelling (C9), the system is near steady state with respect to both DIC and  $\text{NO}_3^-$ . Over the slope after upwelling (G6),  $\text{NO}_3^-$  fluxes are close to steady state (Table 2.3b) but there is still a significant net advective flux of DIC (Table 2.3a) because of horizontal gradients. The DIC budgets from both shelf stations are dominated by the advective term due to very strong horizontal gradients. The VICC (C4) experiences a large net loss of DIC because concentrations there are much larger than they are in surrounding waters. This loss is likely compensated for by along-shore supply of DIC from the Juan de Fuca Strait (A1), not included in this analysis. In contrast, there is large net advective import of DIC on the outer shelf after upwelling (G4) due to intense biological drawdown of DIC. Advective fluxes of nitrogen are important to the daily budgets over the outer shelf but they are of the same order as or less than other terms. Horizontal  $\text{NO}_3^-$  gradients are not as large. (At C4 there is a small advective import of  $\text{NO}_3^-$ , rather than export that would be expected, because of non-homogeneities in  $\text{NO}_3^-$  within the VICC.)

Table 2.3: Terms in the daily DIC (a) and  $\text{NO}_3^-$  (b) budgets for the upper mixed layer in the Vancouver Island Coastal Current (C4), after downwelling (C9) and after upwelling on the outer shelf (G4) and slope (G6) July 1998. All units are  $\mu\text{M d}^{-1}$ . Biological uptake of  $\text{NO}_3^-$  was estimated from carbon uptake measurements assuming a C:N uptake of 6.6.

	C4	C9	G4	G6
advection	$-11 \pm 5$	$-1.0 \pm 0.2$	$20 \pm 10$	$-3 \pm 1$
biological uptake	$-8 \pm 2$	$-1.2 \pm 0.6$	$-7 \pm 3^1$	$-1.4 \pm 0.6^1$
vertical flux	$4 \pm 2$	$1.2 \pm 0.6$	$5 \pm 3$	$1.0 \pm 0.5$
gas flux	$-0.05 \pm 0.03$	$0.003 \pm 0.001$	$0.3 \pm 0.1$	$0.04 \pm 0.01$
remineralization	$0.3 \pm 0.2$	$0.3 \pm 0.2$	$0.3 \pm 0.2$	$0.3 \pm 0.2$
$\frac{d\text{DIC}}{dt}$	$-15 \pm 6$	$-1 \pm 1$	$20 \pm 10$	$-3 \pm 1$

Table 2.3a

	C4	C9	G4	G6
advection	$1.3 \pm 0.5$	$0.04 \pm 0.01$	$0.7 \pm 0.2$	$0.0 \pm 0.1$
biological uptake	$-1 \pm 1$	$-0.2 \pm 0.2$	$-1 \pm 1$	$-0.2 \pm 0.2$
vertical flux	$0.2 \pm 0.1$	$0.04 \pm 0.02$	$0.5 \pm 0.3$	$0.10 \pm 0.05$
remineralization	$0.05 \pm 0.03$	$0.05 \pm 0.03$	$0.05 \pm 0.03$	$0.05 \pm 0.03$
$\frac{d\text{NO}_3^-}{dt}$	$1 \pm 1$	$-0.1 \pm 0.2$	$0 \pm 1$	$-0.1 \pm 0.2$

Table 2.3b

[1] Biological uptake at G4 and G6 were assumed to be the same as at G3 and G7, respectively.

The biological uptake of carbon is closely balanced by the vertical flux at all stations except C4 where alongshore DIC import from the Juan de Fuca Strait is expected. Estimates of biological nitrogen uptake (using the Redfield C:N ratio) were larger than vertical fluxes at all stations, and an order of magnitude larger at C4 and C9. As seen in Figure 2.11, the uptake of  $\text{NO}_3^-$  is less than that predicted by the Redfield ratio on the C line so it is likely that the nitrogen uptakes estimated in the budget are too high. After upwelling (G4, G6), however, when there was no evidence of excess biological carbon uptake (Figure 2.11), nitrogen uptake was of the same order as the estimated vertical flux (Table 2.3).

In the daily budgets  $\text{CO}_2$  gas flux is insignificant, though it is large after upwelling at G4 and is likely underestimated in the VICC as the only  $p\text{CO}_2$  estimate available at C4 was from 10 m and was much lower than neighbouring surface values (Table 2.3). Estimated remineralization fluxes of both carbon and nitrogen are also small, but significant at the slope stations where  $pp$  was much lower and the system was closer to steady state.

## 2.4 Conclusions

The VICC is known to have a strong influence on  $pp$  over the shelf off southern Vancouver Island (Mackas et al., 1980; Crawford and Dewey, 1989). I show that the VICC has an equally strong influence on the inorganic carbon system. In this area, surface DIC is very high, causing  $p\text{CO}_2$  to exceed 1000 ppm. Gas evasion from the VICC could easily balance or exceed invasion over the outer shelf where biological drawdown is episodically high during the summer due to  $pp$  associated with upwelling events. It has been predicted that this biological drawdown of DIC could cause a large net invasion of  $\text{CO}_2$  in coastal upwelling regions (Friederich et al., 1994). Although these periods of high  $\text{CO}_2$  invasion

occur, the  $p\text{CO}_2$  of subsurface water over the shelf is very high and when it is mixed into the surface at times of the year when  $pp$  is light limited, substantial gas evasion is likely and may balance summer invasion (Section 3.4.2).

The high subsurface  $p\text{CO}_2$  over the shelf is due to high DIC concentrations. These high concentrations are a result of exceptionally high  $pp$ , and particulate flux from surface waters, which is rapidly remineralized over the shelf in a small volume of water relative to the open ocean, thereby concentrating the remineralized DIC.

The C:N ratio of biological uptake appears to be higher during the period of summer downwelling when nitrogen was limiting (exceeding the Redfield ratio), but close to the Redfield ratio following an upwelling event. Despite the excess carbon uptake at times, the POC:PON ratio remained relatively constant. This excess carbon is probably excreted as DOC, as it is not incorporated into the phytoplankton.

The C:chl $a$  ratio varied widely and was lowest after upwelling when new nitrogen had been supplied. C:chl $a$  increased where nitrogen was limiting likely due to some combination of mortality of phytoplankton and a decrease in cellular chl $a$  in viable cells.

The daily DIC budget was dominated by cross-shore advection over the shelf where  $pp$  was high producing strong horizontal gradients in DIC. Horizontal gradients in  $\text{NO}_3^-$  were much smaller and so  $pp$  and vertical mixing terms were usually of the same order.

In the following chapter I present the model that I developed for this system. Annual cycles (not just summer) are modelled. In Chapter 4 these data are compared to model results.

## Chapter 3

### Model Development and Major Results

#### 3.1 Introduction

It is becoming an accepted fact that the large anthropogenic increase in atmospheric CO<sub>2</sub> is influencing our climate (Crowley, 2000) and so great importance is being placed on understanding the global carbon system. The ocean holds the largest active carbon reservoir on Earth (Siegenthaler and Sarmiento, 1993) and ultimately sets the atmospheric CO<sub>2</sub> concentration (Najjar, 1992). Accurate and well-tested oceanic carbon models are required to interpolate sparse data and to predict future CO<sub>2</sub> levels.

Simple ocean box models have demonstrated the importance of biology in setting the carbon capacity of the ocean by drawing down the surface partial pressure of CO<sub>2</sub> ( $p\text{CO}_2$ ) and transporting organic carbon into the deep ocean via sedimenting organic detritus, where remineralization occurs (Sarmiento, 1992). This process has been termed the biological pump (Volk and Hoffert, 1985). A disproportionate amount of carbon is fixed and vertically exported in coastal waters, particularly in upwelling regions (Eppley and Peterson, 1979; Harrison et al., 1987). Therefore it is expected that coastal upwelling regions form an important part of the biological pump.

Despite the global importance of coastal regions they are seldom included in current global numerical ocean models because resolution is not high enough to deal with the smaller spatial scales and inherent non-homogeneity. It is one of the major weaknesses of these models (Doney, 1999). Bulk ocean models and budgets have been used to consider

coastal processes in a global context. For example, (Christensen, 1994) suggested, using a box model, that over large time scales (1000s of years) coastal denitrification has an important effect on atmospheric  $p\text{CO}_2$ , and that organic carbon export to the deep sea does not. Another modelling study indicated that net heterotrophy over continental margins has influenced the global carbon budget over the last 100s of years (Mackenzie et al., 1998). Also, it has been shown that the effect of terrestrial inputs (particularly anthropogenic) on coastal eutrophication can impact the annual global carbon budget (Smith and Hollibaugh, 1993). Tsunagai et al. (1999) suggest that continental shelf areas absorb atmospheric  $\text{CO}_2$  and transport it into the subsurface layers of the open ocean based on carbon data from the East China Sea.

Coastal upwelling brings intermediate depth (100 – 250 m), nutrient-rich waters to the surface, fueling high primary production (Smith, 1994). These waters also have higher inorganic carbon concentrations and so could be a source of  $\text{CO}_2$  to the atmosphere (Christensen, 1994). However, the few inorganic carbon data which have been reported from coastal upwelling regions show strong biological drawdown of  $p\text{CO}_2$  (as at station G4, Table 2.1) and suggest that such regions may be net sinks for atmospheric  $\text{CO}_2$  (Friederich et al., 1994; Simpson, 1986; Simpson and Zirino, 1980). These studies did not investigate the winter season.

There are detailed physical models of coastal upwelling (e.g. Allen et al., 1995; Fed-eriuk and Allen, 1995), and for downwelling (Allen and Newberger, 1996), however they apply to short time scales. Current computer speed does not allow such detailed models to be run for full year simulations. Two-dimensional physical models of an upwelling event have been coupled with nitrogen based biological models (Wroblewski, 1977; Batchelder et al., 2000). Again, biological cycles were not modelled over the winter season and over longer time scales. There are no previous models specific to coastal upwelling regions which include a carbon cycle.

We have developed a simple model of a coastal upwelling region which incorporates a biological and a carbon cycle over all seasons. The system that I am modelling is complex and non-homogeneous. Furthermore, few measurements exist of many relevant quantities. Thus, my primary objective was to develop a model which produced sensible results and then to identify the parameters that strongly influence the system and need to be measured. I provide estimates of net annual primary production ( $pp$ ),  $\text{CO}_2$  gas exchange and carbon and nitrogen mass exchange between the model system and the open ocean.

### 3.2 Model

Our goal is to model the system as simply as possible and obtain reasonable seasonal cycles compared with available data. I only include those processes occurring on time scales of days (weeks) to years that are necessary to determine net carbon fluxes. Horizontally the model distinguishes between the shelf, slope and offshore regions and there are two levels in the vertical (Figure 3.1). The upper layer is the mixed layer where primary production occurs while in the lower layer only remineralization occurs. The system has 42 ordinary differential equations, which are solved by a standard Runge-Kutta method (Press et al., 1992) using an adaptive stepper with a time step of 0.1 d or less.

I first define the modelled quantities (state variables). I model salinity ( $S$ ) and two currencies (carbon and nitrogen) for each state variable. Model structure is separated into physical and biological components, whereas the chemical portion (gas flux calculation) is described last.

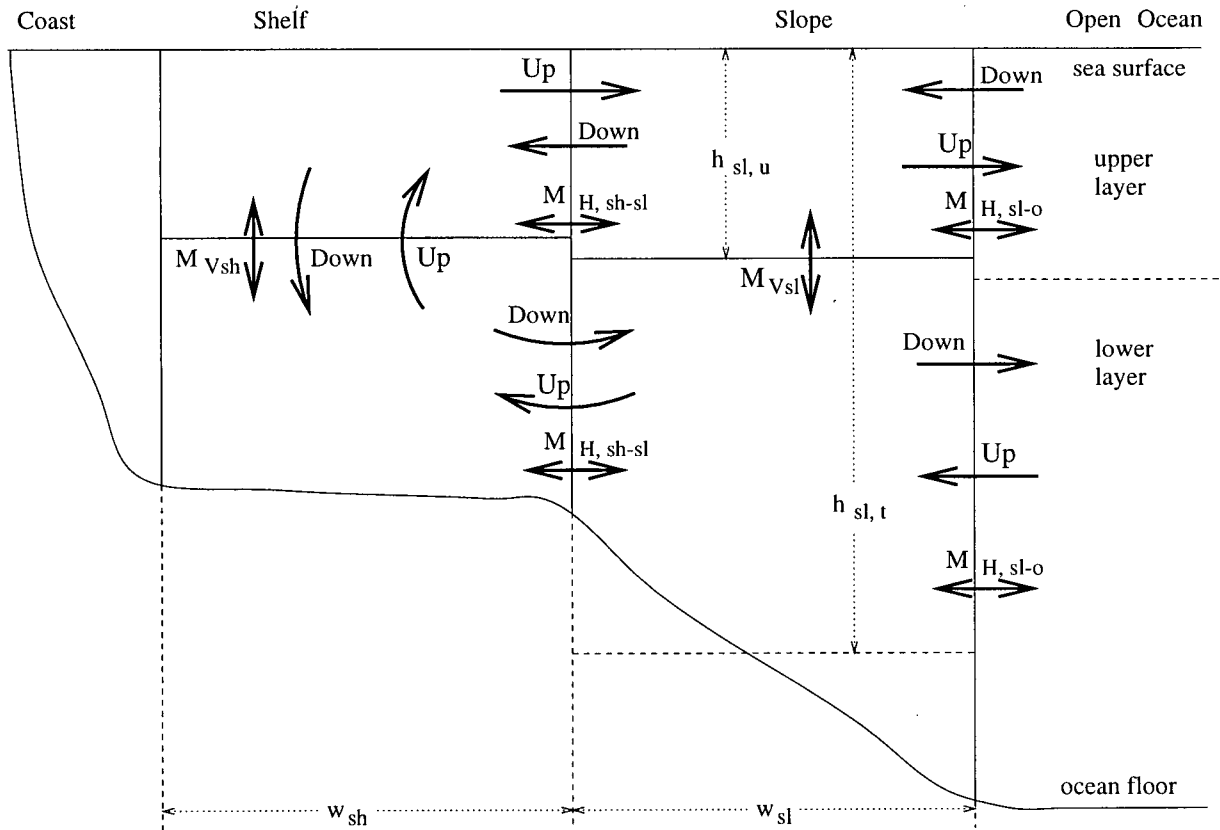


Figure 3.1: Vertical cross-section through a coastal upwelling system showing the geometry of the model. Illustrated are the physical processes. Physical advection between shelf, slope and open ocean with **Up** representing upwelling flux ( $\mathbf{Up} = A \cdot w_{sh}$ ) and **Down** downwelling flux ( $\mathbf{Down} = D \cdot w_{sh}$ ) where  $w_{sh}$  is the width of the shelf box. The vertical mixing fluxes are:  $\mathbf{M}_{Vsh} = M_V \cdot w_{sh}$  and  $\mathbf{M}_{Vsl} = M_V \cdot w_{sl}$  where  $w_{sl}$  is the width of the slope box. The changes in mixed layer depth between horizontal regions approximate sloping isopycnals. The horizontal mixing fluxes are:  $\mathbf{M}_{H,sh-sl} = M_H \cdot h_{sh,u}$  and  $\mathbf{M}_{H,sl-oc} = M_H \cdot h_{sl,u}$  in the upper layer and  $\mathbf{M}_{H,sh-sl} = M_H \cdot (h_t - h - u)_{sh}$  and  $\mathbf{M}_{H,sl-oc} = M_H \cdot (h_t - h - u)_{sl}$  in the lower layer where  $M_H$  is the horizontal mixing coefficient.

### 3.2.1 Currencies

Carbon and nitrogen are the two currencies that are used in the model. Carbon is the currency of particular interest and nitrogen is modelled as the biologically limiting nutrient (Hutchings et al., 1994). While it is possible that other macronutrients might be limiting at times (e.g. silicic acid (Dugdale et al., 1995)) they occur in such similar ratios (with nitrogen) to the biological demands that choosing one will not greatly affect my model. Micronutrients such as iron are rarely limiting close to the coast (although iron limitation has been observed in coastal California (Hutchins and Bruland, 1998)). Each currency has its own set of parameters. Carbon is exchanged at the air-sea interface whereas nitrogen is not. The dissolved inorganic nitrogen (DIN) pool does not include  $N_2$ , or processes involving  $N_2$  such as nitrogen fixation and denitrification. Calcium carbonate formation is not modelled.

### 3.2.2 State Variables

Three state variables are modelled for each currency (Table 3.1): dissolved organic (DO), particulate organic (PO) and dissolved inorganic (DI). What is important in the model is whether organic matter sinks or does not. Thus the model definition of the DO pool is organic matter which is non-living and non-sinking while the non-living PO pool sinks and so is found only in the lower layer. The living PO pool can control its buoyancy and does not sink so it stays in the upper layer. Because of the time scales of interest, only the semi-labile portion of the total DO (which includes about 30% of the operationally defined DO (Carlson and Ducklow, 1995; Carlson et al., 1994)) is modelled. This pool has remineralization time scales of months to years. Labile pools are difficult to estimate and measure and can have faster remineralization rates than the model time scales (*ibid.*). Fluxes associated with the refractory pool are negligible despite its large size (about 70%

of the measurable DO matter) because of its long lifetime (order 1000 yr). The difference between PO and DO matter is traditionally defined by standard filter size ( $0.45 \mu\text{m}$ ), which will make my DO pool larger than the reported semi-labile fraction, while my total organic TO pools should be comparable after the refractory portion is subtracted. The DI pools include all forms of inorganic materials which are biologically accessible. The DIN pool is made up of nitrate, ammonium and nitrite, and the dissolved inorganic carbon (DIC) pool of bicarbonate, carbonate and carbon dioxide.

Table 3.1: State variables for each currency (units  $\mu\text{M}$ ).

DIC	dissolved inorganic carbon	DIN	dissolved inorganic nitrogen
DOC	dissolved organic carbon	DON	dissolved organic nitrogen
POC	particulate organic carbon	PON	particulate organic nitrogen

Salinity is modelled as a state variable as a physical check on the model and also to determine several quantities (including alkalinity) in the carbonate system necessary to calculate  $p\text{CO}_2$ .

### 3.2.3 Physical Circulation

The model consists of 6 boxes, a surface box and a lower box for each horizontal region: shelf, slope and open ocean (Figure 3.1). Physical parameters and geometry are presented in Table 3.2. All state variables are subject to the circulation with the exception of PO matter which is advected (both vertically and horizontally) and mixed horizontally but is not vertically mixed or entrained because of partitioning between viable (non-sinking, upper layer) and non-viable (sinking, lower layer) fractions.

Table 3.2: Physical parameters and geometry with values used in the model runs. Values in parenthesis were calculated from time dependent functions within the model. Ranges show seasonal variation.

$\bar{A}$ -	average upwelling velocity	0.785	m d <sup>-1</sup>
$t_u$	upwelling season length	145	d
$C$ -	flux per length along coast from VICC	(0.009 - 0.082)	m d <sup>-1</sup>
$\bar{D}$ -	average downwelling velocity: typical, ENSO	0.7, 2.8	m d <sup>-1</sup>
$t_d$	downwelling season length	65	d
$M_H$ -	horizontal mixing	20	m d <sup>-1</sup>
$M_V$ -	vertical mixing	0.2	m d <sup>-1</sup>
$P$ -	precipitation	(0.002 - 0.013)	m d <sup>-1</sup>
$R$ -	flux per length along coast from terrigenous runoff	(0.003 - 0.024)	m d <sup>-1</sup>
$d_m$ -	depth of mixing below $h_u$	2	m
$e_l$ -	entrainment to the lower layer	(- 0.007 - 0)	d <sup>-1</sup>
$e_u$ -	entrainment to the upper layer	(0 - 0.055)	d <sup>-1</sup>
$h_{pp}$ -	permanent pycnocline: shelf, slope	73, 43	m
$h_t$ -	total depth: shelf, slope	120, 400	m
$h_u$ -	depth of upper layer: shelf	(10 - 40)	m
	depth of upper layer: slope	(15 - 70)	m
$w_{sh}$ -	shelf width	20	km
$w_{sl}$ -	slope width	10	km

## Advection

Upwelling circulation (flux **Up**, vertical velocity  $A$ : Figure 3.1) is based on current meter data analyzed by Lentz (1992) from four coastal upwelling regions. From these data, he shows that all upwelling occurs inside the shelf break. In the model, intermediate depth water advects from the outer ocean through the lower layers of the slope and shelf and then into the surface over the shelf. Our shelf box does not include that part of the inner-shelf which is landward of the upwelling center. When there are important inputs from the inner shelf, these are modelled as a mixing process (see section on buoyancy fluxes). The model equivalent of the upwelling front is the offshore edge of the slope box. The extent of advection between the coast and open ocean through the front is unknown (Smith, 1994; Mackas and Yelland, 1999). In my model the full upwelled volume is advected through the front, recognizing that this represents a maximum export flux from the system to the open ocean and that a portion of it may be advected in the along-shore current.

Downwelling circulation is shown by the flux **Down** (vertical velocity  $D$ ) in Figure 3.1. Although downwelling is actually a depression of the pycnocline at the coast, salinities are reproduced reasonably well when representing it by advection. Offshore surface water is advected onshore to the shelf where it sinks into the lower layer and flows offshore in the deep boxes. The open ocean is considered an infinite source and sink with respect to the shelf and slope system.

Along-shore advection is not modelled, although along-shore velocities are strong in coastal upwelling systems (Smith, 1994). We assume that the along-shore gradients in state variables are small and thus along-shore advection does not affect the model. This assumption may be incorrect at times; however, it provides us with a starting point for this modelling exercise.

### Entrainment and mixing

The upper layer depth ( $h_u$ ) is the mixed layer depth which varies seasonally. When  $h_u$  changes with time ( $t$ ) entrainment ( $e$ ) occurs into the layer which becomes thicker. It is unrealistic to entrain or mix averaged lower layer concentrations into the upper layer because density profiles do not conform to a perfect two layer structure, particularly in late summer and early fall. Instead there is some gradient structure between the bottom of the mixed layer and the nearly homogeneous lower layer. We approximated this structure by modelling a permanent pycnocline ( $h_{pp}$ ) (different for each horizontal region and fixed in time) with a linear density gradient from it to the bottom of the upper box (Figure 3.2) ensuring that  $h_u < h_{pp}$ . The upper box and the region below the pycnocline have uniform concentrations. Thus entrainment rates are:

$$e_u = MAX \left( \frac{dh_u}{dt} \cdot (h_{pp} + h_u)^{-1} , 0 \right) \quad (3.1a)$$

$$e_l = MIN \left( \frac{dh_u}{dt} \cdot (2h_t - h_{pp} - h_u)^{-1} , 0 \right) \quad (3.1b)$$

for the upper and lower layer, respectively, where  $h_t$  is the total depth of the water column. Likewise the vertical mixing coefficient ( $M_V$ ) is scaled by  $d_m (h_{pp} - h_u)^{-1}$  for ( $h_u \leq (h_{pp} - d_m)$ ) so that mixing occurs between the upper layer and the fluid centered at a depth of  $d_m$  below the interface.

The ordinary differential equations for the state variable salinity demonstrate the model simulation of the physical circulation (Appendix B).

#### 3.2.4 Biological Model

The biological model is a two layer system. State variables are related to one another by biological fluxes (Figure 3.3). In addition, dissolved state variables (DI, DO,  $S$ ) are exchanged between levels by mixing and entrainment (Figure 3.3) as well as by

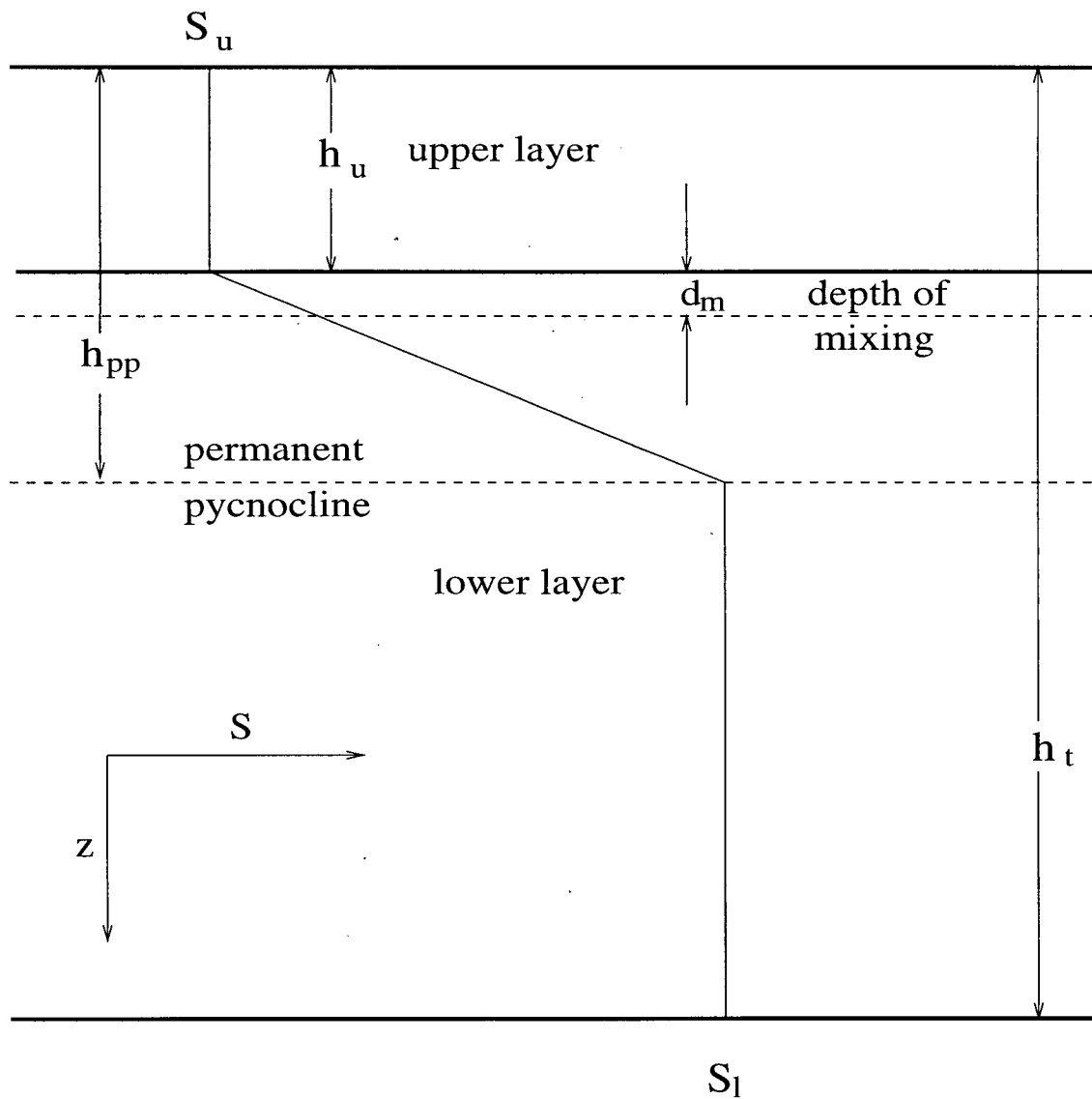


Figure 3.2: The vertical structure of model concentrations using salinity ( $S$ ) as an example. The linear gradient between the upper layer and the permanent pycnocline allows for more realistic vertical entrainment and mixing between layers.

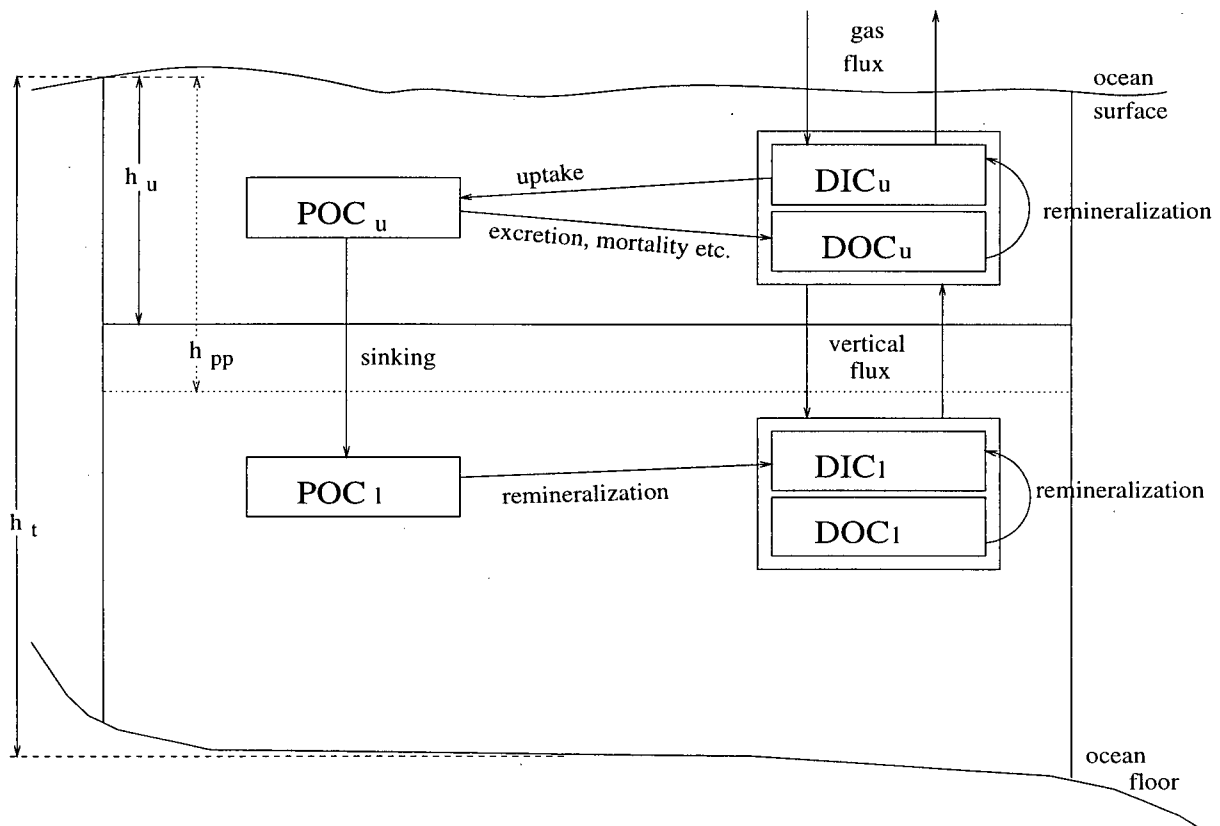


Figure 3.3: The biological model with fluxes shown for the two layer system using carbon as a currency.

advection (Figure 3.1). PO matter can only sink into the lower layer (or be advected between vertical levels). This system was embedded into each of the horizontal shelf and slope regions in the physical circulation model described above. (Note that all state variables, dissolved and particulate are subject to horizontal advection.) Biological source-sink processes were not modelled in the open ocean system. Open ocean state variable concentrations were specified using data (described below).

Using carbon as a currency, the general ordinary differential equations for the upper layer are

$$\frac{dDIC_u}{dt} = -pp - pc + r_d DOC_u + \frac{G}{h_u} + V + X + H \quad (3.2a)$$

$$\frac{d\text{POC}_u}{dt} = pp - s \text{POC}_u \cdot \text{loss} + X + H \quad (3.2b)$$

$$\frac{d\text{DOC}_u}{dt} = (1 - p) s \text{POC}_u \cdot \text{loss} + pc - r_d \text{DOC}_u + V + X + H \quad (3.2c)$$

where  $pp$  is primary production,  $r_d$  is the DOC remineralization rate,  $G$  is the gas flux and  $pc$  is excess carbon uptake (described below). Physical terms are represented by  $V$  (vertical mixing and entrainment),  $X$  (advection) and  $H$  (horizontal mixing). In (3.2b) the second term on the left hand side is the decay of the upper (living) POC pool where  $s$  is the decay rate and  $\text{loss}$  is a dimensionless function dependent on growth conditions. The fraction of this decay flux that sinks into the lower layer as particulate flux is  $p$ . In the lower layer

$$\frac{d\text{DIC}_l}{dt} = r_d \text{DOC}_l + r_p \text{POC}_l + V + X + H \quad (3.2d)$$

$$\frac{d\text{POC}_l}{dt} = \frac{s \cdot p \cdot h_u \cdot \text{loss}}{h_t - h_u} \text{POC}_u - r_p \text{POC}_l + X + H \quad (3.2e)$$

$$\frac{d\text{DOC}_l}{dt} = -r_d \text{DOC}_l + V + X + H \quad (3.2f)$$

where  $r_p$  is the POC remineralization rate. Values of biological parameters are shown in Table 3.3. Fluxes are described below and illustrated in Figure 3.3. The equations are identical for nitrogen, except that there is no gas flux or excess uptake ( $pc$ ).

I model the living PO pool as temperate diatoms, which dominate primary production in coastal upwelling systems where there are large fluxes of nutrients into the euphotic zone (Hutchings et al., 1994). Diatoms have high growth rates and their populations often crash suddenly when nutrients become limiting. Sinking rates of single cells can be high (up to  $10 \text{ m d}^{-1}$  in rare cases) and an order of magnitude higher when cells coagulate and become marine snow (Smetacek, 1985; Alldredge and Silver, 1988). Values of the  $f$ -ratio (Dugdale and Goering, 1967) are high ( $> 0.5$ ) (Harrison et al., 1987).

Inorganic nutrients are taken up by the surface (living) PO pool which is the modelled primary production ( $pp$ ) via Michaelis-Menten kinetics. This uptake is limited by light

Table 3.3: Biological parameters and values used for model runs. Values in parenthesis are results of model calculations. Ranges show seasonal variation.

$I_0$	daily averaged $I_{PAR}$ at the surface	47 – 301	$W m^{-2}$
$I_{PAR}$	photosynthetically available radiation		$W m^{-2}$
$I_{SAT}$	light intensity at which $vm$ is reached	50	$W m^{-2}$
$K_n$	half saturation constant for nitrogen uptake	0.1	$\mu M$
$K_{sl}$	half sat. constant for PO decay due to light lim.	0.06	–
$K_{sn}$	half sat. constant for PO decay due to N lim.	0.1	$\mu M$
$\alpha$	slope of $vm$ vs. $I_{PAR}$ curve at $I_{PAR}=0$	(0.028 – 0.04)	$d^{-1}(W m^{-2})^{-1}$
$chl_r$	chlorophyll reduction factor	0.2	–
$k_p$	$I_{PAR}$ attenuation coefficient for PON	0.06	$m^{-1}(\mu M N)^{-1}$
$k_w$	$I_{PAR}$ attenuation coefficient for sea water	0.04	$m^{-1}$
$p$	particulate fraction of flux leaving $PO_u$ pool	0.6	–
$p_0$	active surface PO concentration (C or N)		$\mu M$
$pc$	excess carbon uptake		$\mu M C d^{-1}$
$pp$	primary production (C or N)		$\mu M d^{-1}$
$r_d$	dissolved organic matter decay rate: C, N	0.005, 0.0065	$d^{-1}$
$r_p$	particulate organic matter decay rate	0.2	$d^{-1}$
$s$	decay rate of surface PO pool	0.0385	$d^{-1}$
$vm$	maximum growth rate for phytoplankton	(1.4 – 2.0)	$d^{-1}$
$vm_0$	maximum growth rate for phytoplankton at 0 K	$5.696 \times 10^{-9}$	$d^{-1}$

and the nutrient nitrogen such that only one factor is limiting at any one time:

$$pp = vm \cdot p_0 \text{ MIN} \left( \overline{light}, \frac{\text{DIN}}{\text{DIN} + K_n} \right) \quad (3.3)$$

where  $p_0$  is the active portion of the living PO pool (C or N) defined below,  $vm$  is the maximum uptake rate,  $K_n$  is the half saturation constant for nitrogen and

$$light = 1 - \exp(-\alpha I_{PAR}(z)/vm) \quad (3.4)$$

(Denman and Pena, 1999) where  $\alpha$  is the growth rate per light intensity at low light levels. This function must be integrated with respect to  $z$  (the vertical coordinate) over the upper layer depth to obtain the average light level,  $\overline{light}$ . (There is no primary production below the model upper layer.) The photosynthetically available radiation  $I_{PAR}$  is

$$I_{PAR}(z) = I_0 \exp\{(k_w + k_p \text{ PON})z\} \quad (3.5)$$

(Fasham, 1995) where  $I_0$  is the daily averaged  $I_{PAR}$  at the surface,  $k_w$  is the extinction coefficient of light in water and  $k_p$  is attenuation coefficient for PON. Annual model production is equivalent to annual net production.

During winter, modelled  $pp$  was higher than expected even though integrated light levels were realistic. Since many diatoms go into non-sinking resting stages when growth conditions are not favorable (Garrison, 1984) we chose to make part of the surface PO pool dormant during the winter months. Thus the active fraction of the PO (C or N) is

$$p_0 = \text{PO}(1 - \exp(-0.1 \text{ W}^{-1}\text{m}^2(I_0(\text{noon}) - 43 \text{ Wm}^{-2}))) \quad (3.6)$$

where  $I_0(\text{noon})$  is  $I_{PAR}$  at mid-day.

### Excess carbon uptake

In the model, additional uptake of DIC ( $pc$ ) can occur when DIN is limiting but light is not

$$pc = chl_r(vm \cdot p_0 \cdot \overline{light} - pp) \quad (3.7)$$

where  $chl_r$  is a factor to account for the reduction of cellular chlorophyll  $a$  ( $chl_a$ ) relative to carbon. Variable uptake ratios of DIC:DIN that are greater than the Redfield ratio (Redfield et al., 1963) were observed in my data (Section 2.3.4) and have been observed by others (Sambrotto et al., 1993). In an attempt to model this excess uptake we assume that phytoplankton still respond to light and process carbon regardless of nutrient limitation (as shown in Figure 2.11), but with an increased C:chl $a$  ratio. In the absence of DIN, however, carbon is not incorporated into the cell. Live phytoplankton maintain a C:N ratio in a narrow range close to the Redfield ratio (confirmed by my data, Table 2.2), while C:chl $a$  (likewise N:chl $a$ ) ratios vary widely (Table 2.2) and are highest when nutrients are limiting but light is not (Sakshaug et al., 1989; Taylor et al., 1997). DOC:DON ratios are usually well above POC:PON (Redfield) ratios (Hill, 1999; C. S. Wong pers. com.). Thus we model the excess carbon uptake as passing directly into the DOC pool (3.2a, 3.2c).

Loss from the living (upper) PO pool is first order decay (3.2b). The decay rate  $s$  is scaled by a dimensionless loss function dependent on either nutrient or light limitation

$$loss = MAX \left( 9 - 8 \cdot \frac{DIN}{DIN + K_{sn}^2}, 6 - 5 \cdot \frac{\overline{light}^2}{\overline{light}^2 + K_{sl}^2} \right) \quad (3.8)$$

where  $K_{sn}$  is the half saturation constant for PO decay due to nitrogen limitation and  $K_{sl}$  is that for light limitation. The numerical coefficients were chosen so that model equivalent sinking rates ( $s \cdot loss \cdot p \cdot h_u$ ) are in the range of diatom single-cell sinking rates under nutrient and light limitation, respectively (Bienfang et al., 1982 and Bienfang et

al., 1983). The total decay flux is partitioned between the lower PO and upper DO pools (3.2f, 3.2c), so that the fraction  $p$  goes into the lower PO pool. In a one-dimensional system in steady state,  $p$  is a first order approximation of the  $f$ -ratio, as all particulate flux sinks immediately to the lower box while the dissolved portion stays in the surface. Transfers between trophic levels are not modelled. Non-living organic matter (DO and lower PO pools) remineralizes (3.2c, 3.2e, 3.2f) to DI pools (3.2a, 3.2d) via first order exponential decay at their respective decay rates ( $r_d$ ,  $r_p$ ) which are different for each currency.

### 3.2.5 Gas Flux

The surface partial pressure of CO<sub>2</sub> ( $p\text{CO}_{2w}$ ) was calculated from modelled DIC and alkalinity (TA) using the relationships of Skirrow (1975), prescribed sea surface temperatures and modelled  $S$ . The sea surface salinities are fresher than the averaged box value so they were extrapolated by subtracting  $\Delta S$  from  $S_u$ . Model DIC was diluted by the same amount to determine surface DIC. A linear relation between measured TA and salinity in the study area (Figure 2.8) was used to estimate TA. The single negative charge associated with modelled DIN (assuming that the bulk of the DIN is nitrate) was then subtracted to estimate carbonate TA.<sup>1</sup> Annual variability of atmospheric  $p\text{CO}_{2a}$  was prescribed (Manning, 1993). Gas flux ( $G$ ) is

$$G = sol \cdot k (p\text{CO}_{2a} - p\text{CO}_{2w}) \quad (3.9)$$

where  $sol$  is the solubility of CO<sub>2</sub> and  $k$  is the piston velocity. (Note, this equation is identical to Equation 2.1, repeated here for the reader's convenience.) The relationship of Wanninkhof (1992) for  $k$  based on long term averaged wind was used.

<sup>1</sup>The uptake of nitrate by phytoplankton is accompanied by an increase in TA.

### 3.3 Physical Forcing

The external physical forcing makes the model specific to a particular coastal upwelling region. We present results for the west coast of Vancouver Island, Canada. Up and downwelling circulation, light, mixed layer depth and buoyancy fluxes are all forced by external functions based on local data and are described below.

#### 3.3.1 Upwelling and Downwelling

In my study area upwelling is forced partially by local winds in the traditional way (Lentz, 1992), but also in response to the stronger upwelling centers further south (Oregon and California) via shelf waves (Freeland and Denman, 1982). For this reason upwelling and downwelling were based on local ocean current (rather than wind) data. The upwelling index of Thomson and Ware (1996) was used to specify the average timing of the seasons as well as the frequency and relative strength of up- and downwelling events. Average vertical velocities (Freeland and Denman, 1982; Freeland and McIntosh, 1989) set the average strength of up- and downwelling (Figure 3.4). A smoothed version of this forcing function with the same averaged velocities and seasonal timing was also used to compare the effects of smooth versus realistic forcing (Figure 3.4). Forcing during El Niño Southern-Oscillation (ENSO) years was based on Hsieh et al. (1995), who showed that during a typical ENSO year in my study area downwelling strength is enhanced while upwelling strength remains constant.

#### 3.3.2 Light, Wind, Temperature and Salinity

Sea surface measurements of  $I_{PAR}$  from Crawford and Whitney (*in prep.*) and Harris (2000) at latitudes of  $49^{\circ} - 50^{\circ}N$  were used to set the annual light cycle. The Pacific Northwest experiences thick cloud cover during a large part of the year so light availability

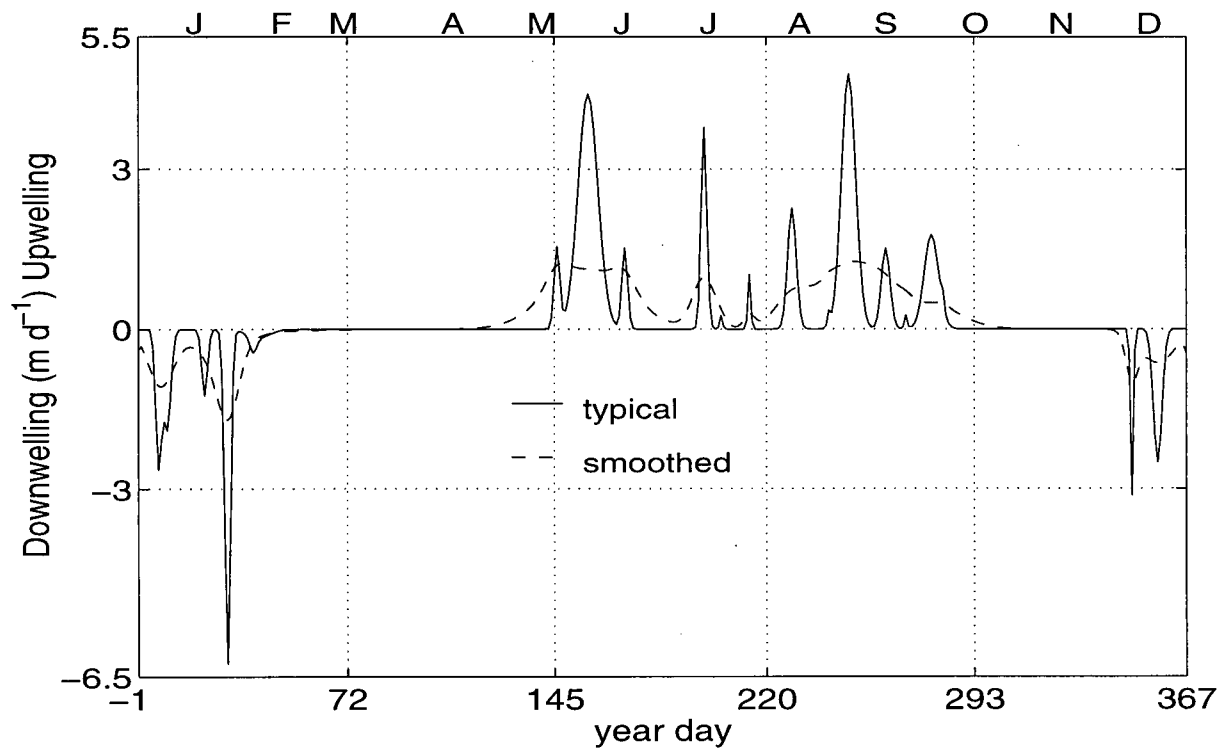


Figure 3.4: A typical year of realistic external forcing. Positive values are  $A$  during the upwelling season and negative values are  $D$  during the downwelling season. The hashed curve shows smoothed forcing for the same integrated flux as the typical year.

is often low. Wind data (Faucher et al., 1999) were averaged over the seasons to calculate the piston velocity. Long term averaged temperature data from *Inst. of Ocean Sci., Pat. Bay B.C.* at <http://www.ios.bc.ca/ios/osap/data/lighthouse/bcsop.htm> and R. Brown (I.O.S. pers. com.) were used to prescribe a typical seasonal cycle in temperature. The amount of surface freshening,  $\Delta S$ , relative to the average box value for shelf and slope was 0.2 and 0.03, respectively.

### 3.3.3 Buoyancy flux

Coastal fresh water additions are very important to my model as they dilute both DIC and alkalinity and so have a major impact on  $p\text{CO}_2$ . The west coast of Vancouver Island experiences about  $3 \text{ m}\cdot\text{yr}^{-1}$  of rain (BCDA, n.d.), most of which falls in the late fall and early winter. Buoyancy flux is added to the model via rainfall ( $P$ ) over both the shelf and slope and also as terrigenous run-off ( $R$ ) into the shelf box (Figure 3.5). The run-off has a low concentration of DIC (based on regressions from data in the study area (Figure 2.8), and since the area is relatively pristine, very low concentrations of organic matter are assumed. The annual cycle of run-off volume was scaled from Thomson et al. (1989) to account for mixing in the inner-shelf (Appendix C). The buoyancy fluxes are presented in Appendix C.

A buoyancy current, the Vancouver Island Coastal Current (VICC), flows northward year round over the inner-shelf (Freeland et al., 1984) and provides a large flux of DIN (Pawlowicz, 1999) although gradients of other state variables are assumed small (Appendix C). The VICC is modelled like run-off as a scaled flux into the surface shelf box based on peak values from Pawlowicz and Farmer (1998) and a seasonal cycle from Thomson et al. (1989). The additional volume added to the shelf and slope surface boxes exits the system in the alongshore current (Figure 3.5).

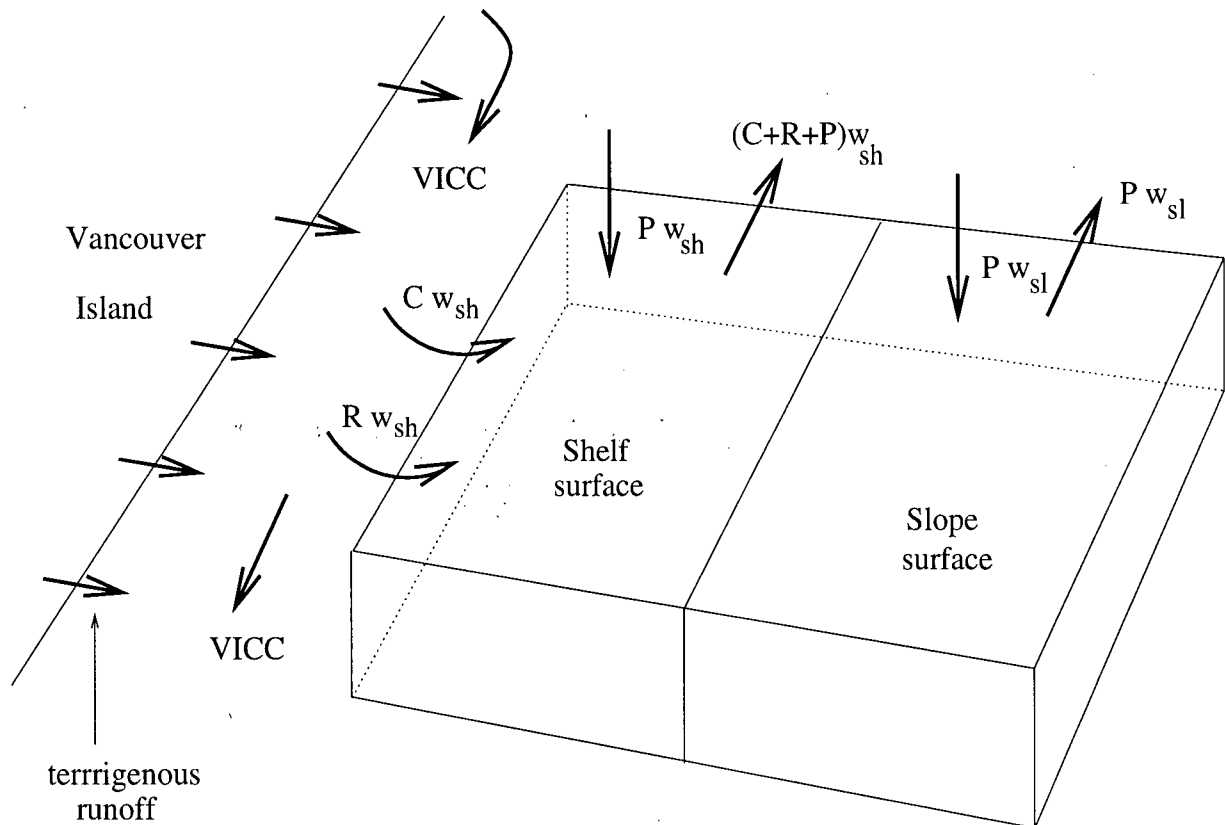


Figure 3.5: A schematic of the upper layer shelf and slope boxes showing buoyancy fluxes. Buoyancy fluxes (volume per length coastline) from precipitation are  $P w_{sh}$  and  $P w_{sl}$ . Buoyancy fluxes (volume per length coastline) from the inner shelf are from terrigenous runoff,  $R w_{sh}$  and from the VICC,  $C w_{sh}$ .

### 3.3.4 Mixed Layer Depth

The depth of the upper box ( $h_u$ ) is the mixed layer depth. Annual mixed layer depth variability was prescribed using the results of Thomson and Fine (2000) for both shelf and slope (Appendix D). On top of this average, additional variability at storm frequencies (periods of 5 and 10 d) was added (Appendix D). The amplitudes of this variation were modulated so that forcing was weaker during the summer months.

### 3.3.5 Open Ocean

Seasonal variations in all surface ocean state variable concentrations were forced (Appendix E) based on the data of Whitney et al. (1998), Wong et al. (1997), Bishop et al. (1999), Whitney and Freeland (1999), C. S. Wong (pers. com.) and R. Brown (pers. com.) Constant deep open ocean concentrations were estimated from the same data (Appendix E).

### 3.3.6 Parameter Choice

#### Biological

Biological parameters are challenging to choose. Single numbers are used to represent many processes and may also be species dependent. Often the processes are poorly understood and non-linear. Field measurements are difficult to make and usually scarce. We used data from many sources combined with steady state solutions of the biological model to constrain parameters.

Maximum growth rates ( $vm$ ) are temperature dependent following the standard  $Q_{10}$  rule,

$$vm = vm_0 \exp(0.069K^{-1} \cdot T) \quad (3.10)$$

where  $vm_0$  would be the maximum growth rate at a temperature of 0 K and  $T$  is the

average temperature in the upper layer. Field data (Harrison and Platt, 1986) were used to set growth rates. In this data compilation the saturation light intensity  $I_{sat}$  varied less than  $\alpha$  throughout the year for similar sea surface temperatures and light intensities as in my study area, so it was kept constant in the model and  $\alpha$  (uptake per  $I_{PAR}$  at low light intensity) was calculated from

$$\alpha = \frac{vm(T)}{I_{sat}} \quad (3.11)$$

To make  $vm$  and  $\alpha$  independent of  $chl_a$  we assumed that active phytoplankton had a C:chl $a$  ratio of 35.

The particle remineralization rate ( $r_p$ ) for lower layer PO matter was set using measured remineralization depth scales from sediment traps (Martin et al., 1987; Timothy and Pond, 1997). The depth scales were combined with the sinking rate associated with the particle flux that sediment traps measure ( $100 \text{ m d}^{-1}$  (Suess, 1980)).

To deal with the most poorly known parameters (e.g. the decay of the living PO pool ( $s$ ) which represents many processes) quasi-steady state solutions were found for a simplified two box version of the biological model (Figure 3.3, Equation F.2) (Appendix F). Known values (or ranges of values) of parameters and state variables were used to constrain the equations and to provide a solution for  $s$  and to narrow the range for the remineralization rate of DO matter ( $r_d$ ) (Table 3.3).

### Physical

Physical parameters were set by tuning the seasonal salinity and DIN cycle to match data (Chapter 4). Parameters were constrained to ranges based on local measurements (see section Upwelling and Downwelling) and numerical simulations (Eurin, 1999) in the study area.

## 3.4 Results

### 3.4.1 Primary Production

The response to the typical up- and downwelling forcing (Figure 3.4) by DIN and primary production presented over the shelf and over the slope (Figures 3.6 and 3.7) shows the classic spring bloom (Sverdrup, 1953) followed by an abrupt crash when DIN in the upper layer becomes depleted (occurring later over the slope). Storm mixing and entrainment provide DIN for small bursts of primary production until the upwelling season begins (year day 145). Upwelled fluxes into the upper layer are large so that upper layer DIN builds up faster than the biota can draw it down, so sharp peaks in DIN and  $pp$  over the shelf occur (Figure 3.6). Much of the upwelled DIN is taken up over the shelf before it can be advected offshore into the upper slope box. Thus, over the slope these peaks are much smaller and only occur for large upwelling events (Figure 3.7). In the fall, DIN increases in the surface mainly due to entrainment and reduced demand because of decreasing light availability. In the lower shelf layer (Figure 3.6 lower panel) DIN decreases as the nutricline becomes depressed during the short winter downwelling season (year days 349 – 45). DIN increases throughout the upwelling season (year days 145 – 285) due both to advection from the open ocean and remineralization. DIN in the lower slope box (Figure 3.7 lower panel) behaves similarly but with less variation throughout the year. Net annual primary production for the typically forced case is 410 and 330  $\text{g C m}^{-2}\text{yr}^{-1}$  for the shelf and slope, respectively. Model  $pp$  is higher than expected (around 250  $\text{g C m}^{-2}\text{yr}^{-1}$  (P. Harrison, pers. com.)) but is in agreement with recent measurements (Harris, 2000).

In the surface shelf box, DIN supplied by upwelling is responsible for 50% of  $pp$ , while mixing and entrainment provide 35% and the VICC 15%. Over the inner shelf, which we do not model, the VICC is likely the major nutrient source. Over the slope upwelled

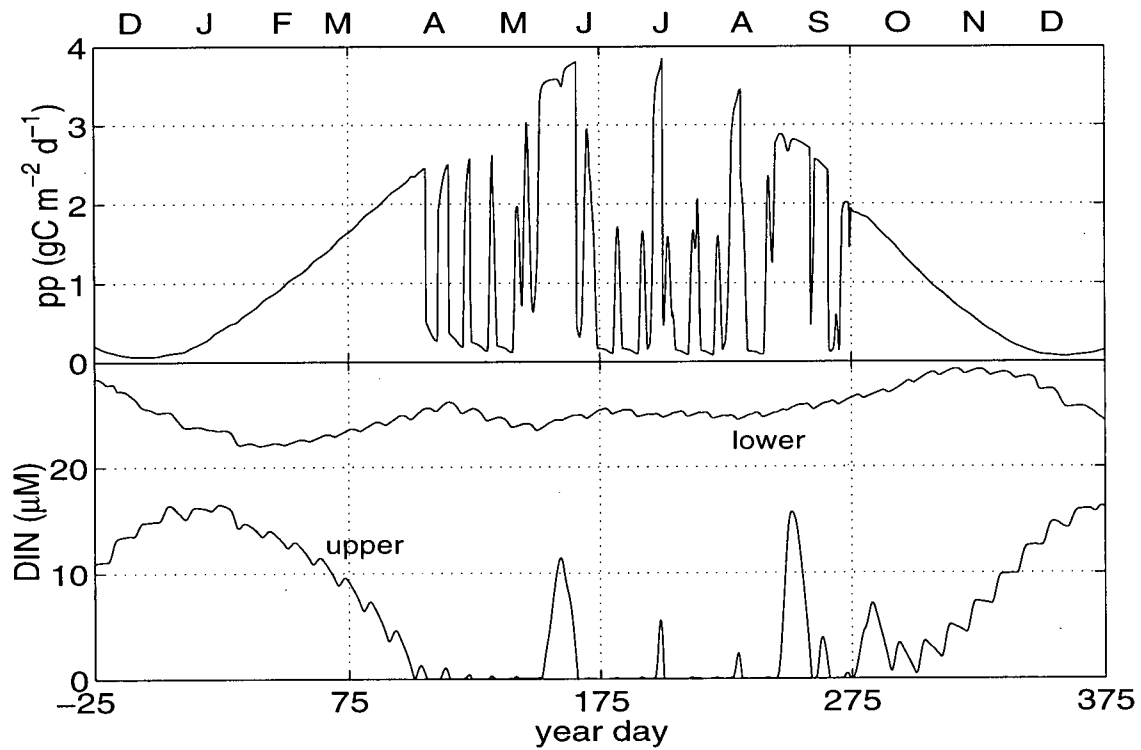


Figure 3.6: Integrated shelf primary production (upper panel) and upper and lower layer shelf DIN (lower panel) for a typical year. (Upper layer depths are shown in Figure D.1.) Advective forcing is shown in Figure 3.4. The modulating wave in DIN is caused by entrainment in response to storm forcing. Time is in year days where year day 0 is Jan. 1.

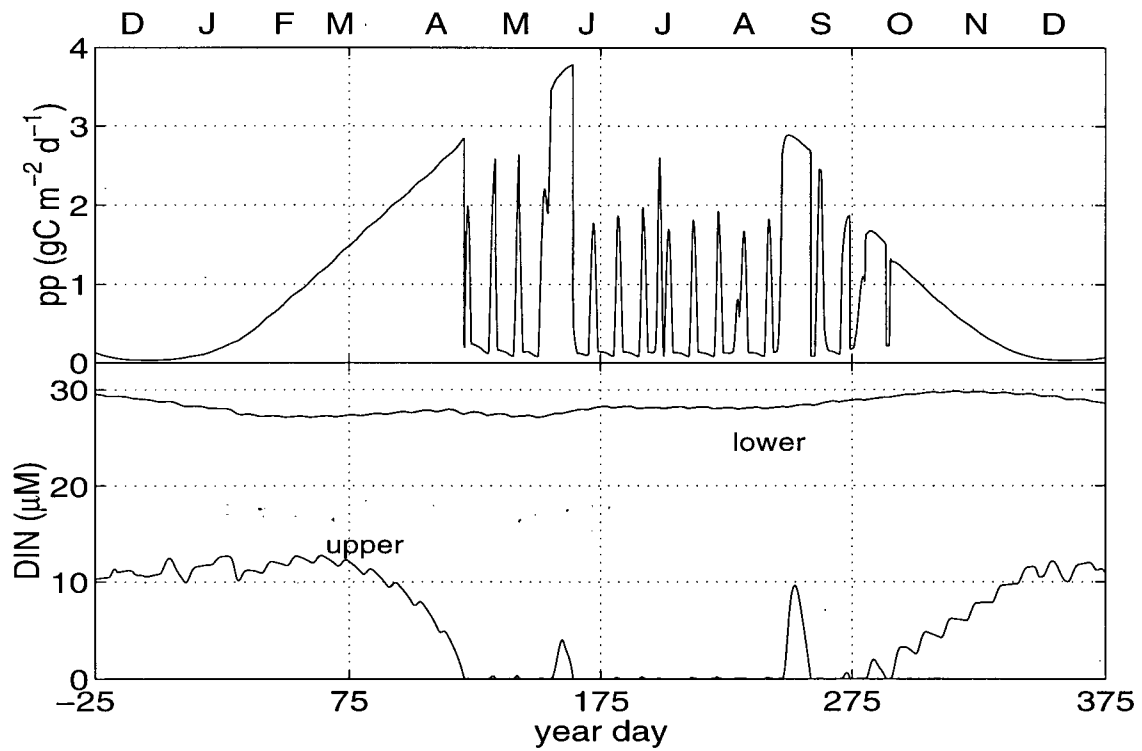


Figure 3.7: Slope primary production (upper panel) and upper and lower layer slope DIN (lower panel) for a typical year. Advective forcing is shown in Figure 3.4. The modulating wave in DIN is caused by entrainment in response to storm forcing. Time is in year days where year day 0 is Jan. 1.

DIN fuels 30 – 35% of the  $pp$ , mixing 65 – 70% and the VICC less than 5%.

Primary production is mainly controlled by light availability in my study area when physical forcing is realistic; i.e. not smoothed in time (Figure 3.4). The maximum possible daily  $pp$  when nutrients are not limiting is controlled by  $I_{PAR}$  through the biological uptake parameters,  $\alpha$  and to a lesser degree  $vm$ . When the model  $pp$  drops during the summer it is nutrient limited or briefly light limited through PO matter self shading. Because  $I_{PAR}$  is usually below  $I_{SAT}$  throughout the upper layer, the model is not sensitive to changes in  $vm$ . Increasing  $vm_0$  by 35% (but maintaining  $\alpha$  through a comparable increase in  $I_{SAT}$ ) has no effect on model  $pp$ . At low light levels  $\alpha$  is important. Increasing  $\alpha$  by 35% (with  $vm_0$  constant) causes  $pp$  to increase by 10% as the maximum possible daily  $pp$  is higher. (See Appendix G for a summary of sensitivity analysis.) However, changing the way that nutrients are delivered to the euphotic zone has a major effect on  $pp$ .

When forcing is smoothed (peak width of each event increased by a factor of 4) (Figure 3.4) but integrated up- and downwelling flux is the same, primary production increases significantly over the shelf ( $510 \text{ g C m}^{-2}\text{yr}^{-1}$ ), but decreases over the slope ( $280 \text{ g C m}^{-2}\text{yr}^{-1}$ ). There is higher primary production in the system because the peak upwelled DIN fluxes are small enough that the biota can respond before the DIN is horizontally advected into the open ocean. In the more sporadic (typical) case some DIN is advected out of the system during strong events before it can be utilized by the biota. The effect of this higher production (20%) under smooth forcing is to maintain a larger nutrient inventory in the system (about 6% in nitrogen) despite the same net advected nitrogen flux into the system. Much of the additional primary production is remineralized over the shelf and so more nutrients are retained.

Nutrient inventory is clearly influenced by primary production as in the example above. Of the physical parameters, the most important to nutrient inventory are the

average up- and downwelling velocities ( $\bar{A}$  and  $\bar{D}$ ), in particular the ratio of total annual fluxes ( $\bar{A}t_u:\bar{D}t_d$ ) where  $t_u$  and  $t_d$  are the lengths of the up- and downwelling seasons, respectively. Horizontal mixing is less important. The higher  $\bar{A}t_u:\bar{D}t_d$ , the higher the nutrient inventory over the shelf. Some of the increased nutrient supply is used in  $pp$ . Increasing this ratio to 3.2 ( $\bar{A} = 0.865$  and  $\bar{D} = 0.6$  with unchanged season durations,  $t_u$  and  $t_d$ ) from 2.5 (typical value) causes a 2 - 3% increase in  $pp$  and an increase in total nitrogen inventory by 6%. Also, the nutrient concentration in the lower layer of the neighboring open ocean (the depth of upwelling) is very important, as this water is advected onshore each summer.

Increasing the fraction  $p$  of the decay flux from the surface PO pool which sinks and becomes PO in the lower layer also increases nutrient inventory (6% with a change in  $p$  from 0.3 to 0.7) and therefore primary production (10% for the same change). With the higher  $p$ , more remineralization occurs over the shelf as the particulate rate ( $r_p$ ) is an order of magnitude higher than the dissolved rate ( $r_d$ ). In addition, it occurs in the lower layer where it is more likely to be retained in the system as most  $pp$  occurs during the upwelling season. In the case where  $p$  is low, there is higher horizontal export of DO matter out of the system in the surface layer. Doubling the rates of PO remineralization ( $r_p$ ) has little effect on either nutrient inventory or  $pp$ , as the original rate was high enough that close to complete remineralization already occurred within the system. Doubling the remineralization rates of DO matter  $r_d$  increases the nutrient inventory only slightly (< 1%), but increases total  $pp$  by 5% as the excess remineralization occurs mostly in the surface and so is quickly taken up by the biota.

When up- and downwelling circulation is shut off completely, the model behaves more like an oligotrophic ocean. Primary production decreases to half and is nutrient limited during the entire summer. DIN concentrations are lower everywhere in the system. Surface DIN is 30% less in the winter over the shelf and is zero throughout the summer.

The total nitrogen inventory decreases by 25%.

## ENSO

Simulations of ENSO show effects of interannual variability in forcing and that winter forcing can affect the summer season. During ENSO years, modelled downwelling is enhanced while upwelling remains the same. Despite the same upwelled flux during the summer, primary production is lower (about 20% from increasing  $\bar{D}$  from 0.7 to 2.8). The nutrient inventory in the system is decreased because the nutricline is so strongly depressed during the winter that the summer upwelled water has lower DIN (Figure 3.8). This effect can clearly be seen in the DIN concentration of the lower shelf box (lower panel, Figure 3.8) which drops to 11  $\mu\text{M}$  during the ENSO winter. If the nutricline in the open ocean were also depressed or if summer upwelling were decreased, the effects of ENSO would be enhanced. After one winter of increased downwelling the system takes about four years to reach its previous steady state nutrient inventory (Figure 3.8), though in the second year after ENSO primary production is within 5% of its initial value (but less nutrient is advected out of the system). These results suggest that ENSO events occurring at frequencies higher than every four years decrease the nutrient inventory and production in the system over the long term.

## Residence Time

The residence time for water over the shelf in the model is on the order of weeks in the surface layer ( $\sim 10$  d in the summer and  $\sim 50$  d in the winter) and  $\sim 4$  months in the lower layer. These times seem reasonable relative to the natural system, however the strong along-shore circulation is not modelled and could shorten them substantially depending on the along-shore extent of the model (larger spatial scale, less effect on residence time). In the case of the ENSO example above, the spatial extent of the physical forcing is

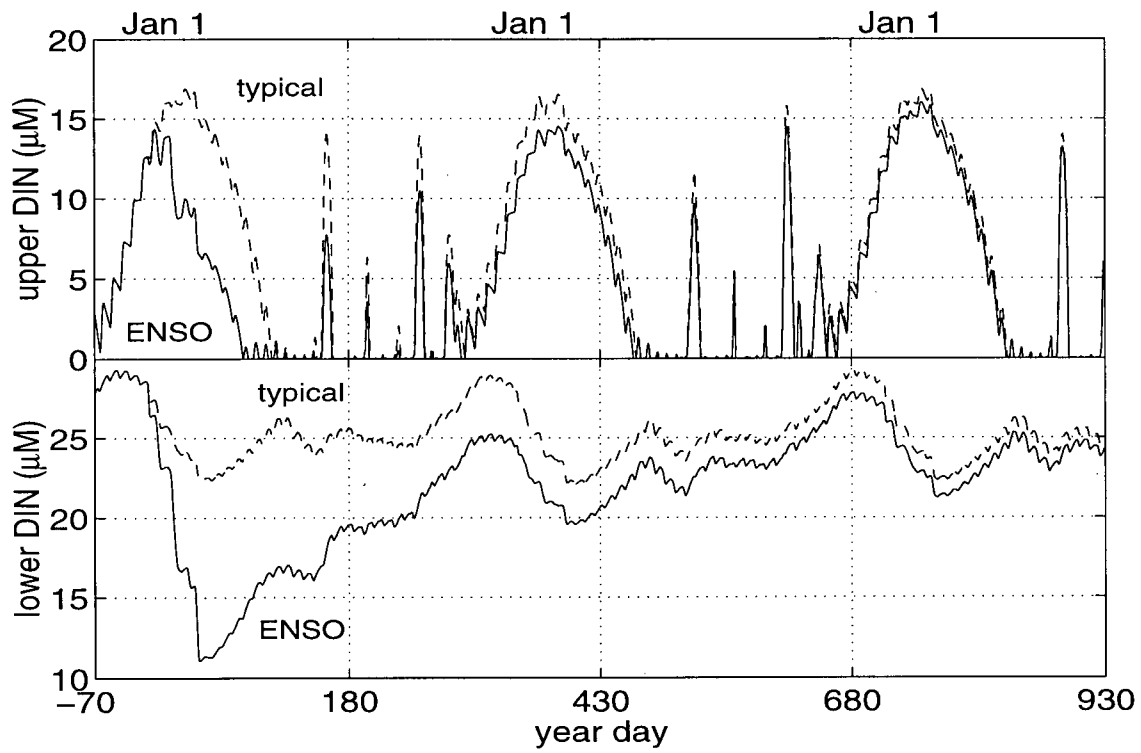


Figure 3.8: Shelf DIN in upper layer (upper panel) and shelf DIN in lower layer (lower panel) for 3 years. ENSO response (solid curve) to ENSO forcing during the first year (followed by typical forcing in the second and third year) is compared to 3 years of typical forcing (dashed curve).

large (order 1000 km) and so my model results would not be greatly affected by the addition of the along-shore circulation. In addition residence time for nutrients is longer because nutrients are incorporated into the POM, some of which sinks into the lower layer, retaining nutrients in the system.

### 3.4.2 Gas Flux

For all model configurations there is net air-sea CO<sub>2</sub> evasion during the winter and invasion during the summer, when *pp* draws down surface DIC (Figure 3.9, upper panel). However net annual CO<sub>2</sub> flux is very small compared to seasonal fluxes. For the typically forced case (Figure 3.9) there is net annual invasion ( $6 \text{ g Cm}^{-2}\text{yr}^{-1}$  which is  $2 \times 10^5 \text{ g C yr}^{-1}$  per m coastline). Over the shelf, surface *p*CO<sub>2</sub> varies over a larger range (200 – 550 ppm) than over the slope (200 – 450 ppm) (Figure 3.9, lower panel). The highest model *p*CO<sub>2</sub> occurs over the shelf in response to strong upwelling events (year days 159 and 251). While these values seem high, surface measurements of 525 ppm have been recorded during an upwelling event in the area (F. Whitney pers. com.). During most of the summer *p*CO<sub>2</sub> is around 200 – 250 ppm, which compares well with measurements (Tables 2.1 and 2.2). In winter, model *p*CO<sub>2</sub> is very high due to low alkalinity (from high rainfall), and increased DIC (from vertical mixing). *p*CO<sub>2</sub> is highest over the shelf where the surface waters are highest in DIC and are freshest. Primary production draws *p*CO<sub>2</sub> down earlier in the spring over the shelf than over the slope (Figure 3.9) but otherwise the model output is similar for both.

Variations in model parameters do affect *p*CO<sub>2</sub>; however, summer *p*CO<sub>2</sub> is remarkably insensitive as long as up- and downwelling circulation is not set to zero. Only large changes in assumed deep ocean DIC concentration or setting excess carbon uptake (*pc*) to zero cause summer *p*CO<sub>2</sub> to vary from the typically forced case. Most variations appear during the winter season even for differing *pp*.

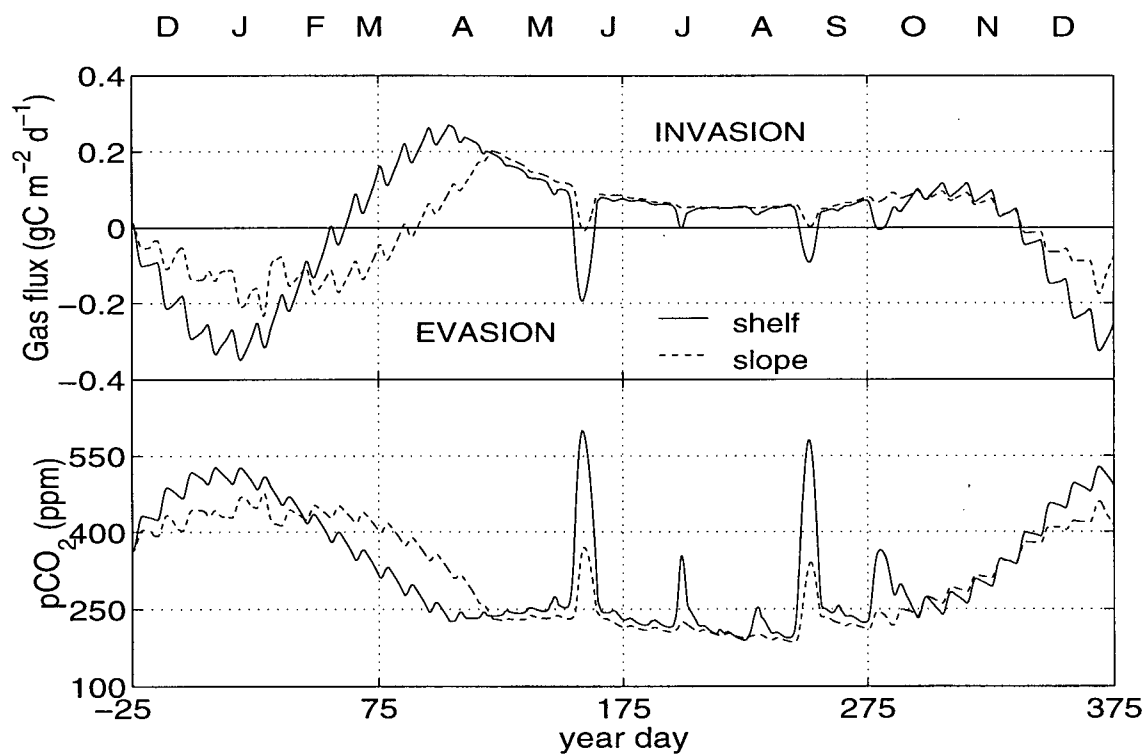


Figure 3.9: Model gas flux (upper panel) and  $p\text{CO}_2$  (lower panel) for shelf (solid curve) and slope (dashed curve). Positive gas flux is from the atmosphere (invasion).

Increasing carbon inventories (by either using smoothed forcing with the same  $\overline{A}t_u:\overline{D}t_d$  ratio or by increasing  $\overline{A}t_u:\overline{D}t_d$  to 3.2 with realistic forcing) causes winter and fall  $p\text{CO}_2$  to increase by 20 – 30 ppm, while summer values are unchanged. There is still net annual  $\text{CO}_2$  invasion but it is significantly decreased (Table 3.4). There is higher invasion in the smoothed case because there are no high  $p\text{CO}_2$  peaks in summer from upwelling. Doubling the remineralization rate of DOC ( $r_d$ ) does not change summer  $p\text{CO}_2$  but increases fall and winter  $p\text{CO}_2$  by about 50 ppm. Decreasing nutrient inventory by lowering  $p$  to 0.3 makes for lower winter  $p\text{CO}_2$  (by 40 ppm) increasing the net gas invasion (Table 3.4).

Table 3.4: Comparison of gas flux for different model runs. Shelf  $p\text{CO}_2$  were averaged over the month of January to represent maximum winter values and over June and July to represent minimum summer values. The average gas flux to the ocean  $\overline{G}$  was calculated by weighting annual flux over the shelf by two relative to the slope to account for its larger area.

Model run	Shelf $\overline{p\text{CO}_2}$ (January) (ppm)	Shelf $\overline{p\text{CO}_2}$ (June and July) (ppm)	Shelf and slope $\overline{G}$ ( $\text{g m}^{-2}\text{yr}^{-1}$ )
typical	505	230	6
$\overline{A}t_u:\overline{D}t_d = 3.2$	530	230	1
smooth forcing	530	230	3
$r_d$ s doubled	540	230	-1
$p = 0.3$	470	230	14
ENSO	435	230	22
$\alpha$ increased 35%	470	230	19
$pc = 0$	505	310	0.6
$\overline{A} = \overline{D} = 0$	450	270	14

Winter  $p\text{CO}_2$  is lowered in the case of ENSO forcing (enhanced downwelling). The depression of the pycnocline and the concentration decrease of DIC is strong and so winter  $p\text{CO}_2$  decreases by about 70 – 80 ppm, while summer values remain the same (Table 3.4). Winter and spring  $p\text{CO}_2$  are lowered (40 – 50 ppm) when  $pp$  is increased (10%) by increasing the biological parameter  $\alpha$  (35%) while summer values remain unchanged

despite higher daily  $pp$ . In both the above examples there is larger net annual  $\text{CO}_2$  invasion (about  $20 \text{ g Cm}^{-2} \text{ yr}^{-1}$ ).

When there is no excess DIC uptake by the surface PO pool,  $p\text{CO}_2$  is significantly higher, as much as 80 – 90 ppm, during the summer (Table 3.4). The carbon inventory does not change though, so winter  $p\text{CO}_2$  is not affected. Net annual gas invasion decreases relative to the typical case to near zero. In this scenario, however, model DIC between upwelling events is higher than measured (Table 2.1 and 2.2).

Shutting off the up- and downwelling circulation entirely causes a 40 ppm increase in summer  $p\text{CO}_2$  as  $pp$  is reduced by about half. Net annual  $\text{CO}_2$  invasion still increases (by a factor of 2) because of decreases in winter and fall  $p\text{CO}_2$ . With no upwelling circulation, nutrient inventories are significantly less, causing fall and winter DIC concentrations to be lower. A much larger portion of the summer DIC drawdown in this scenario however is due to  $pc$ . If it were not for this excess uptake of carbon there would be close to zero net annual  $\text{CO}_2$  flux.

### 3.4.3 Net Annual Exchange Fluxes between the Model and the Open Ocean

For both carbon and nitrogen, the dominant annual exchange flux is the import flux of DI nutrients into the lower slope box from the open ocean (Table 3.5). This nitrogen input is balanced mainly by export of PON from the upper layer to the surface open ocean (50%). Lower layer exports of PON are very small, two orders of magnitude less than surface exports. A further 20% of the DIN import is exported to the open ocean as DON, mainly in the upper layer (Table 3.5) while 10% leaves as DIN in the upper layer. The remaining 20% leaves the system in the along-shore surface current as a result of the buoyancy fluxes. While there is a net import of DIN from the VICC, a much larger alongshore export occurs as DON and PON.

In the case of carbon, most (75%) of the lower layer DIC import flux returns to the

Table 3.5: Net annual input to the model system from the ocean. Exchanges with the open ocean occur between the slope boxes and the open ocean in upper and lower layers. Net along-shore fluxes occur from upper shelf and slope boxes. Negative fluxes are out of the model system and positive fluxes are into the model system. All units are per length of coastline (in m) ( $\text{kg yr}^{-1}\text{m}^{-1}$ ).

open ocean exchange flux	Nitrogen $\text{kgN yr}^{-1}\text{m}^{-1}$	Carbon $\text{kg C yr}^{-1}\text{m}^{-1}$
upper DI	- 60	- $3 \times 10^4$
lower DI	600	$4 \times 10^4$
upper DO	- 100	- 2000
lower DO	- 20	- 200
upper PO	- 300	- 2000
lower PO	- 3	- 20
along-shore exchange flux	- 120	- 6000
gas flux	0	200

open ocean as DIC in the upper layer (Table 3.5) because the fraction of biological DIC drawdown is so much smaller than that of DIN. Only 10% of the carbon import leaves as organic carbon in the surface layer in equal fractions of DOC and POC. 15% of the imported DIC is exported in the along-shore surface current due to buoyancy fluxes, mostly as DIC over the shelf.<sup>2</sup> Although gas flux provides an additional net import of carbon, it is 2 orders of magnitude less than the lower layer import of DIC.

The C:N ratio of the PO export is 6.7 (set in the model), while the C:N ratio of the model DO export is in the range of 10-20 (higher because of excess carbon uptake). The ratio of total TOC:TON export is about 10 which agrees well with depth integrated measurements in the upwelling region along the Oregon coast (Hill, 1999).

When upwelling strength is increased relative to downwelling strength ( $\overline{A}t_u:\overline{D}t_d=3.2$ ), both lower layer DI imports increase by 20%. Almost all of the excess DIC import is exported into the surface ocean as DIC. About half of the excess DIN leaves in the surface

<sup>2</sup>The along-shore volume flux is only that part required to balance the buoyancy volume flux.

as DIN while the other half is converted to organic nitrogen which is then exported into the surface ocean. When  $pp$  is increased through smooth forcing, DIC exchanges are unchanged but there is no longer any DIN export in the upper layer. There is a shift (factor of 2) in organic matter export in the surface from POC to DOC. Likewise, increasing  $pp$  (10%) by raising  $\alpha$  does not affect DIC exchange while DIN export to the surface ocean is much lower (60%). Organic matter exports increase in both layers by 10 – 20%.

If up- and downwelling circulation is shut off, exchange fluxes with the open ocean decrease by an order of magnitude. Import of DIC still occurs in the lower layer but it is balanced mainly by the export of DOC rather than DIC in the upper layer.

### 3.5 Discussion and Conclusions

To develop this model we made several additions which are non-standard relative to the biological models reviewed by Fasham (1993). These additions were necessary to produce reasonable results. Physically, a permanent pycnocline was added to create more realistic vertical variability in state variables (Figure 3.2). Without this variability, entrained and mixed fluxes were too large, particularly during late summer and fall. Entraining averaged lower layer DIN at these times made fall surface DIN unrealistically high and produced a very large fall phytoplankton bloom. Biologically, winter  $pp$  was too high despite realistic light levels. High  $pp$  during the winter meant that surface nutrients did not attain measured spring values and the resultant spring bloom was much smaller than expected. To solve this problem we made a portion of the living PO pool dormant during the winter months (Equation 3.6) representing the formation of non-sinking resting stages by diatoms. We also modelled excess uptake of DIC during times of nutrient limitation (Equation 3.7) so that summer surface DIC values reflected measured values. This excess

flux was added to the DOC pool, thereby increasing the model TOC:TON ratio from the Redfield ratio to a more realistic value of about 10. Raising the DON remineralization rate relative to that of DOC also raises the TOC:TON ratio. In addition, my characterization of non-living organic matter as sinking (PO) or non-sinking (DO) is unique. Because the living PO pool maintained quite large concentrations even when nitrogen and light became limiting we made the decay rate of this pool increase at these times. We based increased losses on changes in phytoplankton single-cell sinking rates. This representation produced much better results than a mathematical representation of zooplankton grazing (Appendix G).

Results show that the winter season is very important in determining model fluxes, despite the fact that the major biological fluxes occur during the summer. Downwelling strength has a major impact on lower layer nutrient concentrations over the shelf and in turn  $pp$  the following summer. Interannual variability (such as ENSO events) affects the system over time scales of 3-5 years. Furthermore, it is differences in winter (not summer) surface  $p\text{CO}_2$  that cause differences in modelled net annual  $\text{CO}_2$  flux. During the winter the lower layer is thoroughly mixed and entrained into the surface layer over the shelf. Because of this winter mixing, nutrient inventories in the system have a strong influence on both  $pp$  and  $p\text{CO}_2$ . The primary influences on nutrient inventory are the ratio of up- and downwelling strengths,  $pp$  and  $p$  (mainly because more organic matter is remineralized at a higher rate when  $p$  is increased). In addition, the nature of advective forcing is very important. Realistic and more sporadic forcing versus smoothed forcing (Figure 3.4) yields significantly lower  $pp$  and nutrient inventory. Fresh water inputs during winter also exert strong control over  $p\text{CO}_2$  by lowering TA.

The model parameters which are most important to predict the system are the offshore lower layer inorganic nutrient concentrations,  $\alpha$  (particularly at mid-high latitudes),  $p$  and  $r_d$ . The former is generally known while the three latter parameters are not as

well known. The most poorly known are  $p$  and  $r_d$ , which determine the character of the non-living organic matter, whether sinking or non-sinking, and the remineralization rates.

It is difficult to calculate  $\text{CO}_2$  gas flux accurately so we do not pretend that the results of my simple model yield firm numbers. Our model does show the chief influences on gas flux and also indicates that within the system there is usually net invasion even when the parameters are stretched to their limits (the exception is the doubling of  $r_d$  which causes small evasion). However, the fate of this carbon influx is most likely evasion in the neighboring surface ocean.

The model suggests that the largest influence on the global carbon budget from coastal upwelling regions is ventilating intermediate depth oceanic DIC through large imports of DIC into the lower layer of the system, most of which exits back to the open ocean in the surface layer. Furthermore this advected surface flux is relatively deplete in DIN. Rather than provide a strong portion of the biological pump, the high  $pp$  makes very high nutrient inventories, which are well ventilated over the shelf in winter. Horizontal exports of organic matter to the open ocean are also large but they occur mostly in the upper layer. There is very little export of organic matter in the lower layer. The surface organic carbon export is split roughly equally into DO and PO so that some of it may sink in the open ocean but most of it is likely to be remineralized in the surface. Thus, while coastal upwelling regions have disproportionately high  $pp$  and  $p\text{CO}_2$  drawdown, they are unlikely to sequester atmospheric carbon via the biological pump. The dynamic physical processes in winter ventilate the DIC which accumulates in the lower layer during the summer and the advective circulation transports large quantities of intermediate depth ocean water, rich in DIC, to the surface.

## Chapter 4

### State Variable Results and Comparison with Data

Annual cycles of each of the model state variables are presented for both layers in the shelf and slope region for the model configuration described in Section 3.2 (parameters in Tables 3.2 and 3.3). Salinity and DIN cycles are described along with a discussion of how these results were used to tune the physical model. Next, dissolved inorganic carbon (DIC), the particulate organic (PO) state variables (nitrogen, PON; carbon, POC) and the dissolved organic (DO) state variables (nitrogen, DON; carbon, DOC) are presented and where possible compared with the data that were obtained as part of this research (Chapter 2). Finally, modelled primary production (*pp*) and partial pressure of carbon dioxide ( $p\text{CO}_2$ ) are compared with the data.

#### 4.1 Salinity and Dissolved Inorganic Nitrogen

The annual cycle of salinity is shown in Figure 4.1 for upper and lower levels over the shelf (lower panel) and the slope (upper panel). Over the shelf there are appreciable buoyancy fluxes (causing freshening) to the surface throughout the year. Terrigenous runoff and precipitation are strongest during the fall and winter, and during the summer the inner-shelf buoyancy current (Vancouver Island Coastal Current, VICC) is at its maximum (as it is fed by snow and ice melt from the mountains). Advective fluxes balance this freshening by bringing higher salinity water into the upper layer of the shelf. In the summer this flux comes from below (more saline lower waters) and in the winter it comes from offshore (more saline ocean surface waters). The net effect is that surface waters are

freshest in fall, winter and spring, and saltier during the summer upwelling season (year days 145 – 285). Upwelling events are seen in salinity peaks. The winter downwelling season (year days 349 – 45) also causes salinity to increase (although much less). The lower shelf salinity becomes fresher during the downwelling season (when the upper shelf water is advected into it) and more saline during the upwelling season, peaking in salinity in early fall. The upper layer over the slope (Figure 4.1, upper panel) receives rainfall during the winter and fall, balancing the onshore advection of open ocean waters (that are higher in salinity) during the downwelling season. The upper slope layer is freshest during the summer upwelling season when surface shelf water is advected offshore. Storm mixing (period of 10 d) causes small oscillations (most noticeable in the upper layer) due to entrainment.

The annual cycle of DIN is shown in Figure 4.2 (slope - upper panel; and shelf - lower panel) for a regular model run. This cycle has been discussed in detail in the previous chapter (Section 3.4.1). The main features in the upper layer DIN cycle are the winter build up produced by vertical mixing and entrainment when primary production is low, followed by the drawdown in spring when light availability allows *pp* to increase. During the upwelling season (year days 145 – 285) there are occasional peaks in DIN that are quickly taken up by the biota. Winter nutrient build up of DIN is higher over the shelf relative to the slope (as are summer upwelling peaks). Upwelling peaks in DIN only show over the slope when events are strong enough that surface DIN can be advected from the shelf (where upwelling occurs) to the slope faster than it can be utilized by the shelf biota. In the lower layers there is a decrease in DIN during the winter downwelling season (year days 349 – 45) due to the depression of the nutricline. Increases in the lower layer occur both from upwelled fluxes (year days 145 – 285) and the remineralization of organic matter (seen mostly in the fall over the shelf). Cycles are similar for both shelf and slope, but more subtle over the slope where overlying production is not as high

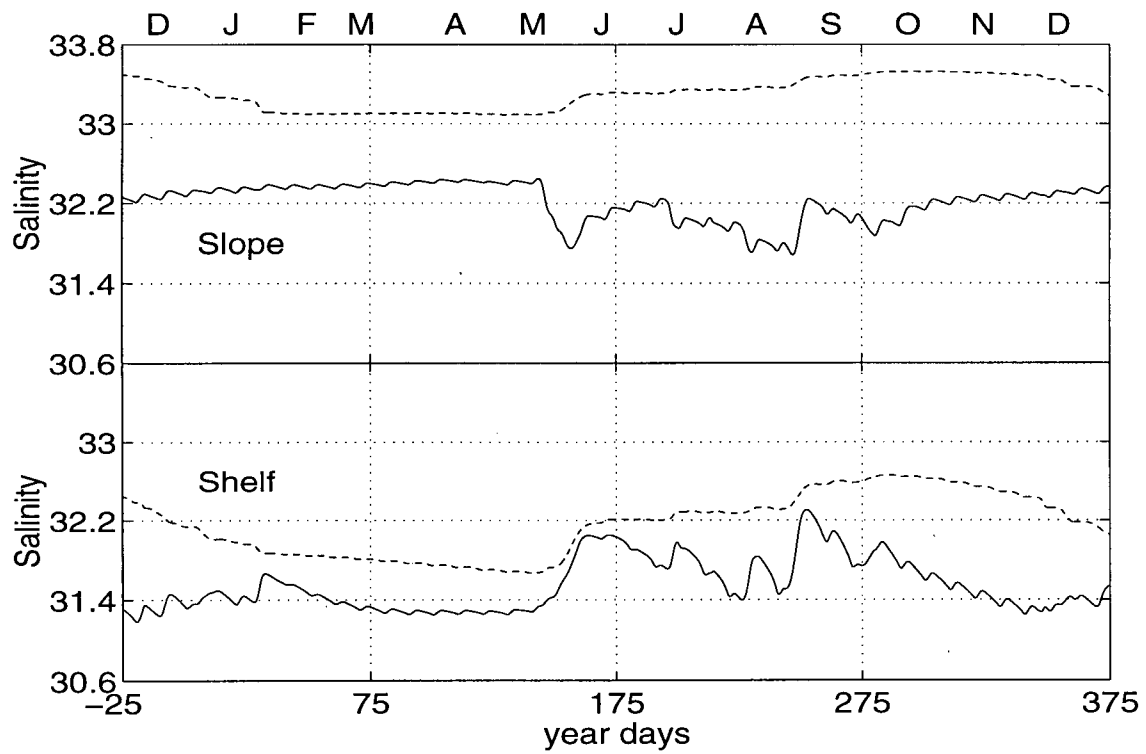


Figure 4.1: The annual salinity cycle for a typical model run (using parameters from Tables 3.2 and 3.3) for upper layers (— solid lines) and lower layers (- - dashed line) over the slope (upper panel) and the shelf ( lower panel).

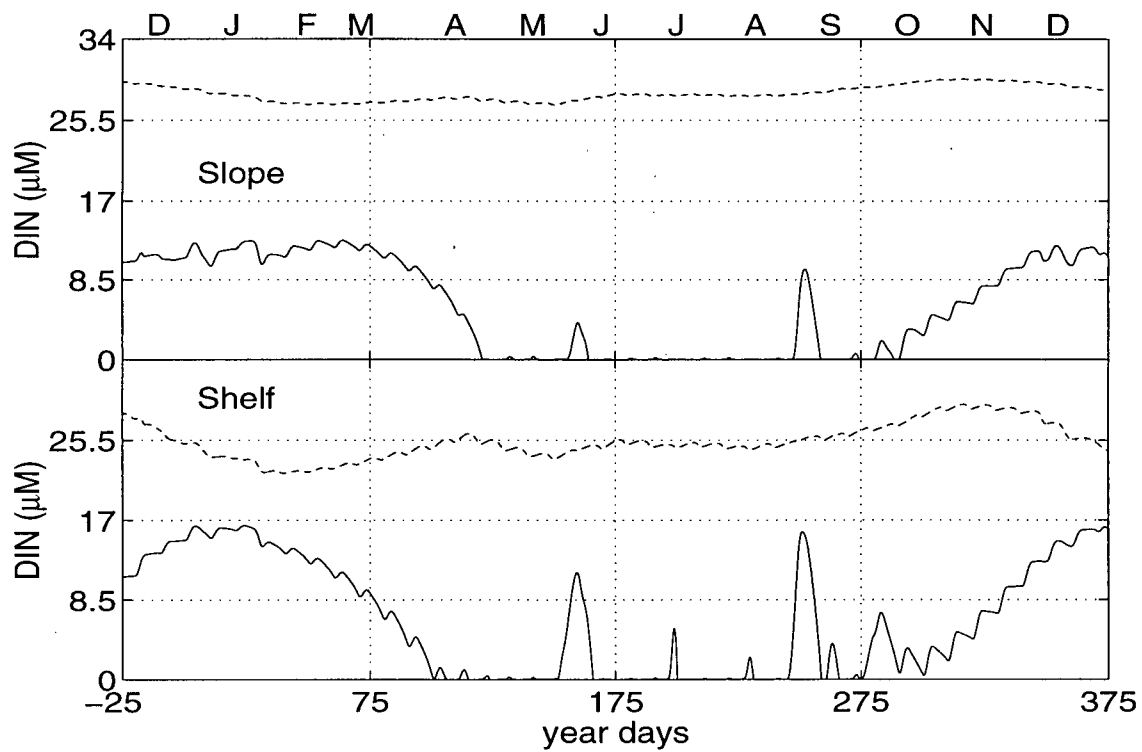


Figure 4.2: The annual dissolved inorganic nitrogen cycle for a typical model run (using parameters from Tables 3.2 and 3.3) for upper layers (— solid lines) and lower layers (- - dashed line) over the slope (upper panel) and the shelf (lower panel).

and the volume of water is considerably larger (and so advective fluxes have less effect). Buoyancy fluxes also affect DIN (dilution by terrigenous runoff and rainfall and addition from the VICC) although fluxes due to the biological cycle dominate.

#### 4.1.1 Tuning the physical model

The physical parameters were tuned so that annual cycles of salinity and DIN compared well with available data (nitrate ( $\text{NO}_3^-$ ) in the case of DIN). Salinity was chosen to tune the physical model because it is not part of the biological cycle and there are considerably

more salinity data available relative to the other state variables.  $\text{NO}_3^-$  data were used to limit the number of potential solutions and because these data are also available (although there are few winter measurements). Data were obtained from R. Brown (Institute of Ocean Sciences data base) from many sites within the study area (collected between 1957 and 1997). To tune the model all physical parameters ( $\bar{A}$ ,  $\bar{D}$ ,  $M_V$ ,  $M_H$ ,  $C$ , and  $R$ ) were allowed to vary within reasonable ranges (within a factor of 2-3 from the typical values presented in Table 3.2). Since advective circulation exerted the strongest control these parameters were varied first and then the mixing parameters (including mixing with the inner shelf) were varied for each set of  $\bar{A}$  and  $\bar{D}$  until the seasonal cycles matched the data as well as possible.

Vertical mixing and entrainment were constrained by modelling salinity. (Entrainment can be changed by varying the amplitudes of storm mixing, Appendix D.) The difference between the integrated values of measured salinities in the upper and in the lower layer (i.e. the 'vertical gradient') is larger than in the model results unless vertical fluxes are small. Decreasing winter downwelling improves model results somewhat; however, I wanted to maintain the upwelling to downwelling ratio ( $\bar{A}t_u:\bar{D}t_d$ ) close to the value measured by Thomson and Ware (1996). Decreasing the magnitude of the upwelling circulation (but maintaining the ratio) introduced other problems (such as surface waters over the shelf remaining too fresh) but did not increase the salinity difference between layers enough to reproduce data. Increasing horizontal mixing provided slight improvement to the modelled vertical differences, but horizontal salinity differences between the shelf and slope remained smaller than observed.

However, when modelled salinity matched the data well (from reducing vertical fluxes) DIN did not match the data. If the vertical flux of DIN into the euphotic zone was reduced throughout the year, levels became too high in the lower layer. This shortcoming was especially obvious during upwelling events when surface values increased to well over 20

$\mu\text{M}$ . Najjar et al. (1992) report a similar difficulty in the equatorial upwelling region of their model. They call it 'nutrient trapping' (implying that either the mixing in the physical model is insufficient or remineralization rates of organic matter are too low).

The physical parameters that were chosen are a compromise to reproduce annual cycles of both salinity and DIN as well as possible, in particular where their values affect the model most. It is important that surface salinity is modelled well because it is used to estimate surface alkalinity (using the linear regression Figure 2.7). Alkalinity is used to calculate surface  $p\text{CO}_2$  and air-sea gas exchange. Lower layer DIN strongly influences primary production so it is also important. Thus my model parameterization reproduces surface salinities and lower layer DIN well, but does not reproduce lower layer shelf salinity as well during the late winter and spring; i.e. the spring transition (lower layer model salinity is approximately 0.7 and 0.3 too low over the shelf and slope, respectively, at this time). During the spring transition, there are no advective fluxes between lower layer boxes in the model and all horizontal exchange occurs via mixing. The lower layer open ocean state variable concentrations (including salinity) are set for a depth range of 150 – 250 m, the expected source of upwelled water. However, mixing occurs over the entire depth interface, which extends well beyond the advective depth range. As such, the average concentration that is mixed should be larger than that specified in the model, causing lower layer shelf and slope salinities to be too low. In addition, along-shore advection is limited in the model. Advected gradients passing through the two-dimensional model could cause some discrepancies with the real world. A suggested improvement in the physical model to overcome this shortcoming is discussed in Chapter 6.

## 4.2 Dissolved Inorganic Carbon

The modelled annual DIC cycle has aspects in common with both the salinity and the DIN cycle because, although DIC is biologically active, it is not limiting (Figure 4.3). During the winter, DIC is mixed into the surface layer and in the spring it is drawn down by the spring phytoplankton bloom. Peaks in surface DIC concentration occur during the summer due to upwelling. These concentrations decrease between the peaks even though DIN is usually limiting due to excess carbon uptake by the biota (Section 3.2.4).

The DIC data (collected between year days 195 – 204, Chapter 2) were integrated over the depths of the model boxes in the upper layer ( $\overline{\text{DIC}}_u$  in Table 4.1). Data were not collected to the bottom of the water column (or the bottom of the model lower box) at most stations so lower layer integrated values ( $\overline{\text{DIC}}_l$ ) are presented with the depths of integration (Table 4.1). It is difficult to compare directly individual data with the model (particularly in the upper layer) as the model was not physically forced in the same way as the natural system, and variability in this forcing is large. Therefore, I have plotted elliptical patches representing all of the data for comparison with the model results (Figure 4.3). The x-axis of the data ellipse is the time period over which all data were gathered and the y-axis of the data ellipse is the range of measured DIC values centered on the average value. The upper layer model values agree well with the data, although if there were no excess carbon uptake, the model DIC would be too high. The modelled lower layer shelf DIC also agrees well. I extrapolated to the depth of the lower box (usually only 15 m beyond the measurements) by assuming that the DIC concentration was constant below the lowest measured DIC. No measurements were made below 200 m (i.e. over more than half of the model lower layer slope box depth), so the lower slope data cannot be directly compared with the model. The integrated lower layer slope data in Table 4.1 represent an intermediate depth band relative to the upper

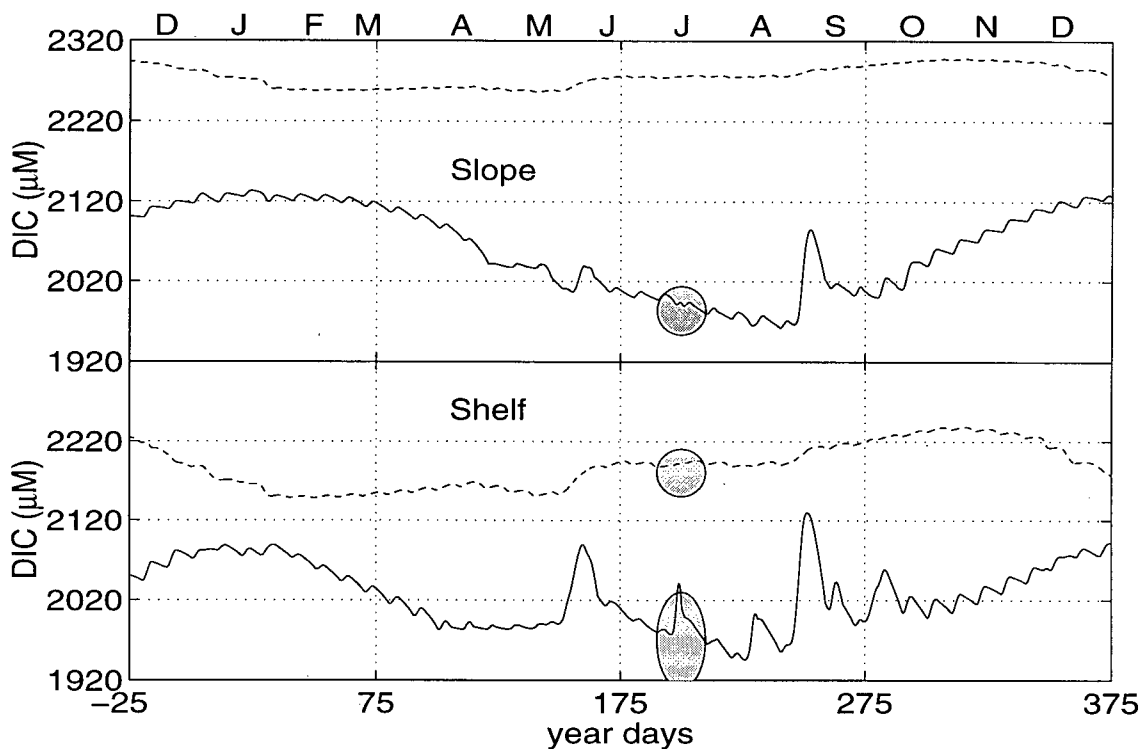


Figure 4.3: The annual dissolved inorganic carbon cycle for a typical model run (using parameters from Tables 3.2 and 3.3) for upper layers (— solid lines) and lower layers (- - dashed line) over the slope (upper panel) and the shelf (lower panel). Data integrated over the depths of the model boxes (Table 4.1) are shown by the grey patches.

and lower model values.

The annual cycle in modelled lower layer DIC is similar to that of DIN. Concentrations decrease during the downwelling season and increase in the summer due to upwelling, and also increase in the fall due to remineralization. Again the cycle is more pronounced over the shelf because the volume of water is smaller and overlying production is larger relative to the slope.

Table 4.1: Integrated DIC data for comparison with model values in the surface,  $\overline{\text{DIC}}_u$  (integrated over the upper layer depth) and in the lower layer,  $\overline{\text{DIC}}_l$  (range of depths for integration in the right column – data were not collected all the way to the bottom of the water column – the depth of the model shelf and slope are 120 and 400 m, respectively). Values are split into inner-shelf, outer-shelf and slope regions. Where there is an obvious source of water for inner-shelf stations (VICC; BS - Barkley Sound) it is indicated in the ‘physical’ column. The physical regime (after upwelling - up; downwelling - down; relaxation - relax) for outer-shelf and slope is indicated in the ‘physical’ column. For the lower stations the integration depths are shown in the right column.

Stn	Surface		Lower	
	$\overline{\text{DIC}}_u$ ( $\mu\text{M}$ )	physical regime	$\overline{\text{DIC}}_l$ ( $\mu\text{M}$ )	depth range (m)
Inner-Shelf				
A1	1980	VICC	2197	20 – 200
C1	1964	BS/VICC	2125	20 – 88
C2	2072	VICC	2139	20 – 100
C4	2062	VICC	2178	20 – 150
C7	2038	VICC	2185	20 – 100
D1	2007	VICC	2083	20 – 30
G1	1987	—	2126	20 – 48
Outer-Shelf				
A2	1980	Down	2193	20 – 100
C7	2038	VICC/Down	2185	20 – 100
C8	1968	Down	2146	20 – 150
D6	1969	Relax	2136	20 – 125
G4	1903	Up	2162	20 – 125
Slope				
A9	2002	Down	2151	20 – 200
C9	2000	Down	2133	20 – 200
C10	2000	Down	2113	20 – 125
C11	1988	Down	2137	20 – 200
D7	1967	Relax	2154	20 – 200
G6	1950	Up	2122	20 – 200

### 4.3 Particulate Organic Matter

The model annual cycles in PON (Figure 4.4) and POC (Figure 4.5) are identical in shape because incorporation of carbon and nitrogen into the particulate organic matter (POM) follows the Redfield ratio and the model remineralization rate of PON is the same as POC. In the surface, the model POM represents the biota. In the lower layer, it is non-living and remineralization occurs. Thus upper layer POM is low during the winter and increases in the spring and summer when primary production is high (after the initial bloom mainly in response to upwelling events). When nitrogen becomes depleted, POM decreases rapidly as the decay of this pool is dependent on the availability of nitrogen. This nitrogen dependence leads to the modelled crash of diatom blooms. A portion ( $p$ ) of the large decay flux sinks into the lower layer as a pulse of phytodetritus. The remainder ( $1-p$ ) of the decay flux passes into the DOM pool and is assumed to be suspended non-living POM (the model surface POM represents viable phytoplankton). In the lower layer POM concentrations are always much lower, since remineralization occurs rapidly. Increases in lower layer POM are seen after surface blooms and are larger over the shelf mainly because the POM flux is confined to a smaller volume of water and also because overlying productivity is higher.

PON and POC data were collected at four stations (outer-shelf, C4 and G3; slope C9 and G7) during this study (year days 196 and 204, Chapter 2), and were integrated over the the model upper layer depth (Table 4.2). Additional data collected at C4 and C9 in May 1998 (year days 135 and 136) (D. Varela, pers. com.) are also shown in Table 4.2. The modelled values reproduce the data, although they span a greater range than the data. There are no observations that are as high as the maximum model values. However, no data were collected during upwelling events (when the maximum model values occur). The C line (July) was sampled at the end of an unusual period of summer downwelling

(Section 2.3.1) when POM is expected to be low (values at C4 reflect the VICC nutrient source). The G line was sampled after upwelling and measurements were not made within the main upwelled plume (centered on G4, Figure 2.10). Thus, maximum POM values are not expected in these data. However, measurements made in the Oregon upwelling region (Hill, 1999) include maximum values similar to the model (PON, 12 – 16  $\mu\text{M}$ ; POC, 90 - 110  $\mu\text{M}$  between year days 199 – 218 over the upper 15 – 20 m of the water column). Note that POM measurements are made by filtering water samples and may include non-living POM as well as living, while in the model surface POM is all living.

Table 4.2: Average PON and POC integrated over the model upper layer depth and integrated  $pp$ . The year day (YD) is presented with the calendar day.

Date	Station	$\overline{\text{PON}}$ ( $\mu\text{M}$ )	$\overline{\text{POC}}$ ( $\mu\text{M}$ )	$\overline{pp}$ (g C m <sup>-2</sup> d <sup>-1</sup> )
Vancouver Island Coastal Current				
May 15 / YD135	C4	4.5	35	1.7
July 15 / YD196	C4	6.7	38	2.5
Outer-Shelf				
July 23 / YD204	G3	8.9	52	1.6
Slope				
May 16 / YD136	C9	1.4	9.6	0.3
July 15 / YD196	C9	2.1	13.3	0.6
July 23 / YD204	G7	1.5	8.4	0.9

#### 4.4 Dissolved Organic Matter

The annual cycles of DON and DOC are shown in Figures 4.6 and 4.7, respectively. The production of dissolved organic matter (DOM) differs from that of POM. In the surface layer an increase in the maximum POM occurs when phytoplankton growth conditions are favourable, while maximum increases in DOM occur later, when the POM pool is decaying. Thus, increases in DOM concentration lag increases in POM. In the

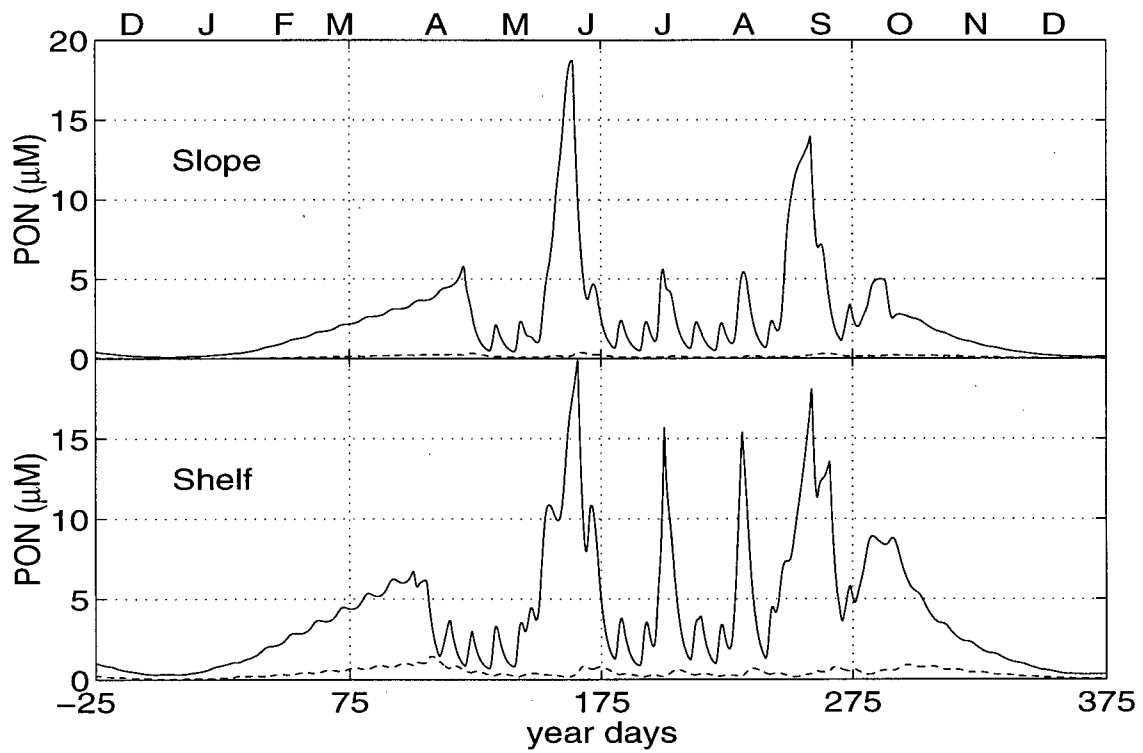


Figure 4.4: The annual particulate organic nitrogen cycle for a typical model run (using parameters from Tables 3.2 and 3.3) for upper layers (— solid lines) and lower layers (- - dashed line) over the slope (upper panel) and the shelf (lower panel).

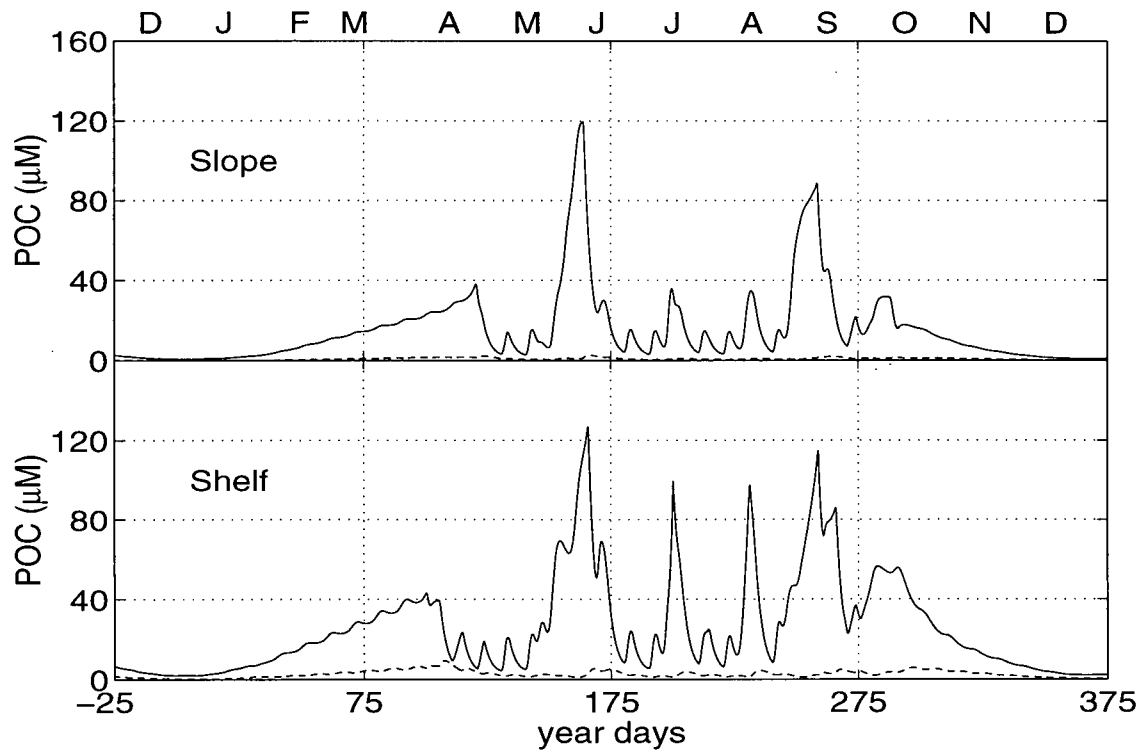


Figure 4.5: The annual particulate organic carbon cycle for a typical model run (using parameters from Tables 3.2 and 3.3) for upper layers (— solid lines) and lower layers (- - dashed line) over the slope (upper panel) and the shelf (lower panel).

lower layer, DOM concentrations are much smaller than in the surface (like POM). As a result, DOM concentrations are noticeably diluted by upwelling events (e.g. events on year days 159 and 199) (while POM increases immediately when an event occurs). Also, remineralization scales for DOM (the semi-labile fraction) are longer than POM so DOM concentrations are higher throughout the year. DOC and DON production are not always coupled because DOC is produced (but not DON) when excess carbon uptake occurs (Section 3.2.4). In addition, the remineralization rate for DON is slightly larger than for DOC.

Over both the shelf and slope, DOM increases in the spring following the initial bloom. DON concentrations stay within the 12  $\mu\text{M}$  range for most of the summer, with occasional decreases when upwelled water causes dilution. DOC concentrations are similar, but since DOC production can occur when DIN is limiting (but DON cannot) they are not as steady as DON and there is an increasing trend throughout the summer. In the lower layer, DOM concentrations are relatively constant. They increase due to vertical mixing and entrainment when DOM concentrations are high in the surface and decrease due to remineralization and also due to dilution by upwelling in the case of the lower shelf (as advection brings lower slope water onto the shelf).

Only the semi-labile fraction of the DOM is modelled. It is difficult to compare the model DOM to data (i.e. bulk measurements) because this fraction is poorly known (it has been estimated to be around 30% in the open ocean (Carlson et al. (1994)). In addition, model 'dissolved' is defined as non-sinking rather than by particle size (which defines measured DOM). Some portions of the measured POM are likely suspended and non-living. Thus, the model DOM is expected to be larger than the measured semi-labile portion. To compare model results with data, total organic (TO) concentrations should be used, recognizing that a portion of the measured TOM is refractory DOM and not present in the model. We collected TOC samples, but unfortunately they were

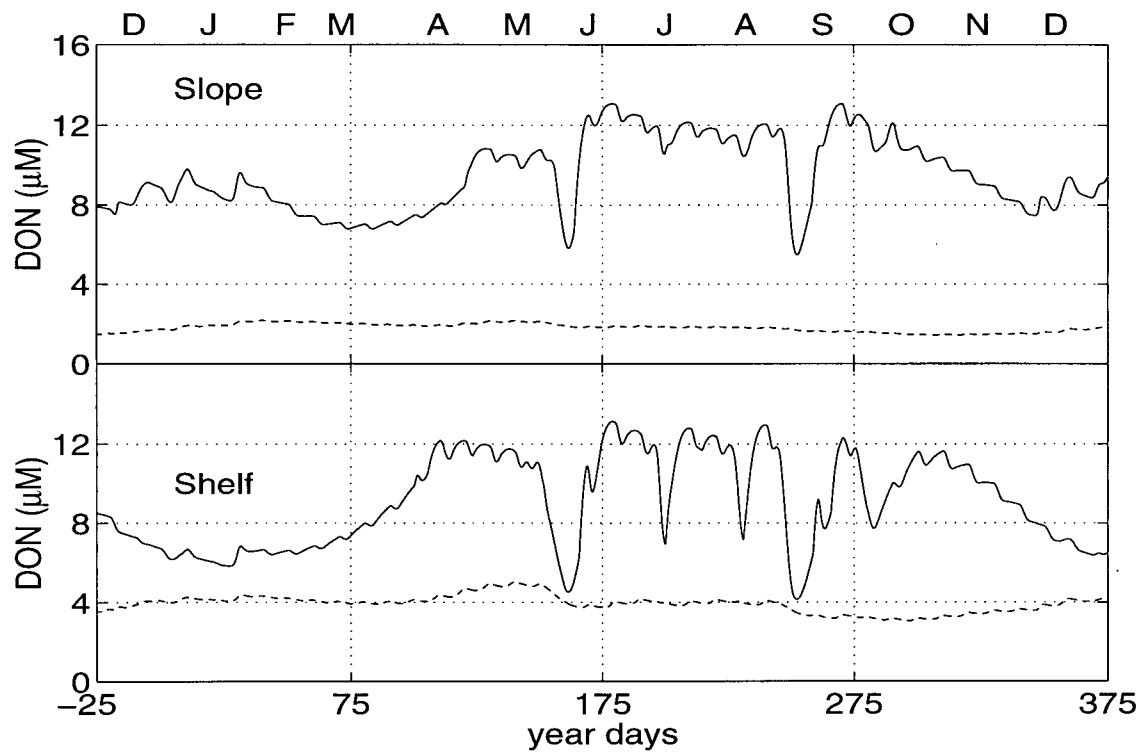


Figure 4.6: The annual dissolved organic nitrogen cycle for a typical model run (using parameters from Tables 3.2 and 3.3) for upper layers (— solid lines) and lower layers (- - dashed line) over the slope (upper panel) and the shelf (lower panel).

contaminated (measured values exceeded what was expected by more than an order of magnitude). As a result, I compare the model results with data from the Oregon upwelling region (Hill, 1999) in the following chapter.

#### 4.5 Comparison of Model Fluxes with Data

The only modelled flux that was directly measured is biological uptake of carbon, i.e. primary production. Daily integrated *pp* measurements over the shelf (C4, G3) and slope (C9, G7) are presented in Table 4.2 along with the POM data (these data were

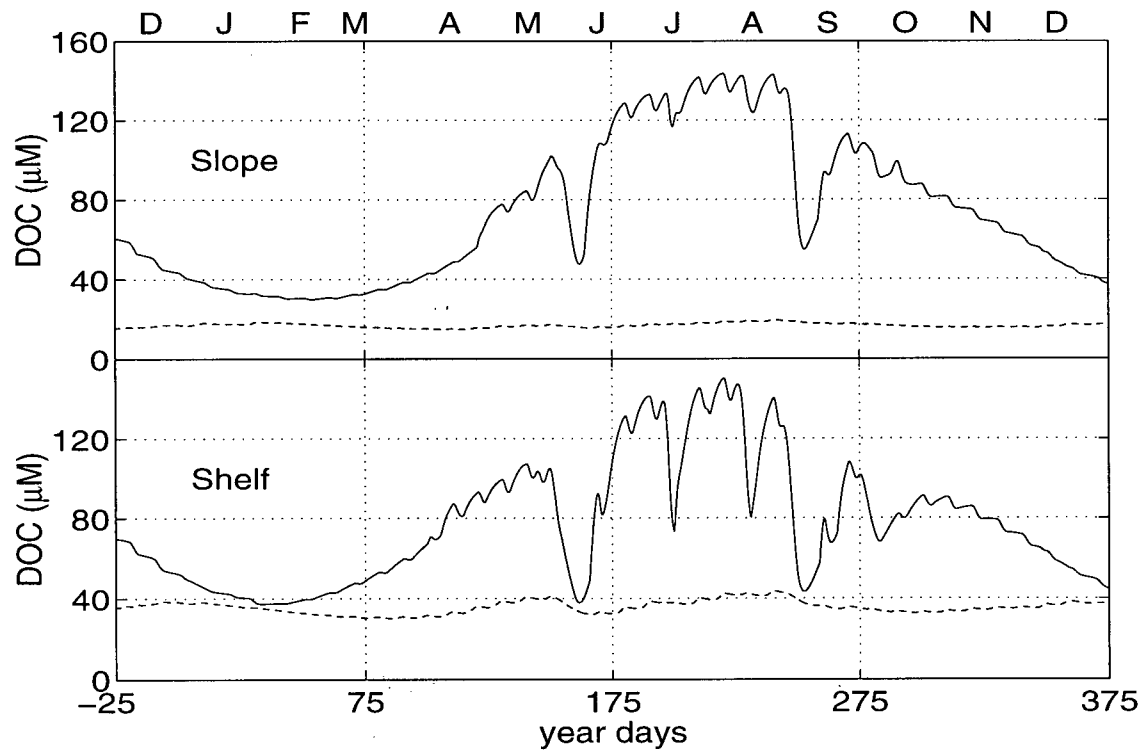


Figure 4.7: The annual dissolved organic carbon cycle for a typical model run (using parameters from Tables 3.2 and 3.3) for upper layers (— solid lines) and lower layers (- - dashed line) over the slope (upper panel) and the shelf (lower panel).

collected at the same time). In May, the model  $pp$  is 1.6 and 0.3 g C m<sup>-2</sup> d<sup>-1</sup> over the shelf and slope, respectively, while in July, model  $pp$  ranges from 0.1 – 3.7 and 0.1 – 2.5 g C m<sup>-2</sup> d<sup>-1</sup> over the shelf and slope, respectively (Figures 3.6 and 3.7). Nutrient depletion between storms and upwelling events are responsible for the low end of the ranges in the July model results, while maximum values occur during upwelling periods. In May, the modelled shelf  $pp$  is similar to the measured  $pp$  at C4 (over the shelf and may be within the VICC). The model slope  $pp$  in May is significantly higher than the measured value. During mid-May in the model the spring bloom is occurring in both the shelf and slope region. The July measurements agree well with the model considering that the measurements were not made when  $pp$  was expected to be maximum (discussed above in Section 4.3). The model peaks in  $pp$  have short durations and the average model  $pp$  in July is closer to 1 g C m<sup>-2</sup> d<sup>-1</sup> and < 0.5 g C m<sup>-2</sup> d<sup>-1</sup> over the shelf and slope, respectively. Measured  $pp$  is in the upper half of the model range over the shelf (C4 and G3) which is consistent with the fact that both stations were productive (C4 due to the VICC and G3 due to the influence of the previous upwelling event), but neither were during upwelling events. Over the slope, the measurements fall in the low to middle part of the model range but above average at G7 following upwelling.

Air-sea CO<sub>2</sub> flux is estimated from  $p\text{CO}_2$  in both the data and model. In both cases DIC and alkalinity (TA) were used to calculate  $p\text{CO}_2$ . The model TA was calculated using the TA–salinity regression determined from the data and the modelled salinity was tuned to reproduce the data. Thus, differences in modelled  $p\text{CO}_2$  and data-derived  $p\text{CO}_2$  are the result of differences in modelled and measured DIC (shown in Figure 4.3). There are fewer measured surface  $p\text{CO}_2$  than DIC data as simultaneous surface DIC and TA measurements were not always available (Tables 2.1 and 2.2). In general, the range in the measured  $p\text{CO}_2$  (and thus CO<sub>2</sub> gas flux) is larger than the model range. The high end of the measured range occurs in the VICC (due to high surface DIC) and the low end over

the shelf after upwelling. The model is not able to reproduce the lowest data-derived  $p\text{CO}_2$ .

#### 4.6 Conclusions

The physical parameters in the model were tuned by comparing model salinity and DIN to available data in the study area. The parameters were chosen to reproduce annual cycles of DIN and surface salinity as well as possible (as these cycles are most important to the model). Modelled lower layer salinities are lower than measured salinities during the spring transition period, likely because the model lower layer open ocean salinity reflects the upper portion of the lower box (to model upwelling) rather than an integrated value over the entire vertical interface (between the lower slope and open ocean). The modelled DIC (and thus  $p\text{CO}_2$ ) agrees well with the DIC data presented in Chapter 2, although modelled surface values would be too high if there were no biological excess uptake of carbon. Both measured and modelled surface DIC values cover a large range depending on physical forcing. Model POC and PON follow the Redfield ratio and so have the same seasonal cycles. The modelled POM has high peaks of short duration that are greater than the maximum in the data (Table 4.2), but close to the maximum values collected in the Oregon upwelling region (Hill, 1999). Considering the physical regimes during data collection, both the model POM and  $pp$  seem reasonable compared with the measurements. The annual DOC and DON cycles are similar but not perfectly coupled (as the POC and PON are) because modelled biological C:N uptake ratios are not always constant and the model remineralization rate of DON is slightly higher than DOC. Comparisons of model TOC and TON (TO rather than DO because our model definition differs from the measured) with data (Hill, 1999) are discussed in the following chapter.

## Chapter 5

### Modelling the character of organic matter in a coastal upwelling region

#### 5.1 Introduction

The character of marine organic matter is complex and not well understood (Alperin et al., 1995). It is generally partitioned into either dissolved organic matter (DOM) or particulate organic matter (POM) by particle size. Nitrogen based ecological models (e.g. Spitz et al., 1999) and nitrogen budgets (e.g. Wheeler; 1993) have shown that the size and character of the dissolved organic nitrogen (DON) pool have a large impact on the system. In carbon models, remineralization rates of particulate organic carbon (POC) and dissolved organic carbon (DOC) (as well as the partitioning fraction between the two pools) (Bacastow and Maier-Reimer, 1991; Toggweiler, 1989) and the depths of remineralization (Najjar, 1992) are very important. However, in nature the constituents of each pool have a range of remineralization rates ( $r$ ) and depths ( $d$ ), the latter depending on sinking rates ( $w_s$ ) combined with remineralization rates (i.e.  $d=w_s/r$ ). In models, these ranges are usually represented by single parameters, in the same way that I have done (Chapter 3). In my model (a nitrogen-based ecological model of carbon fluxes), the character of the organic matter (DON, DOC, PON, and POC) is determined by four parameters, the fraction of the flux of non-living organic matter that is particulate rather than dissolved ( $p$ ), the remineralization rate of POM ( $r_p$ ), and the remineralization rates for DOM ( $r_d$ ) for carbon and for nitrogen.

In nature the organic pools are also active, changing form in time through aggregation and disaggregation processes. The aggregation of POM occurs mainly through particle collision and adhesion (Jackson, 1990) and also by biological repackaging (Hill, 1992). Aggregation is important because it can dramatically increase the sinking rates (hence remineralization depths) of POM (Alldredge and Silver, 1988). In the diatom dominated community that I am modelling, large pulses of phytodetritus are expected (Hansen et al., 1995) and have been observed (Peña et al., 1996). Disaggregation may be an important step in the remineralization of POM, allowing free-living, in addition to particle-attached, bacteria access to the organic matter (Karl et al., 1988; Cho and Azam, 1988). While these processes are clearly an important part of the organic matter cycle, they are complicated and difficult to model. As such, they have not been explicitly included in bulk carbon and nitrogen models.

POM flux has been characterized by decay length derived from sediment trap data (Bishop, 1989). Many difficulties exist in interpreting these data because it is unclear how much of the POM flux is being caught by the sediment traps and at which depths (e.g. Timothy and Pond, 1997). Many particles may not sink vertically, rather they are suspended and are easily advected, settling slowly. Two findings are clear however. First, the bulk of the sedimenting flux comes from rare, large particles (McCave, 1975). Second, the large particles have high, extremely variable sinking rates (e.g. marine snow ( $1-370 \text{ m d}^{-1}$ ) (Alldredge and Silver, 1988))

The DOM pool has been separated into three pools according to lability based on open ocean data (Carlson et al., 1994; Carlson and Ducklow, 1995). The labile pool is difficult to measure and has extremely rapid turnover rates (order hours to days). The semi-labile pool makes up about 30% of the measurable DOM and is remineralized over seasonal time scales. The majority (70%) of the pool is considered refractory and has a lifetime of about 1000 yr.

The modelled annual organic matter cycle is discussed and compared with data from the Oregon upwelling region (shown in Appendix H) (Hill, 1999). Model results are also compared with data over the shorter time scales of upwelling events.

## 5.2 Model

Because the depth of remineralization is so important, and the existing sediment trap data applies to the 'sinking' particulate flux, I chose to partition organic matter by whether it sinks or not, rather than by filter pore size, which is the current standard. This choice means that the non-living particulate organic (PO) pools sink into the lower layer immediately (i.e. within one time step of the model) (Section 3.2.4, Figure 3.3). This is justified given that physical aggregation processes are expected to be important in the study area, particularly when PO concentrations (and thus fluxes) are high. Also, it allows more confidence in the value of the remineralization rate of POM ( $r_p$ ) because sediment trap data are available.

The modelled dissolved organic (DO) pools are more difficult to characterize based on data as they do not correspond to the measured pools. The model DO pools include small non-living particles that do not sink (i.e. the non-living suspended portion of the measured POM); as well as traditional DOM. Additionally the model pools represent only the semi-labile portion of the DO, because the refractory portion has such slow remineralization rates that fluxes associated with them are negligible over the time-scales of interest.

To compare model results directly with data, the total organic (TO) pools are used, so that the differences in the DO and PO definition do not matter. Thus, the model TO pools are expected to be the same as the measured TO pools once the refractory portion has been subtracted.

### 5.3 Results

Hill (1999) collected organic carbon, organic nitrogen and *chl a* data from selected depths between the surface and 50 m at a single station over the outer Oregon shelf throughout the course of a year. For two months during the upwelling season, sampling was weekly and during the rest of the year samples were collected roughly monthly (Figures H.1 and H.2). These data show that during upwelling DOC is diluted, while DON, POC and PON increase (Hill, 1999). Following an upwelling event, DOC increases and POC and PON decrease. He suggests that all the increases are associated with high primary production (*pp*) in response to upwelled nutrients and the decrease in POC and PON occurs when nutrients become exhausted. These results are logical and the model confirms them with the exception of the increase in DON during upwelling.

A time series of model DOC, DON, POC and DIN that includes two upwelling events of varying strength and duration (the first strong and long, centered on day 159; the second moderate and short, centered on day 199) is presented in Figures 5.1 and 5.2 for the upper shelf and slope boxes, respectively. The model parameters, advective and storm forcing (Tables 3.2 and 3.3, Figure 3.4 and Appendix D, respectively) were set for a typical model run as described in Section 3.2. Only POC (not PON) is shown as the C:N ratio in the POM is set. Upwelling occurs over the shelf (Figure 5.1) so the upwelling events and responses are strongest there. DIN is shown in the lower panel of each figure (note that the DIN scale in the slope plot is reduced by a factor of three). The first event is large and extends over about one week and DIN is advected into the slope box causing a noticeable peak (Figure 5.2). The second event is much shorter; any DIN that is advected to the slope is used up too quickly to accumulate. However, a response still occurs as an increase in POC (Figure 5.2). POC (lower panel in each figure, with a slightly reduced POC scale over the slope) increases in response to upwelled fluxes and

also to entrainment from storm forcing, the latter causing modulation at 10 d periods. The response in POC over the shelf to the strong upwelling event (day 159) extends over many days because POC is being advected to the slope as it is being produced. The peak in POC occurs after advection decreases.

DOC and DON are shown in the upper panel of each figure (scales do not differ between shelf and slope). While they are not perfectly coupled (they have slightly different remineralization rates and their production is not always coupled (Section 3.2)) their trends are similar, as expected. Between upwelling events (days 125 – 150, 175 – 195 and 225 – 250), after the initial increase associated with the bloom, DON decreases due to remineralization (and decreased production) while DOC increases as light is not limiting and there is continued DOC production because of the excess carbon uptake term (which slightly exceeds DOC remineralization). Over the shelf, upwelling dilutes both DOC and DON (Figure 5.1, days 151 – 165) and then both increase as they are produced by the resultant phytoplankton bloom. Dilution is expected as the upwelled water from the lower layer has low concentrations of DOM. For either DOC or DON to increase or to remain constant over the shelf (as in the case of DON in the Oregon data), their vertical gradients would have to be small. Small gradients between blooms would imply that the remineralization rates of DOC and DON were fast, so that they could only accumulate in the surface layer when production was high.

Over the slope (Figure 5.2) dilution of DOC and DON in the surface box are not necessarily expected because the source of advected water is the surface shelf box. The response to the first upwelling event over the slope is the same as over the shelf. This event is large enough that DIN and water replete in DOM are advected horizontally. However, the narrow, moderate event is different. In this case POC is advected from the shelf to the slope and the dilution of DOC and DON is small.

Our DOM pools differ from those in the Oregon data however. In Figure 5.3 we

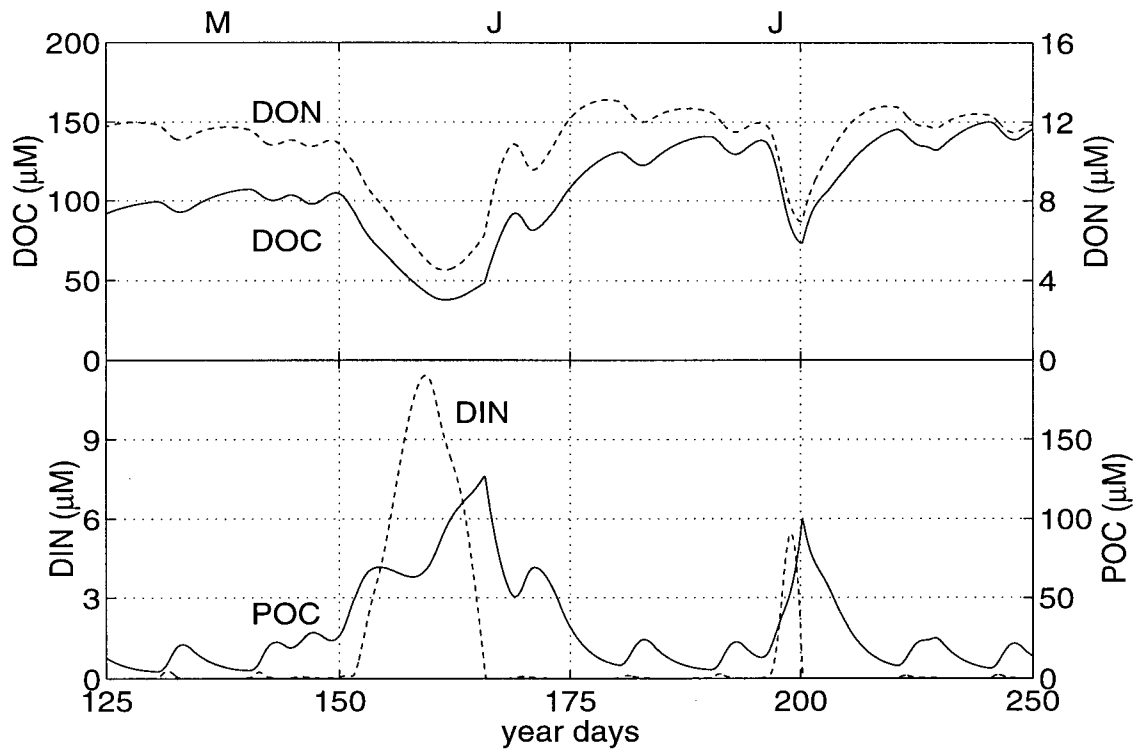


Figure 5.1: DIN (- - dashed line) with POC (— solid line) (lower panel), and DOC (— solid line) and DON (- - dashed line) (upper panel) over two upwelling events (the first centered on day 159 and the second on day 199) all in the surface shelf box.

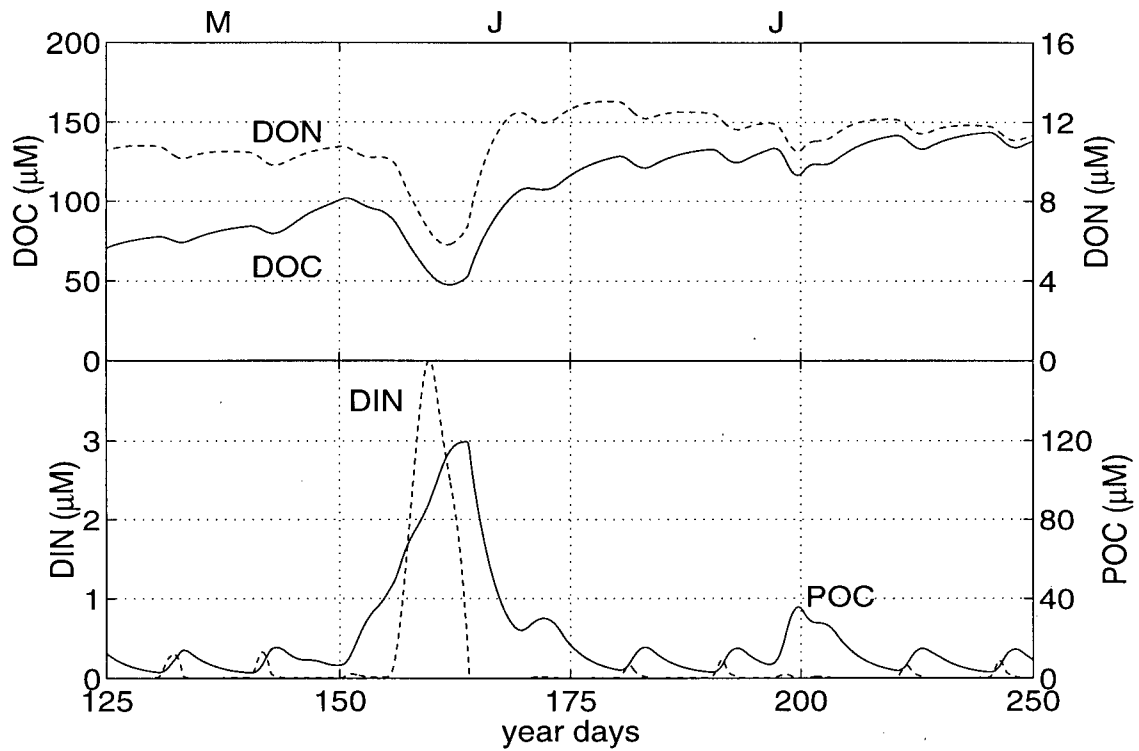


Figure 5.2: DIN (--- dashed line) with POC (— solid line) (lower panel), and DOC (— solid line) and dissolved organic nitrogen (--- dashed line) (upper panel) over two upwelling events (the first centered on day 159 and the second on day 199) in the surface slope box.

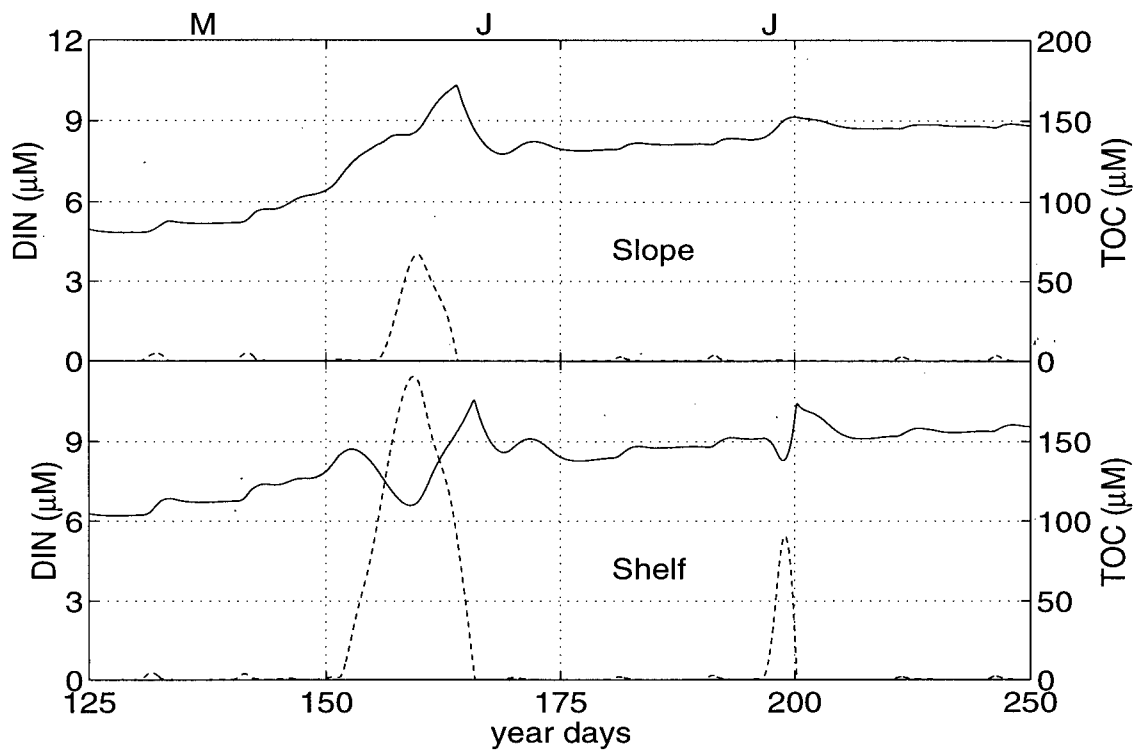


Figure 5.3: DIN (— dashed line) with TOC (— solid line) over the shelf (lower panel) and slope (upper panel) during two upwelling events (the first centered on day 159 and the second on day 199).

present the shelf and slope responses in TOC to compare with the Oregon data. (TON behaves similarly.) DIN in each panel increases with upwelling. Over the shelf TOC is briefly diluted in response to both upwelling events, but increases immediately afterwards. Furthermore, the smaller event causes little dilution and only for a short interval. The response is quite different over the slope. There is no dilution of TOC by upwelling. The increase in TOC occurs immediately because TOC is advected from the surface shelf box to the slope and is produced locally by increased biological uptake (by the POC fraction) due to advected DIN.

The modelled annual cycles of TOC (Figure 5.4) and TON (Figure 5.5) follow the Oregon data reasonably well (Figures H.1 and H.2). The total organic matter (TOM) concentrations in the surface layer are high over the summer, varying due to advection, mixing and primary production and then decrease to less than 30% of their summer concentrations during winter when production is low. The absolute values of the model TOC and TON are similar to observations. The modelled TOM is  $\sim 20\%$  less than the measured TOM over the shelf in summer and winter (and  $\sim 30\%$  less over the slope in winter). (Differences are more difficult to estimate in winter, particularly with TON, because measured values are low and data are more sparse.) The measured TOM includes pools of all lability while the modelled TOM only includes the semi-labile DOM and the relatively labile POM. Thus, the model results suggest that the refractory DOM pool makes up about 20% of the TOM, which is much less than what has been estimated in the open ocean (approximately 70%, Carlson et al., 1994; Carlson and Ducklow, 1995).

The ratios of model DOC:DON range from 7.5 (when  $pp$  is highest) to 12 (when  $pp$  is not high). Depth integrated (over the upper 50 m of the water column) values of DOC:DON from the Oregon data range from 9 (in mid-summer) to 15 (in fall). Because our model DOM includes not only the measured DOM, but also some (non-sinking) POM, which has a C:N ratio of 6.6, this comparison with data is reasonable. The measured TOC:TON ratio ranges from 8 – 14. Our model TOC:TON is lower, 7 – 11.5; however, the refractory portion is missing from our results and that portion may have a higher C:N ratio.

#### 5.4 Discussion and Conclusions

Our model reproduces the upwelling responses of the Oregon DOM and POM data reasonably well. In the model, DOM is diluted by upwelled water and then increases following

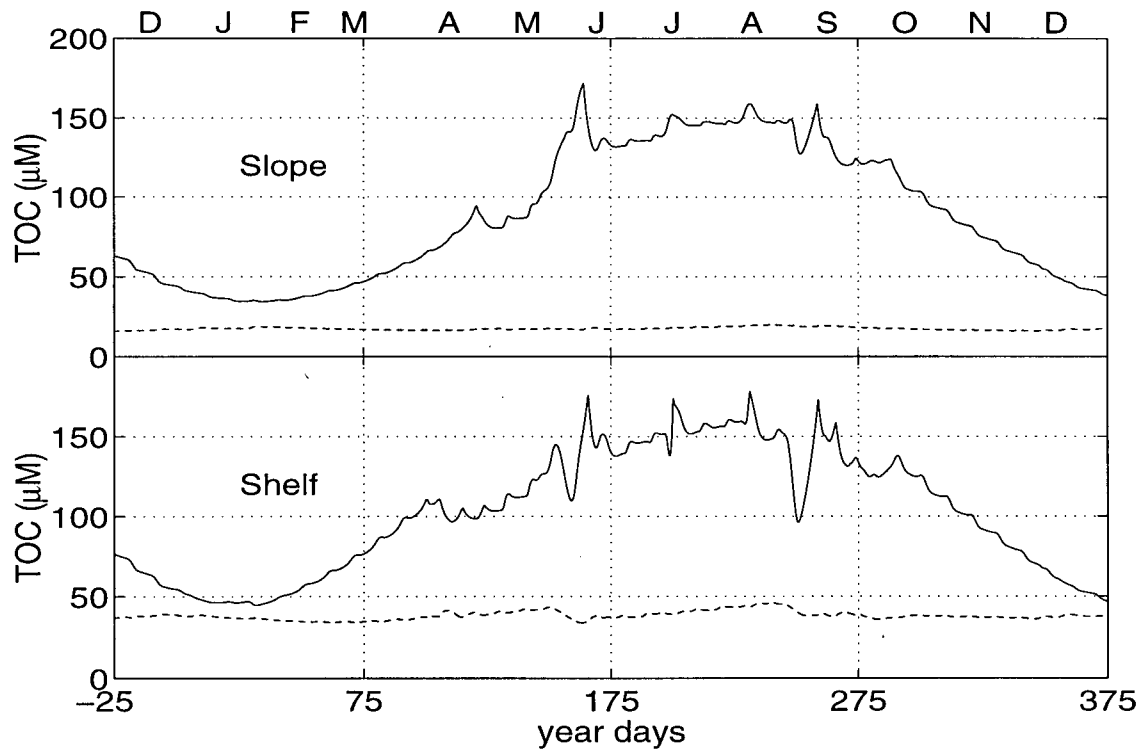


Figure 5.4: The annual cycle of TOC for the shelf (lower panel) and the slope (upper panel) boxes for the upper layer (— solid line) and the lower layer (- - dashed line).

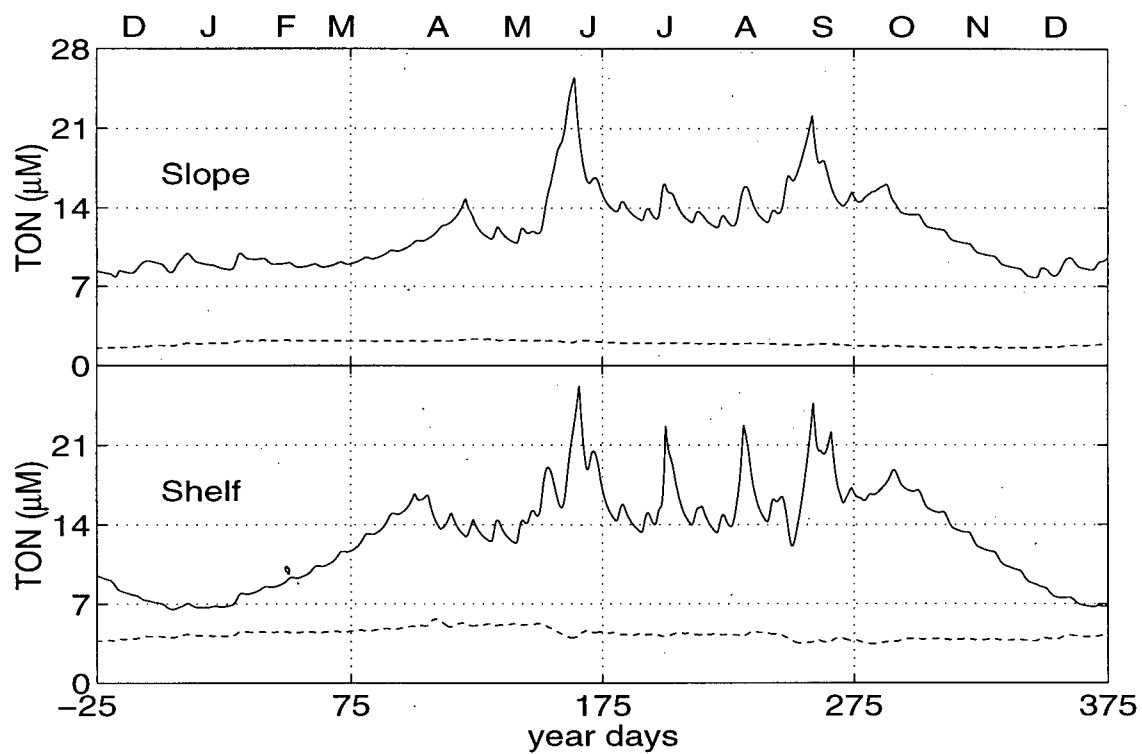


Figure 5.5: The annual cycle of TON for the shelf (lower panel) and the slope (upper panel) boxes for the upper layer (— solid line) and the lower layer (- - dashed line).

a phytoplankton bloom. POC increases with upwelling due to primary production in response to DIN supply. Our model shows the dilution of DON (or TON); however, the data do not. Upwelled water has lower DOM concentrations unless time scales of remineralization are shorter than is expected (seasonal). Therefore, dilution of surface DOM is expected to occur directly over an upwelled plume. The dilution of TOM is less than for DOM and lasts for a shorter time because the POM fraction increases so rapidly. Off-shore of the main upwelling, where the effects of upwelling are still evident (slope region), increases in TOM can occur. It is possible that the data were not collected directly over the upwelled plume and so dilution was not observed. It is also possible that the temporal resolution (order 7 days) was not high enough to observe the dilution, especially if the upwelling pulse was short, as in our second example. It is interesting that, in the data, DOC was diluted upon upwelling but DON was not. The model cannot reproduce this decoupling of nitrogen and carbon whether DOM or TOM is considered. However, it has been suggested that the production of DON and DOC is indeed decoupled (P. Wheeler, pers. com.). Perhaps production of DON in nature is more closely related to primary production (i.e. production of POM) than is DOC. Also, the water collected in the Oregon study was not immediately subsampled for DOM and quick frozen. Although the delay period was only 3 – 6 h, perhaps conditions (such as darkness) between sampling and filtering stimulated phytoplankton to excrete DON.

Both the modelled TOC and TON pools are larger than expected if the refractory portion of the DOM were 70%. If my model is correct (and the DO matter could be well characterized by only one remineralization rate) then results would suggest that the refractory portion makes up  $\sim 20\%$  of the TOM, i.e.  $< 25\%$  of the DOM. The model remineralization rates were constrained by winter and summer quasi-steady state solutions (Appendix F). To obtain these solutions, primary production was specified, rather

than model determined. In winter, when little organic matter is produced, the state variables resemble this solution; however, during summer the non-linear solution has higher primary production than was set in the steady state solution and hence higher DOM. Although modelled primary production is higher than was estimated, it is reasonable given recent measurements off Vancouver Island (see comparison in Chapter 4). Primary production was not measured by Hill (1999). The remineralization rates, or the fraction  $p$  that becomes POM (rather than DOM) could be increased so that model DOM would be smaller, but these rates ( $r_d$ ) are already at the high end of their expected range (see Appendix F) and  $p$  is also high (0.6). It is also possible that the refractory portion of the DOM is  $< 70\%$ , particularly in coastal areas where production is high. More realistically the DOM pools could be represented by probability distributions with variable lability as is discussed in the next chapter.

## Chapter 6

### Conclusions and Suggestions for Future Research

Below is a summary of the detailed conclusions presented at the end of the previous four chapters (the data, Chapter 2; the model development and major results, Chapter 3; a comparison of modelled state variable concentrations with data, Chapter 4; and a comparison of modelled organic matter with data from the Oregon upwelling region, Chapter 5) followed by a discussion of ideas for future work stimulated by this research.

#### 6.1 Model development

This modelling exercise was successful in that it reproduces annual cycles of carbon and nitrogen fluxes reasonably and is relatively simple. Data are scarce for many modelled quantities, particularly in the winter, but where data are available they compare well with model results (see Chapters 4 and 5). Shortcomings occur in modelling the organic matter (Chapter 5) and in modelling the flux of inorganic state variables from the deep ocean to the lower slope box (Chapter 4). These shortcomings spark ideas for future work that are described below.

The division of non-living organic matter into particulate and dissolved forms based on sinking versus buoyancy, respectively, rather than particle size, is a useful formulation developed for this model (described in Chapter 5). Also, three additions were made to the basic model (described in the original proposal for this thesis) to obtain reasonable results (described in Chapter 3). These additions differ from any previous modelling exercises of which I am aware. First, the two layer vertical structure was made more realistic

by adding a permanent pycnocline within the lower layer (Figure 3.2, Section 3.2.3). The state variables are modelled to have linear gradients in concentration between the pycnocline (at the lower layer concentration) and the bottom of the mixed layer (at the upper layer concentration). This structure produces more realistic mixed and entrained fluxes into the upper layer. In particular, with the simple two-layer structure too much nitrogen is entrained during the late summer and fall, leading to an unrealistically large fall phytoplankton bloom. Second, primary production was too high during the winter season despite realistic light and nutrient levels. I chose to make a portion of the biota (upper layer particulate organic pools) dormant during the winter. Dormancy is based on surface light levels (Section 3.2.4). Dormant cells represent the formation of non-sinking resting stages by diatoms. The third addition involved decoupling biological uptake of carbon and nitrogen so that carbon uptake is no longer set by the Redfield ratio. The biota are allowed to take-up excess carbon when nitrogen is limiting but light is not, but with reduced cellular chlorophyll (Section 3.2.4). The excess uptake is not incorporated into the biota, but instead passes directly into the dissolved organic carbon pool. Without this excess uptake, modelled dissolved inorganic carbon was greater than measured, and the ratio of total organic carbon to total organic nitrogen was not as high as measured (Hill, 1999). Furthermore, the data (Section 2.3.4) support this mechanism. Carbon was taken up in excess relative to nitrate when nitrate was limiting. The data also show that the ratio of carbon to nitrogen in the particulate organic matter remained relatively constant regardless of nitrate limitation.

## **6.2 Conclusions**

The model results suggest that coastal upwelling regions do not sequester atmospheric carbon, rather they are conduits for sub-surface inorganic carbon to reach the surface

of the open ocean. Lower layer nitrogen and carbon inventories are high over the shelf (relative to the neighbouring open ocean) and so winter mixing brings large quantities of both to the surface. Thus, over the shelf there is substantial CO<sub>2</sub> gas evasion during winter that almost balances gas invasion due to biological drawdown in the summer. The winter season also affects summer primary production, as strong winter downwelling decreases nutrient fluxes during the following summer. Furthermore, data show that the inner-shelf buoyancy current has high dissolved inorganic carbon concentrations and is likely a source of carbon to the atmosphere throughout the year. These results are discussed in the following.

Despite high productivity and export flux of organic matter, coastal upwelling regions do not operate as strong biological pumps. Both the model and the data show that biological drawdown of pCO<sub>2</sub> over the outer shelf is high during the summer in agreement with observations off the Californian (Simpson, 1986; Friederich et al., 1994) and Peruvian coasts (Simpson and Zirino, 1980). However, the model also shows that winter gas evasion almost completely cancels summer gas invasion. The result is a small net annual influx of atmospheric CO<sub>2</sub> to the system (Section 3.4.2) rather than the large flux that was predicted by Friederich et al. (1994). The fate of this absorbed carbon is probably export (mainly by advection) in the form of inorganic carbon or possibly organic carbon (in equal portions of non-living dissolved and living particulate) to the surface layer of the open ocean. If the latter is the case, most of it is likely remineralized in the surface and potentially degassed. Export of organic carbon in the lower layer, especially in particulate form, is almost negligible. Furthermore, the net annual fluxes of inorganic carbon between the open ocean and the model system are large (Section 3.4.3). During the upwelling season inorganic carbon is advected from the open ocean lower layer over the continental shelf and into the surface layer. Some of this carbon is used biologically, but most of it is advected offshore in the surface ocean. Winter advection of carbon

from the model system into the lower layer of the open ocean is significantly less and even during downwelling winter mixing brings DIC into the surface layer. Further south (e.g. California and Peru) where there is little or no downwelling this effect would be expected to be even stronger. With no downwelling there is less export of DIC (and DIN) to the open ocean in the lower layer. In addition the mixed and entrained flux of lower layer DIC into the surface during winter would be larger without the downwelling circulation. Thus, coastal upwelling systems operate as a short circuit path to the surface for sub-surface inorganic carbon, potentially having a large impact on the global carbon budget.

In our study area there is an additional source of carbon from the Vancouver Island Coastal Current (VICC) (although the net carbon flux from the VICC is small relative to the upwelled flux). Carbon system measurements show that the surface  $p\text{CO}_2$  is very high within this current, which could mean that appreciable gas evasion occurs over the southern inner-shelf off Vancouver Island throughout the year (Section 2.3.2). The surface area of this current is not large in a global sense. However, this result provokes questions about inorganic carbon concentrations in other dynamic coastal regimes where mixing is as intense as it is in the Haro Strait (the source of this current) (Pawlowicz and Farmer, 1998).

Both the data and the model show that there are higher nutrient inventories over the outer-shelf relative to offshore (Section 2.3.2 and Section 3.4.1). These high inventories are caused by the high production in the surface waters. The vertically exported organic matter associated with this production is remineralized in a volume of water that is limited by bathymetry, thus concentrating inorganic nutrients relative to deeper waters. Globally, primary production is higher in the coastal ocean (Eppley and Petersen, 1979) than in the open ocean and, if the above result can be extrapolated, it may have implications to the global carbon budget. To obtain a global estimate of the contribution of

continental shelves to CO<sub>2</sub> sequestration by the oceans the many different types of shelf systems (in addition to the coastal upwelling systems) need to be considered separately.

Nitrogen and carbon inventories regulate both primary production and carbon fluxes in the system because over the shelf a large fraction of lower layer water is mixed into the upper layer, especially during fall and winter. In winter, when biological uptake is low, nitrogen and carbon accumulate in the surface and sensitivities to model parameters show most strongly. For example, changes in net annual CO<sub>2</sub> gas exchange (from changes in parameters) are due to different values of the winter pCO<sub>2</sub> (with the exception of removing excess carbon uptake) (Section 3.4.2). Furthermore, the strength of winter downwelling can affect the summer season by decreasing the nitrogen inventory in the system. When downwelling is enhanced and upwelling unchanged (our simulation of El Niño-Southern Oscillation Events), summer production decreases significantly because upwelled water is relatively depleted in nitrogen (Section 3.4.1). With the exception of salinity, few measurements of any of the state variables are available for the winter season and I obtained inorganic carbon data only on one summer cruise in the study area. The results of this thesis show how important winter data are to understand the system, despite the fact that the large biological fluxes all occur in summer.

The most important and least known parameters in the system involve characterization of the non-living organic matter pool (which affects nutrient inventories and thus surface nitrogen and carbon concentrations in the winter). They are the fraction  $p$ , the portion of the decay flux from the biota that goes into the particulate organic pool rather than the dissolved organic pool, and the remineralization rates of dissolved organic matter ( $r_d$ ). The remineralization rate of particulate organic matter (POM),  $r_p$ , is less important because it is high enough that almost all remineralization occurs before POM can be advected out of the system. The model is also sensitive to changes in the phytoplankton growth rate as a function of light intensity at low light levels ( $\alpha$ ), but not maximum

growth rate because light levels are often low throughout the year at mid-latitudes.

### 6.3 Future Research

Some suggestions for future modelling research are discussed below, beginning with the simplest and most practical, and then becoming more grandiose and hypothetical. Ideas for future data-based research are presented last.

The carbon and nitrogen concentrations of lower layer ocean water that are advected and mixed into the model system are important in setting inventories for these concentrations. It was challenging to reproduce salinity and nitrate data with the physical model using fixed lower layer ocean state variable concentrations from the same depth (Chapter 4). These concentrations were limited to data from a depth range of 150 – 250 m, the expected source of upwelled water. Advective fluxes should come from this range; however, horizontally mixed fluxes do not come from a limited depth range. A simple addition to this model would be to separate the source concentrations for mixing (to make them representative of concentrations of state variables integrated over the vertical interface between the lower slope and open ocean boxes) and advection from the lower layer to make them more realistic.

The dissolved organic remineralization rates  $r_d$  for carbon and nitrogen are important in the model. These parameters are poorly known, but it is known that they represent a wide range of remineralization rates. Also the rates that were used in the model are high relative to the expected ranges, but the dissolved organic matter (DOM) pools are larger than expected (Section 5.3). It would be interesting to explore the use of probability distributions (like those used by Hurtt and Armstrong (1996) for phytoplankton size classes) with variable lability for DOM. In particular, when primary production is high, a larger fraction of produced DOM could be made more labile. Probability distributions require

the addition of considerable complexity; however, in the case of DOM this complexity may be useful. An alternate (and simpler) way to implement variable remineralization of DOM would be to model the DOM as two portions (each with its characteristic  $r_d$ ), the more labile and the semi-labile. A saturation function could be used for the fraction ( $x$ ) of the total DOM which is more labile that would asymptote to a maximum fraction (say 0.9) when DOM concentrations were high (e.g.  $x = 0.9 \text{ DOM} / (k + \text{DOM})$ , where  $k$  would be the half-saturation constant).

Future research of the most interest to me would be application of this model to another coastal upwelling region to compare results, in particular net annual export fluxes of carbon between the model system and the open ocean. The area-specific physical parameterization is very important (for example the effect of buoyancy fluxes on alkalinity). Parameterization of one of the highly productive regions farther south (e.g. Oregon or California) should work well. More data are available in these areas and buoyancy fluxes are smaller. Inner-shelf processes may be less complicated (compared with the VICC), although large riverine input of organic matter from the Columbia River would provide a new challenge.

Another interesting challenge would be to introduce zooplankton to the biological model to see what the ecological impacts would be. The first question would be if meaningful results could be obtained using a simple bulk physical model, rather than a vertically resolved one.

An additional exercise (suggested by J. Allen, Oregon State University) would be to compare the physical fluxes (advection, vertical and horizontal mixing) in my model with results from the complex physical coastal upwelling model of Allen et al. (1995) integrated over the box sizes of my model, through an upwelling event. This exercise would provide a good test of the physical reality of the model.

The biological component of the model may have interesting applications to more

complex, vertically-resolved models because of its definition of non-living organic matter (that the particulate fraction sinks and the dissolved does not sink). An additional state variable would be required because living POM and detrital POM would be sometimes found in the same compartment. Also, the sinking rate of the non-living POM would be needed as an additional parameter. Still, if these sinking rates were well related to the compartment size and time-step, the formulation could be useful. It would be interesting to see if there were improvements over bulk models and what the differences between the two approaches would be.

Finally, the model points to a strong need for winter measurements of model quantities and parameters, in particular inorganic carbon and primary production. Winter measurements could test the model results that high carbon inventories are ventilated during the winter season. It would also be interesting to compile existing coastal data sets to see if nitrogen and carbon inventories are higher in coastal areas than in surrounding waters (as discussed above) and to investigate the implications.

## Bibliography

- [1] Alldredge, A. L., and M. W. Silver. 1988. Characteristics, dynamics and significance of marine snow. *Prog. in Oceanog.*, **20**, 41–82.
- [2] Allen, J. S., and P. A. Newberger. 1996. Downwelling circulation on the Oregon continental shelf. Part I: Response to idealized forcing. *J. Phys. Oceanog.*, **26**, 2011–2035.
- [3] Allen, J. S., P. A. Newberger, and J. Federiuk. 1995. Upwelling circulation on the Oregon continental shelf. Part I: Response to idealized forcing. *J. Phys. Oceanog.*, **25**, 1843–1866.
- [4] Allen, S. E., C. Vindeirinho, R. E. Thomson, M. G. G. Foreman, and D. L. Mackas. 2000. *Physical and biological processes over a submarine canyon during an upwelling event. Can. J. Fish. Aquat. Sci., GLOBEC Special Issue*, in press.
- [5] Archer, D., S. Emerson, T. Powell, and C. S. Wong. 1993. Numerical hindcasting of sea surface pCO<sub>2</sub> at weathership Station Papa. *Prog. in Oceanog.*, **32**, 319–351.
- [6] Archer, D. E., and E. Maier-Reimer. 1994. Effects of deep-sea sedimentary calcite preservation on atmospheric CO<sub>2</sub>. *Nature*, **367**, 260–264.
- [7] Bacastow, R., and E. Maier-Reimer. 1991. Dissolved organic carbon in modelling oceanic new production. *Global Biogeochem. Cycles*, **5**, 71–85.
- [8] Barton, E. D., A. Huyer, and R. L. Smith. 1977. Temporal variation observed in the hydrographic regime near Cabo Corveiro in the northwest African upwelling region. *Deep Sea Res.*, **24**, 7–23.
- [9] Batchelder, H. P., C. A. Edwards, and T. M. Powell. 2000. Individual-based models of zooplankton populations in coastal upwelling regions: implications of diel vertical migration on demographic success and nearshore retention. *Prog. in Oceanog.*, submitted.
- [10] BCDA. n.d.. *Climatic Normals 1941–1970*. Victoria, B.C.: British Columbia Dep. of Agriculture.
- [11] Berner, R. A. 1982. Burial of organic carbon and pyrite sulfur in the modern ocean: its geochemical and environmental significance. *Am. J. Sci.*, **282**, 451–473.

- [12] Bienfang, P. K., P. J. Harrison, and L. M. Quarmby. 1982. Sinking rate response to depletion of nitrate, phosphate and silicate in four marine diatoms. *Mar. Biol.*, **67**, 295–302.
- [13] Bienfang, P. K., J. Szyper, and E. Laws. 1983. Sinking rate and pigment responses to light-limitation of a marine diatom: implications to dynamics of chlorophyll maximum layers. *Oceanologica Acta*, **6**, 55–62.
- [14] Bishop, J. K., S. E. Calvert, and M. Y. S. Soon. 1999. Spatial and temporal variability of POC in the Northeast Subarctic Pacific. *Deep Sea Res. II*, **46**, 2699–2733.
- [15] Bishop, J. K. B. 1989. Regional extremes in particulate matter composition and flux: effects on the chemistry of the ocean interior. *Pages 117–137 of: Berger, W., V. S. Smetacek, and G. Wefer (eds), Productivity of the Ocean: Present and Past.* Chichester: John Wiley.
- [16] Boyle, E. 1988. The role of vertical chemical fractionation in controlling Late Quaternary atmospheric carbon dioxide. *Jour. Geophys. Res.*, **93**, 15,701–15,714.
- [17] Calvert, S. E. 1987. Oceanographic controls on the accumulation of organic matter in marine sediments. *Pages 137–151 of: Brooks, J., and A. J. Fleet (eds), Marine petroleum source rocks.* London: Blackwell.
- [18] Carlson, C. A., and H. W. Ducklow. 1995. Dissolved organic carbon in the upper ocean of the central equatorial Pacific Ocean, 1992: Daily and finescale vertical variations. *Deep Sea Res. II*, **42**, 639–656.
- [19] Carlson, C. A., H. W. Ducklow, and A. F. Michaels. 1994. Annual flux of dissolved organic carbon from the euphotic zone in the northwestern Sargasso Sea. *Nature*, **371**, 405–408.
- [20] Cho, B. C., and F. Azam. 1988. Major role of bacteria in biogeochemical fluxes in the ocean's interior. *Nature*, **332**, 441–443.
- [21] Christensen, J. P. 1994. Carbon export from continental shelves, denitrification and atmospheric carbon export. *Cont. Shelf Res.*, **14**, 547–576.
- [22] Christensen, J. P., J. W. Murray, A. H. Devol, and L. A. Codispoti. 1987. Denitrification in continental shelf sediments has major impact on the oceanic nitrogen budget. *Global Biogeochem. Cycles*, **1**(2), 97–116.
- [23] Cochlan, W. P., P. J. Harrison, and K. L. Denman. 1991. Diel periodicity of nitrogen uptake by marine phytoplankton in nitrate-rich environments. *Limnol. Oceanogr.*, **36**(8), 1689–1700.

- [24] Codispoti, L. A., G. E. Friederich, and D. W. Hood. 1986. Variability in the inorganic carbon system of the southeastern Bering Sea shelf during spring 1980 and spring-summer 1981. *Cont. Shelf Res.*, **5**(1/2), 133–160.
- [25] Crawford, W. R., and R. K. Dewey. 1989. Turbulence and mixing: Sources of nutrients on the Vancouver Island continental shelf. *Atmos.-Ocean*, **27**, 428–442.
- [26] Crowley, T. J. 2000. Causes of climate change over the last 1000 years. *Science*, **289**, 270–277.
- [27] Cushing, D. H. 1989. A difference in structure between ecosystems in strongly stratified waters and those that are only weakly stratified. *J. Plank. Res.*, **11**(1), 1–13.
- [28] Denman, K. L., and M. A. Peña. 1999. A coupled 1D biological/physical model of the northeast subarctic Pacific Ocean with iron limitation. *Deep Sea Res. II*, **46**(11-12), 2877–2908.
- [29] Denman, K., E. Hofmann, and H. Marchant. 1996. Marine biotic responses to environmental change and feedbacks to climate. *Pages 487–516 of: Houghton, J. T., and et al. (eds), Climate Change 1995, IPCC.* Cambridge Univ. Press.
- [30] Dickson, A. G., and C. Goyet. 1994. *Handbook of Methods for the Analysis of the Various Parameters of the Carbon Dioxide system in Sea Water; Version 2.* Washington, D.C.: ORNL/CDIAC-74, DOE.
- [31] Doney, S. C. 1999. Marine biogeochemical modelling challenges. *Global Biogeochem. Cycles*, **13**(3), 705–714.
- [32] Doney, S. C., D. M. Glover, and R. G. Najjar. 1996. A new coupled one-dimension biological-physical model for the upper ocean: applications to the JGOFS Bermuda Atlantic Time Series (BATS) site. *Deep Sea Res. II*, **43**, 591–624.
- [33] Dugdale, R. C., and J. J. Goering. 1967. Uptake of new and regenerated forms of nitrogen in primary productivity. *Limnol. Oceanogr.*, **12**, 196–206.
- [34] Dugdale, R. C., F. P. Wilkerson, and H. J. Minas. 1995. The role of a silicate pump in driving new production. *Deep Sea Res. I*, **42**, 697–719.
- [35] Ekman, V. W. 1905. On the influence of the earth's rotation on ocean currents. *Arkiv fur Matematik, Astronomi och Fysik*, **2**(11), 52.
- [36] Eppley, R. W., and B. J. Peterson. 1979. Particulate organic matter flux and planktonic new production in the deep ocean. *Nature*, **282**, 677–680.

- [37] Eurin, D. 1999. *Circulation and cross-shelf exchanges over an irregular topography*. M.Sc. thesis, University of British Columbia, Vancouver, Canada, 215 pages.
- [38] Evans, G. T., and J. S. Parslow. 1985. A model of annual plankton cycles. *Biol. Oceanog.*, **3**(3), 327–347.
- [39] Falkowski, P. G., P. E. Biscaye, and C. Sancetta. 1994. The lateral flux of biogenic particles from the eastern North American continental margin to the North Atlantic ocean. *Deep Sea Res. II*, **41**, 583–601.
- [40] Fasham, M. J. R. 1993. Modelling in the marine biota. *Pages 457–504 of: Heimann, M. (ed), The global carbon cycle*, vol. 73 Supp.
- [41] Fasham, M. J. R. 1995. Variations in the seasonal cycle of biological production in subarctic oceans: A model sensitivity analysis. *Deep Sea Res. Part I*, **42**, 1111–1149.
- [42] Fasham, M. J. R., H. W. Ducklow, and S. M. McKelvie. 1990. A nitrogen-based model of plankton dynamics in the oceanic mixed layer. *J. Mar. Res.*, **48**, 591–639.
- [43] Faucher, M., W. R. Burrows, and L. Pandolfo. 1999. Empirical-statistical reconstruction of surface marine winds along the western coast of Canada. *Clim. Res.*, **11**, 173–190.
- [44] Federiuk, J., and J. S. Allen. 1995. Upwelling circulation on the Oregon continental shelf. Part II: Simulations and comparisons with observations. *J. Phys. Oceanog.*, **25**, 1867–1889.
- [45] Foreman, M. G. G., and R. E. Thomson. 1997. Three-dimensional model simulations of tides and buoyancy currents along the West Coast of Vancouver Island. *J. Phys. Oceanogr.*, **27**, 1300–1325.
- [46] Foreman, M. G. G., R. E. Thomson, and C. L. Smith. 2000. Seasonal current simulations for the western continental margin of Vancouver Island. *J. Geophys. Res.*, **105**, 19,665–19,698.
- [47] Freeland, H. J., and K. L. Denman. 1982. A topographically controlled upwelling center off southern Vancouver Island. *J. Mar. Res.*, **40**, 1069–1093.
- [48] Freeland, H. J., and P. McIntosh. 1989. The vorticity balance on the southern British Columbia continental shelf. *Atmos.-Ocean.*, **27**, 643–657.
- [49] Freeland, H. J., W. R. Crawford, and R. E. Thomson. 1984. Currents along the Pacific coast of Canada. *Atmos.-Ocean.*, **22**, 151–172.

- [50] Friederich, G. E., C. M. Sakamoto, J. T. Pennington, and F. P. Chavez. 1994. On the direction of the air-sea flux of CO<sub>2</sub> in coastal upwelling systems. *Pages 438-445 of: Global fluxes of carbon and its related substances in the coastal sea-ocean-atmosphere system*. Sapporo Hokkaido, Japan: IGBP.
- [51] Frost, B. W. 1987. Grazing control of phytoplankton stock in the open subarctic Pacific Ocean: a model assessing the role of mesozooplankton, particularly the large calanoid copepods *Neocalanus* spp. *Mar. Ecol. Prog. Ser.*, **39**, 49-68.
- [52] Garçon, V. C., F. Thomas, C. S. Wong, and J. F. Minster. 1992. Gaining insight into the seasonal variability of CO<sub>2</sub> at ocean Station P using an upper ocean model. *Deep Sea Res.*, **39**, 921-938.
- [53] Gargett, A. E. 1991. Physical processes and the maintenance of nutrient-rich euphotic zones. *Limnol. Oceanogr.*, **36**(8), 1527-1545.
- [54] Garrison, D. L. 1984. Planktonic Diatoms. *Pages 1-17 of: Steidinger, K. A., and L. M. Walker (eds), Marine Plankton Life Cycle Strategies*. Boca Raton, U.S.A.: CRC Press Inc.
- [55] Hansen, J. L. S., U. Timm, and T. Kiorbe. 1995. Adaptive significance of phytoplankton stickiness with emphasis on the diatom *Skeletonema costatum*. *Mar. Biol.*, **123**, 667-676.
- [56] Harris, S. 2000. *Size fractionated primary production and nutrient distribution on the west coast of Vancouver Island*. M.Sc. thesis, University of British Columbia, Vancouver, Canada, in prep.
- [57] Harrison, W. G., and T. Platt. 1986. Photosynthesis-Irradiance relationships in polar and temperate phytoplankton populations. *Polar Biol.*, **5**, 153-164.
- [58] Harrison, W. G., T. Platt, and M. R. Lewis. 1987. f-ratio and its relationship to ambient nitrate concentration in coastal waters. *J. Plank. Res.*, **9**(1), 235-248.
- [59] Hickey, B., R. E. Thomson, H. Yih, and P. H. LeBlond. 1991. Velocity and temperature fluctuations in a buoyancy-driven current off Vancouver Island. *J. Geophys. Res.*, **96**, 10507-10538.
- [60] Hill, J. K. 1999. *The distribution and partitioning of dissolved organic matter off the Oregon coast: A first look*. M.Sc. thesis, Oregon State University, Corvallis, Oregon, 118 pages.
- [61] Hill, P. S. 1992. Reconciling aggregation theory with observed vertical fluxes following phytoplankton blooms. *J. Geophys. Res.*, **97**(C2), 2295-2308.

- [62] Hsieh, W. W., D. W. Ware, and R. E. Thomson. 1995. Wind-induced upwelling along the west coast of North America, 1899-1988. *Can. J. Fish. Aquat. Sci.*, **52**, 325-334.
- [63] Hurtt, G. C., and R. A. Armstrong. 1996. A pelagic ecosystem model calibrated with BATS data. *Deep Sea Res. II*, **43**(2-3), 653-683.
- [64] Hutchings, L., G. C. Pitcher, T. A. Probyn, and G. W. Bailey. 1994. The chemical and biological consequences of coastal upwelling. *Pages 65-81 of: Summerhayes, C. P., K.-C. Emeis, M. V. Angel, R. L. Smith, and B. Zeitzschel (eds), Upwelling in the ocean: Modern processes and ancient records.* Wiley and Sons Ltd.
- [65] Hutchins, D. A., and K. W. Bruland. 1998. Iron-limited diatom growth and Si:N uptake ratios in a coastal upwelling regime. *Nature*, **393**, 561-564.
- [66] Huthnance, J. 1995. Circulation, exchange and water masses at the ocean margin: the role of physical processes at the shelf edge. *Prog. Oceanography*, **35**, 353-431.
- [67] Jackson, G. A. 1990. A model of the formation of marine algal flocs by physical coagulation processes. *Deep Sea Res.*, **37**(8), 1197-1211.
- [68] Johnson, K. M., A. E. King, and J. M. Sieburth. 1985. Coulometric TCO<sub>2</sub> analysis for marine studies; an introduction. *Mar. Chem.*, **16**, 61-82.
- [69] Johnson, K. M., J. M. Sieburth, P. J. Williams, and L. Brandstrom. 1987. Coulometric total carbon dioxide analysis for marine studies; automation and calibration. *Mar. Chem.*, **21**, 117-133.
- [70] Johnson, K. S., and C. S. Wong. 1979. Biological production and exchange of oxygen and carbon dioxide across the sea surface in Stuart Channel, British Columbia. *Limnol. Oceanogr.*, **24**(3), 474-482.
- [71] Karl, D. M., G. A. Knauer, and J. H. Martin. 1988. Downward flux of particulate organic matter in the ocean: a particle decomposition paradox. *Nature*, **332**, 438-441.
- [72] Kempe, S., and K. Pegler. 1991. Sinks and sources of CO<sub>2</sub> in coastal seas: the North Sea. *Tellus*, **43B**, 224-235.
- [73] Knox, F., and M. B. McElroy. 1984. Changes in atmospheric CO<sub>2</sub>: Influence of the marine biota at high latitude. *J. Geophys. Res.*, **89**, 4629-4637.
- [74] Large, W. G., and S. Pond. 1981. Open ocean momentum flux measurements in moderate to strong winds. *J. Phys. Oceanogr.*, **11**, 324-336.

- [75] Laws, E. A., and T. T. Bannister. 1980. Nutrient and light-limited growth of *Thalassiosira fluviatilis* in continuous culture, with implications for phytoplankton growth in the ocean. *Limnol. Oceanogr.*, **25**(3), 457-473.
- [76] Lentz, S. J. 1992. The surface boundary layer in coastal upwelling regions. *J. Phys. Oceanogr.*, **22**, 1517-1539.
- [77] MacDonald, R. W., and T. F. Pedersen. 1991. Geochemistry of sediments of the western Canadian continental shelf. *Cont. Shelf Res.*, **11**(8-10), 717-735.
- [78] Mackas, D. L. 1992. Seasonal cycle of zooplankton off Southwestern BC 1979-89. *Can. J. Aquat. Sci.*, **49**, 903-921.
- [79] Mackas, D. L., and D. R. Yelland. 1999. Horizontal flux of nutrients and plankton across and along the British Columbia continental margin. *Deep Sea Res. II*, **46**, 2941-2964.
- [80] Mackas, D. L., G. C. Louttet, and M. J. Austin. 1980. Spatial distribution of zooplankton and phytoplankton off Vancouver Island. *Can. J. Aquat. Sci.*, **54**, 2080-2096.
- [81] Mackenzie, R. T., A. Lerman, and L. M. Ver. 1998. Role of the continental margin in the global carbon balance during the past three centuries. *Geology*, **26**, 423-426.
- [82] Manning, M. R. 1993. Seasonal cycles in atmospheric CO<sub>2</sub> concentrations. *Pages 65-94 of: Heimann, M. (ed), The global carbon cycle.* Germany: Springer-Verlag.
- [83] Martin, J. H., G. A. Knauer, D. M. Karl, and W. W. Broenkow. 1987. VERTEX: carbon cycling in the northeast Pacific. *Deep Sea Res.*, **34**, 267-285.
- [84] Matear, R. J. 1995. Parameter optimization and analysis of ecosystem models using simulated annealing: a case study at Station P. *J. Mar. Res.*, **53**, 571-607.
- [85] McGillicuddy, D. J., J. J. McCarthy, and A. R. Robinson. 1995. Coupled physical and biological modelling of the spring bloom in the North Atlantic (I): model formulation and one-dimensional bloom processes. *Deep Sea Res. I*, **42**(8), 1313-1357.
- [86] Millero, F. J., and A. Poisson. 1981. International one-atmosphere equation of state for sea water. *Deep Sea Res.*, **44**, 363-384.
- [87] Millero, F. J., J. Z. Shang, K. Lee, and D. M. Campbell. 1993. Titration alkalinity of seawater. *Mar. Chem.*, **44**, 153-165.
- [88] Najjar, R. G. 1992. Marine biogeochemistry. *Pages 241-280 of: Trenberth, K. E. (ed), Climate system modelling.* Cambridge, U. K.: Cambridge University Press.

- [89] Najjar, R. G., J. L. Sarmiento, and J. R. Toggweiler. 1992. Downward transport and fate of organic matter in the ocean: Simulations with a general circulation model. *Global Biogeochem. Cycles*, **6**(1), 45–76.
- [90] Parsons, T. R., Y. Maita, and C. M. Lalli. 1984. *A Manual of Chemical and Biological Methods for Seawater Analysis*. Oxford, U.K.: Pergamon Press.
- [91] Pawlowicz, R. 1999. A tracer method for determining transport in two-layer systems, applied to the Strait of Georgia/Haro Strait/Juan de Fuca Strait estuarine system. *Estuarine Coastal Shelf Sci.*, submitted.
- [92] Pawlowicz, R., and D. M. Farmer. 1998. Diagnosing vertical mixing in two-layer exchange flows. *J. Geophys. Res.*, **103**(C13), 30,695–30,711.
- [93] Peña, M. A., K. L. Denman, J. R. Forbes, S. E. Calvert, and R. E. Thomson. 1996. Sinking particle fluxes from the euphotic zone over the continental slope of an eastern boundary current region. *J. Mar. Res.*, **54**, 1097–1122.
- [94] Peña, M. A., K. L. Denman, S. E. Calvert, R. E. Thomson, and J. R. Forbes. 1999. The seasonal cycle in sinking particle fluxes off Vancouver Island, British Columbia. *Deep Sea Res. II*, **46**, 2969–2992.
- [95] Pitcher, G. C. 1990. Phytoplankton seed populations of the Cape Peninsula upwelling plume, with particular reference to resting spores of Chaetoceros (Cacillariophyceae) and their role in seeding upwelling waters. *Est. Coast. Shelf Sci.*, **31**, 283–301.
- [96] Press, W. H., S. A. Teukolsky, W. T. Vetterling, and B. P. Flannery. 1992. *Numerical Recipes in C: the art of scientific computing*. 2nd edn. New York, USA: Cambridge University Press.
- [97] Redfield, A. C., B. H. Ketchum, and F. A. Richards. 1963. The influence of organisms on the composition of sea-water. *Chap. 2, pages 26–77 of: The sea: Ideas and observations on progress in the study of the seas*. New York: John Wiley and Sons.
- [98] Sakshaug, E., K. Andersen, and D. A. Kiefer. 1989. A steady state description of growth and light absorption in the marine planktonic diatom *Skeletomema costatum*. *Limnol. Oceanog.*, **34**(1), 198–204.
- [99] Sambrotto, R. N., et al. 1993. Elevated consumption of carbon relative to nitrogen in the surface ocean. *Nature*, **363**, 248–250.
- [100] Sarmiento, J. L. 1992. Biogeochemical ocean models. *Pages 519–551 of: Trenberth, K. E. (ed), Climate system modelling*. Cambridge, U. K.: Cambridge University Press.

- [101] Sarmiento, J. L., and J. R. Toggweiler. 1984. A new model for the role of the oceans in determining atmospheric  $p\text{CO}_2$ . *Nature*, **308**, 621–624.
- [102] Sarmiento, J. L., R. D. Slater, M. J. R. Fasham, H. W. Ducklow, J. R. Toggweiler, and G. T. Evans. 1993. A seasonal three-dimensional ecosystem model of nitrogen cycling in the North Atlantic euphotic zone. *Global Biogeochem. Cycles*, **7**(2), 417–450.
- [103] Shaffer, G. 1993. Effects of the marine biota on global carbon cycling. *Pages 431–455 of: Heimann, M. (ed), The global carbon cycle*. Germany: Springer-Verlag.
- [104] Siegenthaler, U., and J. L. Sarmiento. 1993. Atmospheric carbon dioxide and the ocean. *Nature*, **365**, 119–125.
- [105] Siegenthaler, U., and T. Wenk. 1984. Rapid atmospheric  $\text{CO}_2$  variations and oceanic circulation. *Nature*, **308**, 624–626.
- [106] Simpson, J. J. 1986. Processes affecting upper ocean chemical structure in an eastern boundary current. *Page 246 of: Burton, J. D., P. G. Brewer, and R. Chesselet (eds), Dynamic processes in the chemistry of the upper ocean*. New York: Plenum Pub. Co.
- [107] Simpson, J. J., and A. Zirino. 1980. Biological control of pH in the Peruvian coastal upwelling area. *Deep Sea Res. I*, **27**, 733–744.
- [108] Skirrow, G. 1975. The dissolved gases - carbon dioxide. *Pages 1–192 of: Riley, J. P., and G. Skirrow (eds), Chemical Oceanography*, vol. 2. London: Academic Press.
- [109] Smetacek, V. S. 1985. Role of sinking in diatom life-history cycles: ecological, evolutionary and geological significance. *Mar. Biol.*, **84**, 239–251.
- [110] Smith, R. L. 1994. The physical processes of coastal ocean upwelling systems. *Pages 39–64 of: Summerhayes, C. P., K.-C. Emeis, M. V. Angel, R. L. Smith, and B. Zeitzschel (eds), Upwelling in the ocean: Modern processes and ancient records*. Wiley and Sons Ltd.
- [111] Smith, S. V., and J. T. Hollibaugh. 1993. Coastal metabolism and the oceanic organic carbon cycle. *Rev. Geophys.*, **31**, 75–89.
- [112] Spitz, Y. H., J. Moisan, M. R. Abbott, and J. G. Richman. 1998. Data assimilation and a pelagic ecosystem model: parameterization using time series observations. *J. Mar. Systems*, **16**, 51–68.

- [113] Spitz, Y. H., J. Moisan, and M. R. Abbott. 1999. Configuring an ecosystem model using data from Bermuda-Atlantic Time Series (BATS). *Deep Sea Res. II*, in press.
- [114] Suess, E. 1980. Particulate organic carbon flux in the oceans - surface productivity and oxygen utilization. *Nature*, **288**, 260-263.
- [115] Sverdrup, H. U. 1937. On the process of upwelling. *J. Mar. Res.*, **1**, 155-164.
- [116] Sverdrup, H. U. 1953. On conditions for the vernal blooming of phytoplankton. *J. Cons. Explor. Mer.*, **18**, 287-295.
- [117] Takahashi, T., G. Mathieu, D. W. Chipman, J. Goddard, and L. Ma. 1991. *Carbon dioxide in the surface water of the western equatorial Pacific Ocean*. Final Technical Report to U.S. Department of Energy.
- [118] Taylor, A. H., R. J. Geider, and F. J. Gilbert. 1997. Seasonal and latitudinal dependencies of phytoplankton carbon-to-chlorophyll a ratios: results of a modelling study. *Mar. Ecol. Prog. Ser.*, **152**, 51-66.
- [119] Thomson, R. E., and I. V. Fine. 2000. Estimation of mixed-layer depth with application to the continental margin of Vancouver Island, British Columbia. *J. Phys. Oceanog.*, in prep.
- [120] Thomson, R. E., and D. Ware. 1996. A current velocity index of ocean variability. *J. Geophys. Res.*, **101**, 14297-14310.
- [121] Thomson, R. E., B. M. Hickey, and P. H. LeBlond. 1989. The Vancouver Island coastal current: fisheries barrier and conduit. *Pages 265-296 of: McFarlane, G. A. (ed), Effects of ocean variability on recruitment and an evaluation of parameters used in stock assessment models*, vol. 108. Can. Spec. Publ. Fish. Aquat. Sci.
- [122] Timothy, D. A., and S. Pond. 1997. Describing additional fluxes to deep sediment traps and water-column decay in a coastal environment. *J. Mar. Res.*, **55**, 383-406.
- [123] Toggweiler, J. R. 1989. *Is the downward dissolved organic matter (DOM) flux important in carbon transport?* New York: John Wiley and Sons Ltd.
- [124] Tsunogai, S., S. Watanabe, and T. Sato. 1999. Is there a 'continental shelf pump' for the absorption of atmospheric CO<sub>2</sub>? *Tellus*, **51B**, 701-712.
- [125] Varela, D. E. 2000. *Ammonium, nitrate and urea uptake rates during the spring, summer and fall of 1997-98 in the coastal upwelling region west of Vancouver Island*. in prep. for *Can. J. Fish. Aquat. Sci.*

- [126] Verardo, D. J., P. N. Froelich, and A. McIntyre. 1990. Determination of organic carbon and nitrogen in marine sediments using the Carlo Erba NA-1500 Analyzer. *Deep Sea Res.*, **37**, 157-165.
- [127] Volk, T., and M. I. Hoffert. 1985. Ocean carbon pumps: analysis of relative strengths and efficiencies in ocean-driven atmospheric pCO<sub>2</sub> changes. *Pages 99-110 of: Sundqvist, E. T., and W. S. Broecker (eds), The carbon cycle and atmospheric CO<sub>2</sub>, natural variations archaen to present*, vol. AGU Monograph 32. Washington, D.C.: AGU.
- [128] Wanninkhof, R. 1992. Relationship between gas exchange and wind speed over the ocean. *J. Geophys. Res.*, **97**(C5), 7373-7382.
- [129] Whitney, F. A., and H. J. Freeland. 1999. Variability in upper-ocean water properties in the NE Pacific Ocean. *Deep Sea Res. II*, **46**, 2351-2370.
- [130] Whitney, F. A., C. S. Wong, and P. W. Boyd. 1991. Interannual variability in nitrate supply to surface waters of the Northeast Pacific Ocean. *Mar. Ecol. Prog. Ser.*, **170**, 15-23.
- [131] Wong, C. S., Y. Zhiming, W. K. Johnson, R. J. Matear, and F. A. Whitney. 1997. Dynamics and characterization of marine organic matter. *Pages 107-116 of: Handa, N., E. Tanoue, and T. Hama (eds), Professor Handa's retirement commemorative volume*. Tokyo: Terra Scientific Pub. Co.
- [132] Wood, E. D., F. A. J. Armstrong, and F. A. Richards. 1967. Determination of nitrate in seawater by cadmium-copper reduction to nitrite. *J. Mar. Biol. Ass. U.K.*, **47**, 23-31.
- [133] Wroblewski, J. S. 1977. A model of phytoplankton plume formation during variable Oregon upwelling. *J. Mar. Res.*, **35**, 357-394.

## Appendix A

### Organic Carbon Burial and Denitrification

#### A.1 Burial of organic matter

Over 80% of organic carbon burial in the ocean occurs over continental margins (Berner, 1982). Most of this flux is due to fluvial delivery of organic matter and the high sedimentation rates in such regions. The large marine organic matter flux in coastal upwelling regions contributes to a lesser degree. This flux was considered during the development of the model but it was not included.

There are no organic carbon burial data in my study area so I consider the coastal upwelling region off the Washington coast, several 100 km south of the study area. Estimates of the organic carbon burial flux off the Washington coast ( $1 \text{ g C m}^{-2}\text{yr}^{-1}$  (Berner, 1982)) are two orders of magnitude lower than the remineralization flux from the model lower particulate carbon pool. Clearly this burial flux would not affect the model over the time scales that I am interested in. Furthermore, this flux is expected to be much smaller on the Vancouver Island shelf. The linear sedimentation rate (units length time<sup>-1</sup>), as well as the delivery of organic carbon to the sediments, is very important in determining how much organic carbon is permanently buried (Calvert, 1987). Organic carbon delivery is not expected to be less over the highly productive Washington shelf than in my study area. However, linear sedimentation rates are very small over the Vancouver Island shelf due to negligible terrigenous input relative to the large input from the Columbia River in Washington (MacDonald and Pedersen, 1991). In addition, resuspension of sediments by

winter storms is likely so that permanent burial may not occur at all over the shelf, but it might be important over the slope (T. Pedersen, pers. com.). This resuspension makes it even more likely that the organic matter reaching the sediments will be remineralized rather than permanently buried. Thus, the flux of organic carbon that is buried on the continental margin off the coast of Vancouver Island is expected to be more than two orders of magnitude smaller than the remineralization flux of organic matter below the euphotic zone. Because the burial flux is so small, I modelled all of the particulate flux as an actively recycling pool in the lower layer.

## A.2 Denitrification

Denitrification is an important part of the nitrogen cycle in the ocean over time scales of 1000 yr (e.g. Christensen, 1994). It occurs in suboxic conditions when nitrate ( $\text{NO}_3^-$ ) is used as an electron acceptor to oxidize organic matter and it produces dissolved nitrogen gas ( $\text{N}_2$ ).  $\text{N}_2$  is not biologically accessible to most of the biota (the exception is nitrogen-fixing cyanobacteria), so denitrification is essentially a loss of nitrogen to the system. Using the same arguments as above (Burial section), I compared the results of data from the Washington shelf (Christensen et al., 1987) with modelled fluxes. This comparison shows that denitrification fluxes are expected to be at least two orders of magnitude less than the modelled remineralization flux in the lower layer. Therefore, denitrification is not modelled.

Processes such as organic carbon burial and denitrification in coastal upwelling regions are likely globally significant over time scales much longer than I am modelling. However, they cannot be modelled mechanistically with bulk models. Detailed vertical profiles (of quantities like oxygen) at the sediment water interface are necessary and bulk models are not capable of providing them.

## Appendix B

### Ordinary Differential Equations for Salinity

Full prognostic equations for the state variable salinity ( $S$ ) show physical circulation without the complication of biological or gas fluxes. Subscripts  $u$ ,  $l$ ,  $sh$ ,  $sl$  and  $o$  are upper, lower, shelf, slope and open ocean, respectively. In each equation, the first term on the right hand side is the vertical mixing and entrainment term, followed by terms for upwelling, downwelling and then horizontal mixing. The slope boxes have two interfaces for horizontal mixing. The surface shelf and slope boxes have additional terms ( $B$ ) for buoyancy fluxes (Appendix C).

$$\begin{aligned} \frac{dS_{sh,u}}{dt} = & \left( \frac{M_V \cdot d_m}{h_{sh,u}(h_{pp} - h_u)_{sh}} + e_{sh,u} \right) (S_{sh,l} - S_{sh,u}) + \frac{A}{h_{sh,u}} (S_{sh,l} - S_{sh,u}) \\ & + \frac{D}{hu_{sh}} (S_{sl,u} - S_{sh,u}) + \frac{M_H}{w_{sh}} (S_{sl,u} - S_{sh,u}) + B_{sh} \end{aligned} \quad (\text{B.1})$$

$$\begin{aligned} \frac{dS_{sh,l}}{dt} = & \left( \frac{M_V \cdot d_m}{h_{sh,l}(h_{pp} - h_u)_{sh}} + e_{sh,l} \right) (S_{sh,u} - S_{sh,l}) + \frac{A}{h_{sh,l}} (S_{sl,l} - S_{sh,l}) \\ & + \frac{D}{h_{sh,l}} (S_{sh,u} - S_{sh,l}) + \frac{M_H}{w_{sh}} (S_{sl,l} - S_{sh,l}) \end{aligned} \quad (\text{B.2})$$

$$\begin{aligned} \frac{dS_{sl,u}}{dt} = & \left( \frac{M_V \cdot d_m}{h_{sl,u}(h_{pp} - h_u)_{sl}} + e_{sl,u} \right) (S_{sl,l} - S_{sl,u}) + \frac{A}{h_{sl,u}} (S_{sh,u} - S_{sl,u}) \\ & + \frac{D}{hu_{sl}} (S_{o,u} - S_{sl,u}) + \frac{M_H \cdot h_{sh,u}}{w_{sl} \cdot h_{sl,u}} (S_{sh,u} - S_{sl,u}) \\ & + \frac{M_H}{w_{sl}} (S_{o,u} - S_{sl,u}) + B_{sl} \end{aligned} \quad (\text{B.3})$$

$$\begin{aligned} \frac{dS_{sl,l}}{dt} = & \left( \frac{M_V \cdot d_m}{h_{sl,l}(h_{pp} - h_u)_{sl}} + e_{sl,l} \right) (S_{sl,u} - S_{sl,l}) + \frac{A}{h_{sl,l}} (S_{o,l} - S_{sl,l}) \\ & + \frac{D}{h_{sl,l}} (S_{sh,l} - S_{sl,l}) + \frac{M_H \cdot h_{sh,l}}{w_{sl} \cdot h_{sl,l}} (S_{sh,l} - S_{sl,l}) \\ & + \frac{M_H}{w_{sl}} (S_{o,l} - S_{sh,l}) \end{aligned} \quad (\text{B.4})$$

$$\frac{dS_{o,u}}{dt} = 0 \quad ; \quad \frac{dS_{o,l}}{dt} = 0 \quad (\text{B.5})$$

where  $t$  is time. Definitions and values of physical parameters are presented in Table 3.2. Note that for some state variables (DIN, DOC, and DON) the upper layer open ocean concentrations (Equation B.5) have prescribed seasonal variability (Appendix E).

## Appendix C

### Buoyancy Fluxes

Using salinity ( $S$ ) as a state variable, the shelf box buoyancy fluxes ( $B$ ) are

$$B_{sh} = \frac{P}{h_{sh,u}}(S_p - S_{sh,u}) + \frac{R}{h_{sh,u}}(S_r - S_{sh,u}) + \frac{C}{h_{sh,u}}(S_c - S_{sh,u}) \quad (\text{C.1})$$

and in the surface slope box

$$B_{sl} = \frac{P}{h_{sl,u}}(S_p - S_{sl,u}) \quad (\text{C.2})$$

where  $P$ ,  $R$ , and  $C$  are flux per length of coastline for rainfall, terrigenous run-off and the Vancouver Island Coastal Current (VICC), respectively, with corresponding subscripts in lower-case. Subscripts,  $u$ ,  $sh$  and  $sl$  are upper, shelf and slope, respectively. The coefficients vary in time, for precipitation

$$P = 0.029 \exp(-0.5(3.5 - 2 \cos(\frac{2\pi}{\tau}(t + 20d)))) \text{ m d}^{-1} \quad (\text{C.3})$$

terrigenous runoff

$$R = 0.05 \exp(-0.5(3.5 - 2 \cos(\frac{2\pi}{\tau}(t + 20d)))) \text{ m d}^{-1} \quad (\text{C.4})$$

and the VICC

$$C = 0.5 \exp(-0.6(5 - 2 \cos(\frac{2\pi}{\tau}(t - 150d)))) \text{ m d}^{-1} \quad (\text{C.5})$$

where  $\tau$  is 365 d and phases are relative to Jan. 1. We chose exponential functions to make short, steep peaks ( $P$  and  $R$  peak on year day 345 (December 11) and  $C$  on year day 150 (May 30)) relative to a broader baseline (corresponding to data). All state

State Variable	Inner-shelf Upper Box	Source
DIC	2050	Chapter 2 (summer), C. S. Wong (pers. com.) (winter)
DIN	10	Chapter 2, Pawlowicz (1999)
DOC	40	see text
DON	6	see text
POC	4	see text
PON	0.6	see text
Salinity	32.0	Pawlowicz and Farmer (1998)

Table C.1: Inner-shelf state variables that are mixed into the upper shelf box by the buoyancy flux  $C$ . All data have units of  $\mu\text{M}$  with the exception of salinity. Values are annual averages (seasonal variation is not modelled).

variable concentrations in the precipitation and run-off were set to zero. State variable concentrations in the inner-shelf Buoyancy current are presented in Table C.1.

The average surface DIN value from the Juan de Fuca Strait,  $28 \mu\text{M}$  (Pawlowicz, 1999) was reduced to  $10 \mu\text{M}$  (based on data in Chapter 2) to account for biological uptake of DIN and mixing over the inner shelf. (Note, if the value is changed to  $28 \mu\text{M}$   $pp$  increases by less than 3% so the model is not very sensitive to this change.) Average surface winter and fall measurements of DIC (C. S. Wong, pers. com.) are from Station P01 ( $48.58^\circ\text{N}$ ,  $125.5^\circ\text{W}$ ). There are few organic matter data on which to base the values in Table C.1 (only POM), and none in the winter. I assume that gradients are small between the outer-shelf and the Juan de Fuca Strait in winter and that organic matter concentrations are higher over the shelf (relative to the Juan de Fuca Strait) during summer to set average DOM and POM values within the VICC. These values are arbitrary; however, the model is not sensitive to them (as long as they are the of same order as the values recorded by Wong et al. (1997), Bishop et al. (1999) and C. S. Wong, pers. com).

## Appendix D

### Annual Mixed Layer Depth

Annual variability in mixed layer depth was prescribed (Figure D.1). Variations were added in response to prescribed storm forcing:

$$storm = \left( 4 \cos\left(\frac{2\pi}{10d}t\right) + \cos\left(\frac{2\pi}{5d}(t - 3d)\right) \right) \cdot \left( 1.2 + 0.3 \cos\left(\frac{2\pi}{\tau}(t - 50d)\right) \right) \text{ m} \quad (\text{D.1})$$

where  $t$  is time,  $\tau$  is 365 d and phases are relative to Jan. 1. The first set of large parenthesis contains the storm frequencies (at 10 and 5 d periods, respectively) and the second set contains the annual amplitude variation (so storm forcing is larger in winter relative to summer).

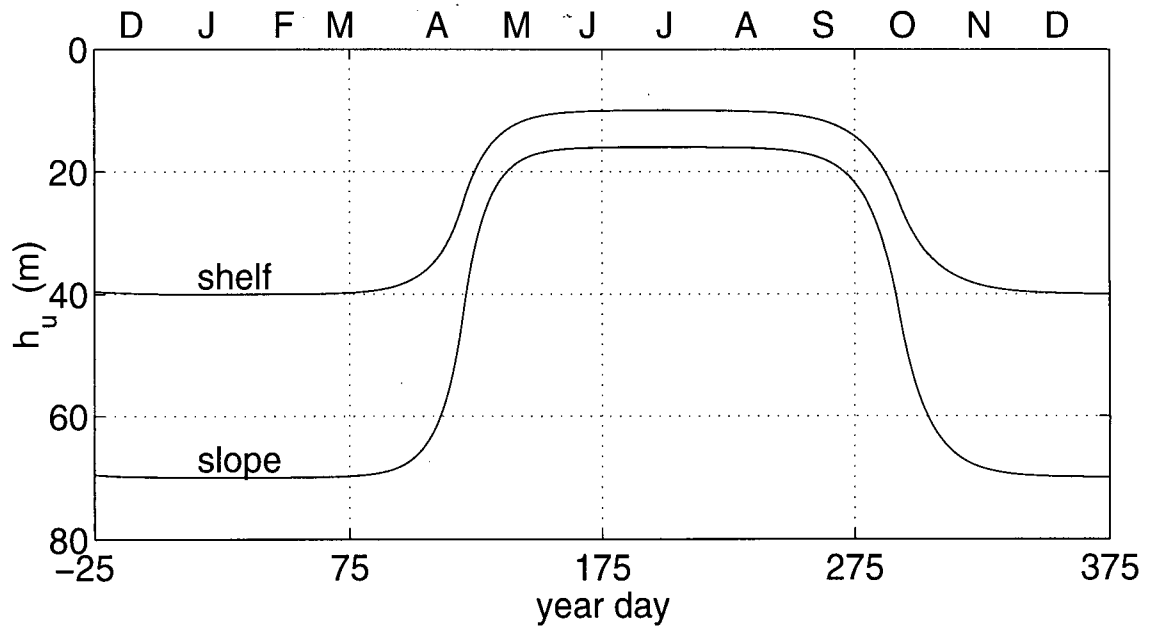


Figure D.1: Seasonal variation in mixed layer depth ( $h_u$ ) for shelf and slope.

## Appendix E

### Open Ocean State Variable Concentrations

The values of the open ocean state variables were specified in the model for the upper and lower layer (Table E.1). Where upper layer values varied significantly throughout the year, annual variation was prescribed (below), while all values remained constant in the lower layer. Lower layer values were chosen to reflect a depth range of 150 – 250 m, the expected source water of upwelled water.

State Variable	Open Ocean		Source
	Upper Box	Lower Box	
DIC	2050	2275	C. S. Wong (pers. com.)
DIN	0 – 8	30	Whitney et al. (1998), R. Brown (pers. com.)
DOC	20 – 30	18	Wong et al. (1997)
DON	2 – 4	1.5	C. S. Wong (pers. com.)
POC	2	0.8	Bishop et al. (1999)
PON	0.3	0.12	see text
Salinity	32.4	33.9	Whitney and Freland (1999), R. Brown (pers. com.)

Table E.1: Open Ocean State Variables. All data are from Stn P04 (48.65°N 126.67°W) and have units of  $\mu\text{M}$  with the exception of salinity. Ranges show annual variation.

Ranges are prescribed using simple sinusoidal functions:

$$\text{DIN} = 4 - 4 \sin\left(\frac{2\pi}{\tau}(t - 40\text{d})\right) \mu\text{M} \quad (\text{E.1})$$

$$\text{DOC} = 25 - 5 \cos\left(\frac{2\pi}{\tau}(t - 40\text{d})\right) \mu\text{M} \quad (\text{E.2})$$

$$\text{DON} = 3 - 1 \cos\left(\frac{2\pi}{\tau}(t - 40\text{d})\right) \mu\text{M} \quad (\text{E.3})$$

where  $t$  is time,  $\tau$  is 365 d and phases are relative to Jan. 1. There are few data on which to base these variations, particularly for the DOM. I use a phase shift of 40 d to coincide with expected natural cycles (eg. DIN concentration builds up during the winter, peaking later than Jan. 1 and has minimum values throughout the summer). It is assumed that DOM is produced during summer and remineralized during winter. For DO concentrations, the semi-labile portion was estimated to be about 30% of the total measured DOM. The Redfield C:N was used to convert POC (Bishop et al., 1999) to PON.

## Appendix F

### Steady State Solutions

Steady state solutions were sought for a simplified version of the two-layer biological model (Equation 3.2) for summer (upwelling) and winter (downwelling) scenarios and they were used to constrain poorly known model parameters. For these solutions the upper layer depth was constant (no entrainment) and the permanent pycnocline was not modelled; therefore, the vertical mixing term ( $V$  in Equations 3.2) reduced to  $M\Delta C/h$  where  $M$  is the mixing coefficient,  $h$  is the box height and  $\Delta C$  is the concentration difference between the upper and lower layer. There are no horizontal mixing or advection terms ( $H$  and  $X$  in Equations 3.2) because the system has only two boxes. Excess carbon uptake ( $pc$ ) and variable loss due to DIN and light limitation were not considered (i.e.  $loss = 1$  and  $pc = 0$ ). Carbon was used as the currency.

#### F.1 Steady State Equations

POC and DOC pools have straightforward solutions. However, the DIC equations are indeterminate (because the system is closed and no pools are dependent on DIC concentration), yielding two expressions for the difference between the upper and lower pool concentrations ( $DIC_l - DIC_u$ ). The equations are:

$$DIC_l - DIC_u = \frac{h_u}{M} \left( \frac{G}{h_u} + \frac{ppz}{h_u} - r_d DOC_u \right) \quad (F.1a)$$

$$POC_u = \frac{ppz}{s h_u} \quad (F.1b)$$

$$\text{DOC}_u = \frac{\frac{(1-p) ppz}{h_u} \left( \frac{M}{h_t - h_u} + r_d \right) \left( \frac{h_t - h_u}{M} \right)}{\left( r_d + \frac{M}{h_t - h_u} \right) \left( \frac{h_t - h_u}{M} \right) \left( r_d + \frac{M}{h_u} \right) - \frac{M}{h_u}} \quad (\text{F.1c})$$

$$\text{DIC}_l - \text{DIC}_u = \frac{h_t - h_u}{M} (r_p \text{POC}_l + r_d \text{DOC}_l) \quad (\text{F.1d})$$

$$\text{POC}_l = \frac{p \cdot ppz}{r_p (h_t - h_u)} \quad (\text{F.1e})$$

$$\text{DOC}_l = \frac{\frac{(1-p) ppz}{h_u}}{\left( r_d + \frac{M}{h_t - h_u} \right) \left( \frac{h_t - h_u}{M} \right) \left( r_d + \frac{M}{h_u} \right) - \frac{M}{h_u}} \quad (\text{F.1f})$$

where subscripts  $u$  and  $l$  denote upper and lower, respectively. The depth of the total water column is  $h_t$  and  $h_u$  is the depth of the upper box.  $M$  is the mixing coefficient,  $G$  is the air-sea gas flux and  $ppz$  is primary production integrated over depth. The rates  $r_d$ ,  $r_p$  and  $s$  are for the remineralization of DOC, the remineralization of POC and the decay of the living POC, respectively. The fraction  $p$  is the portion of the decay flux of living POC that becomes particulate (sinking) versus dissolved (non-sinking).

## F.2 Values for Pools and Parameters

The values for many pools and parameters in the model are not well known. Ranges for all values are presented in Tables F.1 and F.2 for summer and winter, respectively with sources listed in the right column. Where possible direct observations are cited. However, it was often necessary to estimate values indirectly, as described in the text. Summer steady state solutions were obtained by using those values that are best known (there are more measurements available in summer) to constrain ranges for parameters that are not known ( $r_d$  and  $s$ ). The winter solution was then found using the parameter values set by the summer solution.

Table F.1: Values of pools and parameters used to estimate the summer steady state solution for the two-layer biological model. Sources are listed in the right column.

Estimated from data in the study area:			
$h_u$	10 – 50	m	Thomson and Fine (2000)
$h_t$	250	m	see text
$POC_u$	10 – 20	$\mu\text{M}$	Chapter 2
$p\text{CO}_2w^1$	275 – 525	ppm	(F. Whitney, pers. com.)
$sol \cdot k^1$	$9 \times 10^{-6}$	$\text{mol m}^{-2}\text{d}^{-1}\text{ppm}^{-1}$	Faucher et al. (1999)
$ppz$	60 – 170	$\mu\text{M m d}^{-1}$	Skirrow (1975), Wanninkhof (1992) P. Harrison (pers. com.)
M	0.5 – 4	$\text{m d}^{-1}$	Thomson and Ware (1996) Freeland and Denman (1982), Freeland and McIntosh (1989)
Estimated from data offshore from the study area (Stn P04):			
$POC_l$	0.5 – 3	$\mu\text{M}$	Bishop et al. (1999)
$DOC_u$	30 – 50	$\mu\text{M}$	Wong et al. (1997)
$DOC_l$	20 – 30	$\mu\text{M}$	Wong et al. (1997)
Estimated from data (or modelling studies) elsewhere:			
$r_p$	0.2 – 0.3	$\text{d}^{-1}$	Martin et al. (1987), Suess (1980), see text
$\text{DIC}_{l-u}$	0 – 300	$\mu\text{M}$	Redfield et al. (1963), see text
$p$	0.3 – 0.7	–	Bacastow and Maier-Reimer (1991)
$p\text{CO}_2a^1$	380	ppm	extrapolated from Manning (1993)
Solved for:			
$r_d$	0.001 – 0.005	$\text{d}^{-1}$	compared to Carlson and Ducklow (1995), Carlson et al. (1994), Wong et al. (1997)
$s$	0.05 – 0.3	$\text{d}^{-1}$	compared to Denman and Peña(1999)

[1]for estimation of gas flux  $G$ , equation 3.9 described in Section 3.2.5.

The upper layer depth ( $h_u$ ) represents the mixed layer depth (Thomson and Fine, 2000) and the total depth ( $h_t$ ) represents an average of the shelf and slope depths. The range in daily  $ppz$  was estimated assuming a total annual production of  $200 - 250 \text{ g C m}^{-2}\text{yr}^{-1}$  (P. Harrison, pers. com.) combined with seasonal lengths determined by Thomson and Ware (1996). In the upper limit, the total  $ppz$  ( $250 \text{ g C m}^{-2}$ ) occurs during the upwelling season, while for the lower limit,  $ppz$  ( $200 \text{ g C m}^{-2}$ ) is spread equally throughout the year. The mixing coefficient is large because in the two-box system with fixed upper layer depth it represents all vertical physical transport (mixing, entrainment and advection). The range for  $M$  is based on estimated values for the up- and downwelling velocities in the study area (Freeland and Denman, 1982; Freeland and McIntosh, 1989).

The semi-labile fraction of DOM was estimated as  $\sim 30\%$  (as suggested by Carlson et al. (1994) and Carlson and Ducklow (1995)) of the measured DOM (Wong et al., 1997). The remineralization rate for particulate organic matter was determined using decay length scale,  $d$  (Martin et al., 1987), and a sinking rate ( $sr$ ) of  $100 \text{ m d}^{-1}$  (Suess, 1980) (i.e.  $r_p = sr/d$ ). The upper limit for the difference in DIC concentrations between the upper and lower layer ( $\text{DIC}_{l-u}$ ) was determined assuming that biological uptake followed the C:N Redfield ratio and the maximum DIN that could be used in the upper layer was  $40 \mu\text{M}$ .

The range of remineralization rates ( $r_d$ ) determined by steady state equations (Equations F.1) are at the low end of the ranges suggested by Carlson et al. (1994), Carlson and Ducklow (1995) and the data of Wong et al. (1997). The estimated range for the decay rate ( $s$ ) includes the modelled phytoplankton mortality rate of Denman and Peña (1999),  $0.05 \text{ d}^{-1}$  (in their model this flux passes directly to detritus). Note that in my model  $s$  represents other processes as well as phytoplankton mortality.

Winter solutions for DOC and POC are reasonable compared with the data of Wong

Table F.2: Values of pools and parameters used to estimate the winter steady state solution for the two-layer biological model. Sources are listed in the right column.

Estimated from data in the study area:			
$h_u$	50 – 70	m	Thomson and Fine (2000)
$h_t$	250	m	see text
$p\text{CO}_2w^1$	325 – 330	ppm	(F. Whitney pers. com.)
$sol\ k^1$	$120 \times 10^{-6}$	$\text{mol m}^{-2}\text{d}^{-1}\text{ppm}^{-1}$	Faucher et al. (1999)
$ppz$	0 – 10	$\mu\text{M d}^{-1}\text{ m}$	Skirrow (1975), Wanninkhof (1992)
$M$	0.5 – 4	$\text{m d}^{-1}$	see text
			Freeland and Denman (1982), Freeland and McIntosh (1989)
Estimated from data (or modelling studies) elsewhere:			
$r_p$	0.2 – 0.3	$\text{d}^{-1}$	Martin et al. (1987), Suess (1980)
$\text{DIC}_{l-u}$	300	$\mu\text{M}$	Redfield et al. (1963)
$p$	0.3 – 0.7	–	Bacastow and Maier-Reimer (1991)
$p\text{CO}_2a^1$	385	ppm	extrapolated from Manning (1993)
From summer solution:			
$s$	0.05 – 0.3	$\text{d}^{-1}$	see Table F.1
$r_d$	0.001 – 0.005	$\text{d}^{-1}$	see Table F.1
Solved for:			
$\text{DOC}_u$	0 – 30	$\mu\text{M}$	compare to Wong et al. (1997)
$\text{DOC}_l$	0 – 20	$\mu\text{M}$	compare to Wong et al. (1997)
$\text{POC}_u$	0 – 4	$\mu\text{M}$	compare to Bishop et al. (1999)
$\text{POC}_l$	0 – 0.1	$\mu\text{M}$	compare to Bishop et al. (1999)

[1]for estimation of gas flux  $G$ , equation 3.9 described in Section 3.2.5.

et al. (1997) and Bishop et al. (1999).

### F.3 Quasi-Steady Solutions

To obtain solutions, it was necessary to allow the upper layer dissolved pools (but not the particulate pools or lower layer dissolved pools), to vary with time (i.e. have small constant time derivatives) in both seasons. In summer this variation is required because the time scales of DOC production (and DIC uptake) are much shorter than the time scale of DOC remineralization (and DIC production). In winter the upper DIC pool must increase with time to balance remineralization fluxes and the upper DOC pool must decrease with time because production is low. These solutions are quasi-steady state, of the form,  $\text{pool} = a + \beta t$ , where  $a$  and  $\beta$  are constant,  $t$  is time,  $a$  is the time invariant pool size and  $\beta$  is the small time derivative, thus:

$$\frac{dDIC_u}{dt} = -pp + r_d \text{DOC}_u^* + \frac{M}{h_u} (\text{DIC}_l - \text{DIC}_u^*) + \frac{G}{h_u} \quad (\text{F.2a})$$

$$0 = pp - s \text{POC}_u \quad (\text{F.2b})$$

$$\frac{d\text{DOC}_u}{dt} = (1 - p) s \text{POC}_u - r_d \text{DOC}_u^* + \frac{M}{h_u} (\text{DOC}_l - \text{DOC}_u^*) \quad (\text{F.2c})$$

$$0 = r_d \text{DOC}_l + r_p \text{POC}_l - \frac{M}{h_t - h_u} (\text{DIC}_l - \text{DIC}_u^*) \quad (\text{F.2d})$$

$$0 = \frac{s \cdot p \cdot h_u}{h_t - h_u} \text{POC}_u - r_p \text{POC}_l \quad (\text{F.2e})$$

$$0 = -r_d \text{DOC}_l - \frac{M}{h_t - h_u} (\text{DOC}_l - \text{DOC}_u^*) \quad (\text{F.2f})$$

in which  $\beta t$  is assumed negligible compared with  $a$  in terms with the \*,  $pp$  is primary production and the derivatives on the left hand side of the equation are  $\beta$ , e.g.:

$$\beta_{DIC_u} = \frac{dDIC_u}{dt} \quad (\text{F.3})$$

Possible solutions are presented pictorially for summer and winter seasons in Figures F.1 and F.2, respectively.

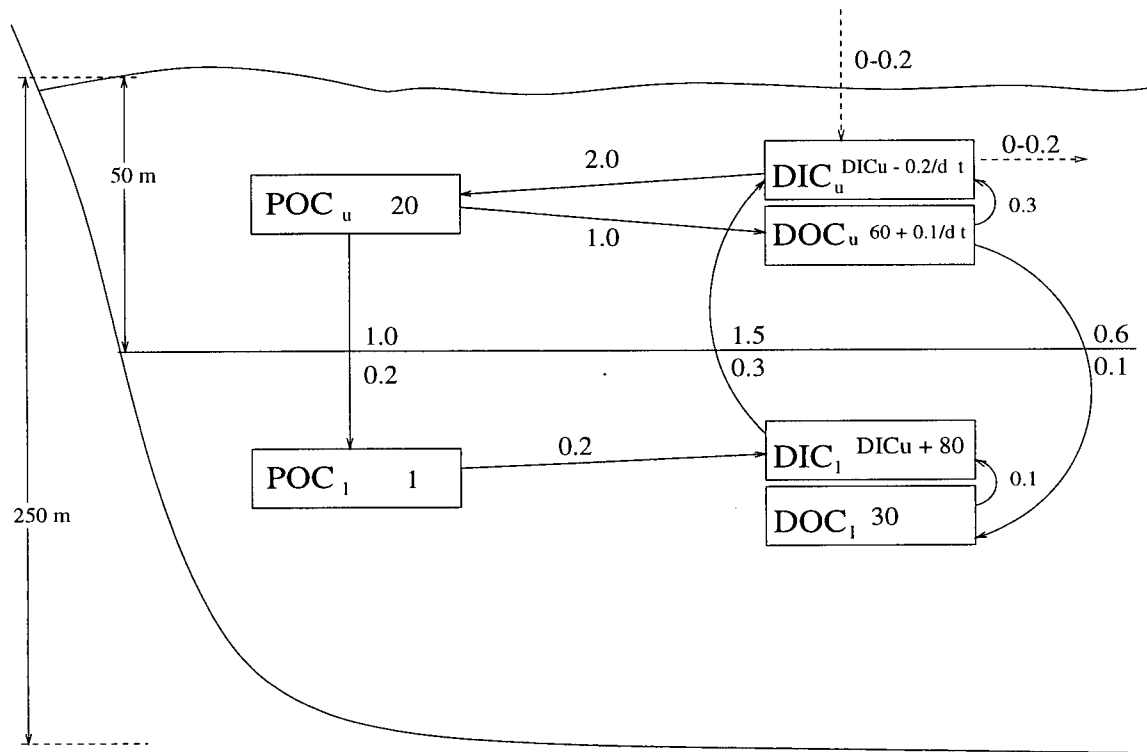


Figure F.1: A possible quasi-steady state summer solution. All pools have units  $\mu\text{M}$ . Fluxes are expressed as a rate of change in concentration (units  $\mu\text{M d}^{-1}$ ) and thus are scaled by box height (causing upper layer fluxes to be 5 times larger than lower layer fluxes). Fluxes passing from one layer to another are shown in terms of both layer geometries (the number in the upper layer corresponds to the the upper layer flux and the number in the lower layer corresponds to the lower layer flux). Upper layer dissolved pools are expressed in the form  $a + \beta t$ . Note that  $\text{DIC}_u$  and  $\text{DIC}_l$  cannot be solved for (Equations F.1a and F.1d). Their difference ( $\text{DIC}_{l-u}$ ) is  $80 \mu\text{M}$ , shown in the lower layer. The potential carbon dioxide gas influx is balanced by horizontal offshore advection.

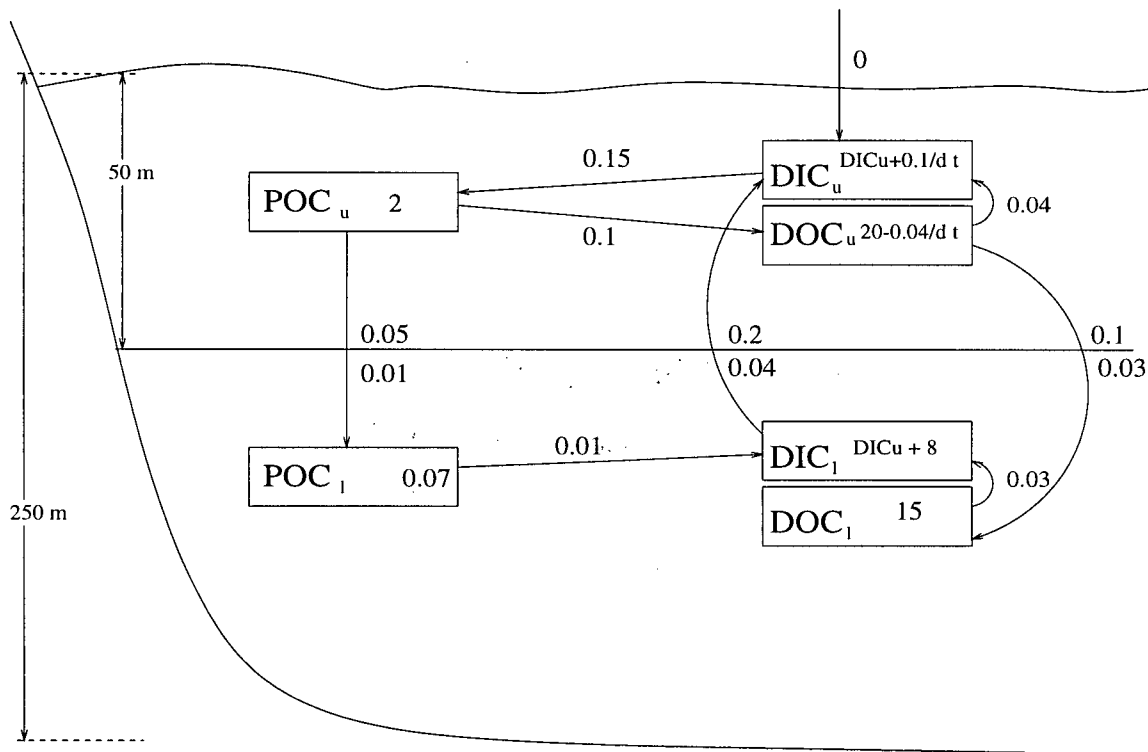


Figure F.2: A possible quasi-steady state winter solution. All pools have units  $\mu M$ . Fluxes are expressed as a rate of change in concentration (units  $\mu M d^{-1}$ ) and thus are scaled by box height (causing the upper layer fluxes to be 5 times larger than lower layer fluxes). Fluxes passing from one layer to another are shown in terms of both layer geometries (the number in the upper layer corresponds to the upper layer flux and the number in the lower layer corresponds to the lower layer flux). Upper layer dissolved pools are expressed in the form  $a + \beta t$ . Note that  $DIC_u$  and  $DIC_l$  cannot be solved for (Equations F.1a and F.1d). Their difference ( $DIC_{l-u}$ ) is  $8 \mu M$ ; shown in the lower layer.

#### F.4 Summary

The steady state equation (F.1) is valuable for understanding the sensitivity of model pools to various parameters. The solution shows that  $pp$  is the dominant flux (much larger than  $G$  or remineralization fluxes) in the surface and the largest possible gas evasion is of the order of the remineralization flux. The solution constrains the value of  $s$  (which represents many processes and is poorly known) and the remineralization rate of model DOC ( $r_d$ ). (Note that in the time dependent solution (Chapters 3, 4 and 5)  $s \cdot loss$  must be compared to the steady state  $s$  because the decay rate in the model is dependent on DIN and light through the  $loss$  term, Equation (3.8)). In all potential solutions for both seasons there is a vertical gradient in DIC, DOC and POC (i.e.,  $DIC_u < DIC_l$ ,  $DOC_u > DOC_l$  and  $POC_u > POC_l$ ), although in winter this gradient is small. Allowing small constant time derivatives in the upper layer dissolved pools is necessary to the solution because the remineralization time scale of dissolved organic matter is longer than its time scale of production.

## Appendix G

### Sensitivity Analysis

Model results relative to changes in model parameters are summarized in Table G.1. All parameters are defined in Tables 3.2 and 3.3. The most important model sensitivities (runs 1 – 9) are discussed in Chapter 3, Results section. Nitrogen inventories influence both net annual primary production ( $pp$ ) and exchange of model quantities between the model system and the open ocean. These inventories are primarily controlled by advective forcing and also by the fraction ( $p$ ) of the decay flux of the biota that sinks into the lower layer as particulate organic matter and the remineralization rate of dissolved organic matter ( $r_d$ ). The model results are not sensitive to changes in maximum phytoplankton growth rate ( $vm$ ) but they are sensitive to  $\alpha$ , the initial slope of the  $vm$  vs.  $I$  curve. Table 3.4 presents the sensitivity of air-sea gas flux to changes in model parameters. Air-sea gas flux during summer is relatively insensitive to parameter changes, while differences (with parameter variation) are seen during the winter season. In addition, it is necessary to model buoyancy fluxes and salinity (so that dilution of both DIC and TA occur together) to obtain reasonable model estimates of  $pCO_2$ .

Runs 10 – 13 show more results of variable up- and downwelling forcing. When downwelling is increased relative to upwelling the modelled  $pp$  and nutrient inventories decrease (run 10, the ENSO case Figure 3.8). When both up- and downwelling are substantially increased (run 11), increased upwelling is not able to overcome the strong depression of the nutricline until late in the upwelling season. Thus, nutrients do not build up over the surface shelf during winter and there is no spring bloom. Most of

the  $pp$  occurs in late summer and fall when nutrients have finally been replenished. Increasing only the upwelling strength while maintaining downwelling (run 12) causes nutrient inventories to increase. However,  $pp$  increases are small (increasing more on the slope relative to the shelf where a maximum  $pp$  is reached) because the biota cannot respond quickly enough to the increased nitrogen supply. Instead, there is more offshore surface advection of DIN. Similarly, the export of DIC to the open ocean in the surface layer is enhanced. When the ratio of up- and downwelling strengths is maintained but the magnitudes decreased, both  $pp$  and nitrogen inventory decreased (as expected). There is little change in surface layer DIN, but lower layer DIN is significantly decreased. Lower layer salinities decrease and do not match measurements as well. Therefore, the effect of downwelling becomes more important relative to upwelling when the magnitudes are decreased. Thus, if both up- and downwelling strengths are decreased in the model, the ratio ( $\bar{A}t_u:\bar{D}t_d$ ) also needs to increase to reproduce seasonal measurements. If the upwelling season is offset to start earlier (run 14) but  $\bar{A}$  and  $\bar{D}$  maintained,  $pp$  increases significantly because nutrients are being supplied when light is most available and they are used more efficiently in the system. There is large interannual variability (over 2 months) in estimated start times of the upwelling season (Thomson and Ware, 1996).

Increased vertical mixing (run 15) brings more nitrogen into the surface layer where it is taken up by the biota. DIN concentrations decrease over the slope and shelf; however, lower layer salinity decreases as well (becoming further from measured values as discussed in Section 4.1.1). Decreased horizontal mixing (run 16) has little effect on  $pp$  or DIN concentrations, but decreases lower shelf salinity significantly (as the horizontal salinity gradient is larger than the horizontal DIN gradient). Model sensitivity to horizontal mixing is also discussed in Section 4.1.1. Changing the frequency of storm forcing (run 17) has no effect on the model as long as integrated vertical fluxes (from entrainment) remain the same and amplitudes are not too large (i.e. so large that the biota does not

take up the nitrogen flux before it can be horizontally mixed or advected out of the system).

Raising the lower layer open ocean concentration of salinity ( $S$ ), DIN and DIC (runs 18, 19 and 20, respectively) causes inventories of the altered state variables to increase. Concentrations of  $S$ , DIN and DIC are significantly higher everywhere in the system. (Similarly, lowering  $S_{o,l}$ ,  $DIC_{o,l}$  and  $DIN_{o,l}$  lower  $S$ , DIC and DIN inventories.) Air-sea gas evasion increases with increasing DIC and decreases with increased salinity (due to increased alkalinity). Runs 21 and 22 show the effect of lowering the lower layer open ocean concentrations of POM and DOM, respectively. In the case of POM the model is not at all sensitive to the change. Similarly, a substantial decrease in the  $DOM_{o,l}$  concentrations (by a factor of 2) has little effect on surface DOM ( $< 1\%$  change) or  $pp$ . However, in the lower layer DOM decreases by 3% over the shelf and by 8% over the slope. The model is more sensitive to changes in  $DOM_{o,l}$  than  $POM_{o,l}$  because the remineralization time scale is much longer for DOM and lower layer POM concentrations are already small. Thus, the depth of upwelling and values of offshore inorganic state variables ( $S$ , DIN and DIC) are important to the results of the model. The model is relatively insensitive to changes in lower layer organic matter concentrations ( $POM_{o,l}$  and  $DOM_{o,l}$ ) as long as they are within the same order of magnitude as in the typical run (Appendix E). Likewise net annual export fluxes from the model system to the open ocean are affected by changes in inorganic concentrations while organic concentrations are only important in lower layer exchange. In the lower layer, setting  $POM_{o,l}$  to zero has little effect, while decreasing  $DOM_{o,l}$  by a factor of 2 causes net export of DOM to the lower layer ocean to increase by  $\sim 10\%$ .

The fraction  $p$  of the biota decay flux which goes into the particulate organic pool, rather than the dissolved organic, was varied as a function of POC (various Michaelis-Menton functions were used),  $p$  increasing to  $p_{max}$  at high POC (as expected in large

diatom dominated communities, particularly if particle coagulation is important) and decreasing with low POC (where smaller plankton such as flagellates are likely to dominate and regenerated production is expected to be more important) (run 23). The net annual  $pp$  is similar in magnitude (within 2%) and shape to the regular model output for  $p_{max}=0.6$  (the constant value used in typical model runs). This result is not surprising because the model is most sensitive to  $p$  when the decay flux of the biota is large, which is when the POC dependent function asymptotes to  $p_{max}$ .

When the decay rate of the biota ( $s$ ) is decreased (run 24) model  $pp$  increases in the fall, winter and spring (net annual increase almost 10%). The increase occurs during periods of light limitation because a larger standing stock ( $POM_u$ ) is maintained to take up available DIN. (Equation (F.1d) shows the dependence of  $POC_u$  on  $s$  in steady state.) The shape of the annual  $pp$  curve is similar.

Likewise, when the dependence of  $s$  on DIN and light availability is decreased (by changing the numerical coefficients in the *loss* equation (3.8) which decreases model equivalent sinking rates) upper layer POM increases (run 25) and is similar to run 24. Primary production is similar (in size and as a function of time). Maximum  $POM_u$  concentrations (during upwelling events) are similar (to typical model run) and are followed by an abrupt decrease when nitrogen becomes limiting. However, in runs 24 and 25,  $POM_u$  pools do not drop to the same levels as in the typical run. Instead they remain  $\sim 20\%$  higher (unrealistically high) between upwelling events.

The loss function (Equation (3.8)) was replaced by a mathematically similar formulation to 'Holling-type-III' zooplankton grazing (eg. Denman and Peña, 1999) (run 26):

$$loss = 1 + \frac{PON_u^2}{PON_u^2 + k_p^2} \quad (G.1)$$

where  $k_p$  is the zooplankton grazing half-saturation constant (with a value of  $0.4 \mu\text{M N}$  from Denman and Peña (1999)). In this scenario, increased decay of the biota occurred

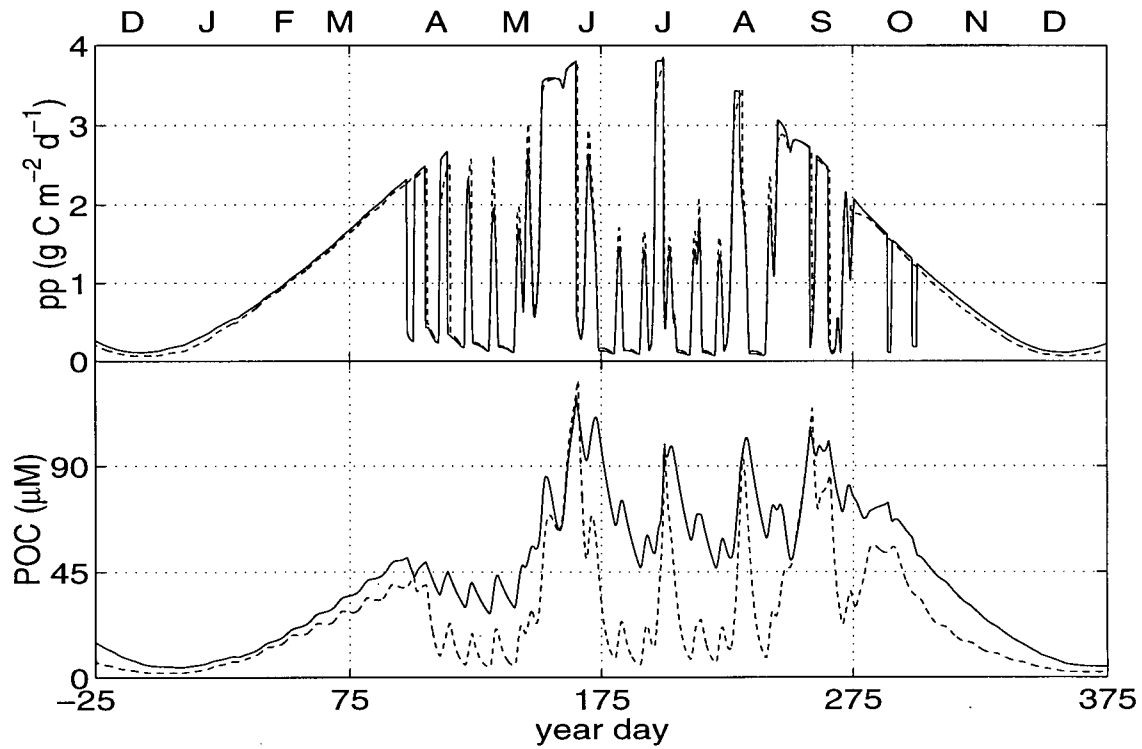


Figure G.1: The annual upper layer POC (lower panel) and  $pp$  (upper panel) cycle over the shelf for a run (run 26, solid line —) in which  $s$  is dependent on upper layer PON using a function similar to zooplankton grazing. The typical cycle is shown by the dashed line - -.

when there were high  $PON_u$  concentrations rather than low  $DIN_u$  concentrations or low light availability. Results of this run are similar to those from runs 24 and 25. Net annual  $pp$  is slightly lower (due to 5% decrease in  $pp$  over the shelf) but the annual cycle follows a similar form (as does nitrogen inventory). POM in the upper layer reaches similar maximum values (during upwelling) as in the typical run (also runs 24 and 25) but does not reach minimum values and in general is more constant throughout the year (Figure G.1).

In the lower layer, POM decreases in summer ( $\sim 50\%$ ) and increases in winter ( $\sim 50\%$ )

for runs 24, 25 and 26. Again run 26 has the lowest annual variation.

### G.1 Summary

The model is sensitive to advective forcing ( $\bar{A}$ ,  $\bar{D}$   $t_{up-0}$ , and smoothing), vertical flux (mixing and entrainment due to seasonal variation in upper layer depth and storm forcing),  $\alpha$ ,  $s$ , characterization of organic matter ( $p$ ,  $r_d$ ) and the inorganic state variable concentrations ( $S_{o,l}$ ,  $DIC_{o,l}$ ,  $DIN_{o,l}$ ) in the lower layer of the open ocean.  $S_{o,l}$  and  $DIN_{o,l}$  data exist in the study area, but there are few  $DIC_{o,l}$  data. In fact most of these parameters are not well known, although the physical parameters and  $\alpha$  can be constrained by measurements. The poorest known parameters are  $s$ ,  $p$  and  $r_d$  ( $s$  and  $r_d$  were constrained by steady state solutions, Appendix F). The model is insensitive to  $vm$ ,  $r_p$  and the organic state variable concentrations ( $DON_{o,l}$ ,  $DOC_{o,l}$ ,  $POC_{o,l}$ ,  $PON_{o,l}$ ) in the lower layer of the open ocean, none of which is well known.  $PON_{o,l}$ ,  $POC_{o,l}$  and  $DOC_{o,l}$  have been measured in the study area, although data are few.

Table G.1: A summary of sensitivity analysis. The new value of the parameter that is varied is presented (the change relative to the typical run is below). Increase and decrease are represented by  $\uparrow$  and  $\downarrow$ , respectively. Model effects are listed in the right column. In this table 'export' and 'import' refer to net annual exchange between the model system and the open ocean (through the vertical slope-open ocean boundary). Export is from the model system and import to the model system. N-inventory is total nitrogen inventory.

Run Number	Parameter Varied	New Value	Comments
1	$vm_0$ <sup>1</sup> , $I_{sat}$	$7.7 \times 10^{-9} \text{d}^{-1}, 67 \text{ Wm}^{-2}$ ( $\uparrow$ 35%, $\uparrow$ 35%)	no effect on $pp$ note, $\alpha$ kept constant
2	$I_{sat}$	$37 \text{ Wm}^{-2}$ ( $\downarrow$ 35%)	note this increases $\alpha$ by 35% $pp$ $\uparrow$ 10% , DIC export unchanged DIN export 60% lower
3	advective forcing	smooth (peak width $\uparrow$ 4 $\times$ )	$pp$ $\uparrow$ 20% (shelf $pp$ $\uparrow$ ; slope $pp$ $\downarrow$ ) N-inventory $\uparrow$ 6%
4	$\bar{A}t_u : \bar{D}t_d$	$3.2$ <sup>2</sup> ( $\uparrow$ 28%)	$pp$ $\uparrow$ 2-3%, N-inventory $\uparrow$ 6% DIC and DIN import $\uparrow$ 20% excess import leaves in surface as DIC DIN and DON
5	$p$	$0.3$ ( $\downarrow$ 0.5 $\times$ )	$pp$ $\downarrow$ 7% N-inventory $\downarrow$ 4%
6	$p$	$0.7$ ( $\uparrow$ 0.1)	$pp$ $\uparrow$ 3% N-inventory $\uparrow$ 2%
7	$r_p$	$0.4 \text{ d}^{-1}$ ( $\uparrow$ 2 $\times$ )	$pp$ unchanged N-inventory unchanged
8	$r_d$ C,N	$0.005 \text{d}^{-1}, 0.0065 \text{d}^{-1}$ ( $\uparrow$ 2 $\times$ )	$pp$ $\uparrow$ 5 % N-inventory $\uparrow$ < 1%

[1]  $vm_0$  would be the phytoplankton growth rate at a temperature of 0 K.

[2]  $\bar{A}=0.865 \text{ m d}^{-1}$  and  $\bar{D}=0.6 \text{ m d}^{-1}$ . Season lengths unchanged.

Table G.1 cont.

Run Number	Parameter Varied	New Value	Comments
9	$\bar{A}, \bar{D}$	0, 0 m d <sup>-1</sup>	<i>pp</i> ↓ 50% N-inventory ↓ 25%
10	$\bar{D}$	2.8m d <sup>-1</sup> <sup>3</sup> (↑ 4 ×)	<i>pp</i> ↓ 20% N-inventory ↓ 14%
11	$\bar{A}, \bar{D}$	3.92, 4.9 m d <sup>-1</sup> <sup>4</sup> (↑ 5 ×, ↑ 7 ×)	spring bloom ↓, fall bloom ↑ due to downwelling
12	$\bar{A}$	2.4 m d <sup>-1</sup> <sup>5</sup> (↑ 3 ×)	<i>pp</i> ↑ 5%, N-inventory ↑ 10%, DIC export into surface ocean enhanced
13	$\bar{A}, \bar{D}$	0.55, 0.42 m d <sup>-1</sup> <sup>6</sup> (↓ 0.6 ×)	<i>pp</i> ↓ 14%, N-inventory ↓ 6% DIN in lower layer ↓ 10 – 15%
14	$t_{up-0}$ <sup>7</sup>	year day 120 (25 days earlier)	<i>pp</i> ↑ 20% N-inventory ↑ 6%
15	$M_V$	1.0 m d <sup>-1</sup> (↑ 10 ×)	<i>pp</i> ↑ 10%, DIN ↓ 12% lower shelf salinity ↓ 0.2
16	$M_H$	2.0 m d <sup>-1</sup> (↓ 0.1 ×)	<i>pp</i> unchanged, lower DIN ↓ 2% lower shelf salinity ↓ 0.3
17	$T_{storm}$ <sup>8</sup>	↑ and ↓	no change in <i>pp</i> , for the same net integrated vertical flux

[3]  $\bar{A}=0.785$  m d<sup>-1</sup> (unchanged). Season lengths unchanged. This is the ENSO case.

[4]  $\bar{A}t_u:\bar{D}t_d=1.8$ . Season lengths unchanged.

[5]  $\bar{A}t_u:\bar{D}t_d=7.6$ . Season lengths unchanged.

[6]  $\bar{A}t_u:\bar{D}t_d=2.5$ . Season lengths unchanged.

[7]  $t_{up-0}$  is the start time of the upwelling season. In this run the spring transition is shortened and the fall transition lengthened.

[8]  $T_{storm}$  are the periods of the storm forcing (10 and 5 d in equation D.1)

Table G.1 cont.

Run Number	Parameter Varied	New Value	Comments
18	$S_{o,l}$ <sup>9</sup>	34.9 ( $\uparrow 1$ )	lower shelf salinity $\uparrow 0.6$ net annual gas invasion $\uparrow 3 \times$
19	$DIN_{o,l}$ <sup>9</sup>	32 $\mu\text{M}$ ( $\uparrow 2 \mu\text{M}$ )	DIN $\uparrow \sim 1 \mu\text{M}$ $pp \uparrow 4\%$
20	$DIC_{o,l}$ <sup>9</sup>	2300 $\mu\text{M}$ ( $\uparrow 25 \mu\text{M}$ )	DIC $\uparrow \sim 10 \mu\text{M}$ , $pp$ same small net gas evasion
21	$POC_{o,l}, PON_{o,l}$ <sup>9</sup>	0, 0 $\mu\text{M}$ ( $\downarrow 0.8, \downarrow 0.12 \mu\text{M}$ )	$< 0.1\%$ POM change in shelf and slope boxes
22	$DOC_{o,l}, DON_{o,l}$ <sup>9</sup>	9, 0.75 $\mu\text{M}$ ( $\downarrow 2 \times$ )	$DOM_u \downarrow < 1\%$ $DOM_l \downarrow 2 - 8 \%$
23	$p$	$f(\text{POC})$ <sup>10</sup>	little change in $pp$ model behaves as if $p=p_{max}$
24	$s$	0.0162 $\text{d}^{-1}$ ( $\downarrow 42\%$ )	$pp \uparrow 10\%$ $POM_u \uparrow \sim 15 - 25\%$
25	$sr_{max}$ <sup>11</sup>	1.1, 0.8 $\text{m d}^{-1}$ ( $\downarrow 50\%, \downarrow 50\%$ )	$pp \uparrow < 1\%$ $POM_u \uparrow 15 - 25\%$
26	$loss$	$f(\text{PON})$ <sup>12</sup>	$pp \downarrow < 3\%$ , $POM_u \uparrow$ and more constant

[9] Subscript  $o, l$  denotes (prescribed) lower layer open ocean state variable concentrations.

[10]  $p=f(\text{POC})$  such that at high POC concentrations  $p$  asymptotes to  $p_{max}$  and decreased to  $p_{min}$  at low POC concentrations. See text.

[11] Maximum DIN and light dependent sinking rates ( $sr_{max}$ ) were lowered by changing the coefficients in Equation (3.8) from (9, 8) and (6, 5) to (4, 3) and (3, 2) for DIN and light dependence, respectively.

[12] Equation (3.8) (dependent on both DIN and light availability) was changed to be dependent on PON, similar to a zooplankton grazing function. See text.

## Appendix H

### Organic Matter data from the Upwelling Region off the Oregon Coast

Organic carbon and nitrogen data from the upwelling region off the Oregon coast over the outer shelf (Hill, 1999) were compared with model results (Chapter 5). Measured annual cycles of organic carbon and nitrogen data are presented in Figures H.1 and H.2, respectively. Integrated (over the upper 50 m where data were collected) organic carbon data from a two month period in summer are presented in Figure H.3. For direct comparison, the model results have been integrated over the upper 50 m (over both the shelf and the slope) during a two month period (Figure H.4). The time periods in Figures H.3 and H.4 are not the same because the Oregon system and the model were not physically forced in the same way. Both periods are centered on a phytoplankton bloom. The difference between the measured TOC and the model TOC should represent the refractory portion of the TOC (Section 5.3). A comparison of integrated TOC in Figures H.3 and H.4 suggests that this portion is  $\sim 45\%$  of the bulk measured TOC. However, when only the mixed layers (upper 10 – 20 m in summer) are compared the difference is less ( $\sim 20\%$ ). This discrepancy occurs because model POC concentrations below the mixed layer are averaged over the entire lower layer depth. In nature (and in the data) POC concentrations immediately below the mixed layer are higher than in deeper waters. Thus, the lower layer contribution to the 50 m integrated model POC is unrealistically low.

Our model results compare reasonably well to these data over single upwelling events

and between maximum and minimum TOM values in summer and winter seasons, respectively (after a refractory portion is subtracted). Differences occur in upwelling response; in the data DON increases during upwelling (DOC is diluted), while in the model both DON and DOC are diluted by upwelling (Section 5.3).

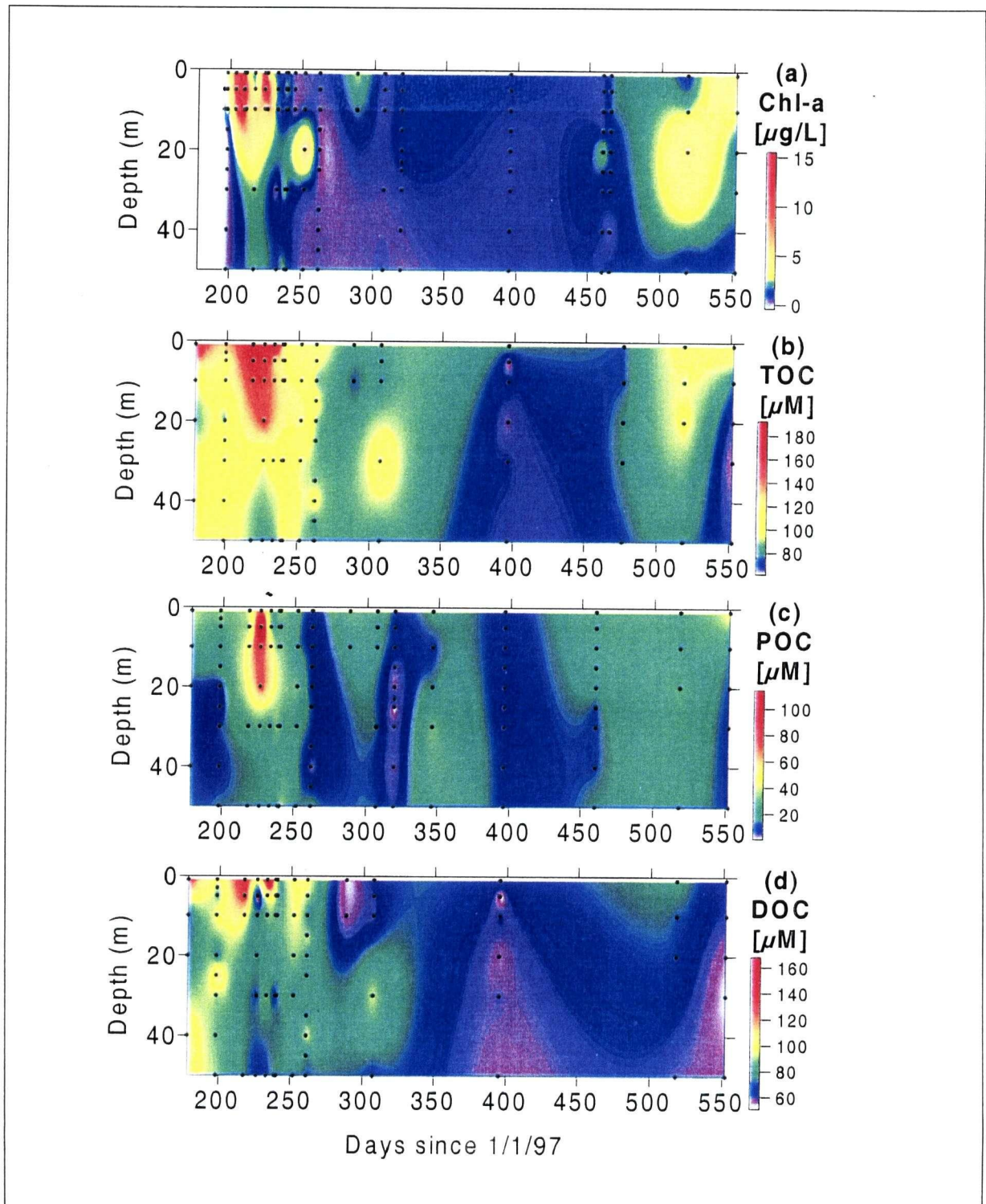


Figure H.1: An annual cycle of chl $a$ , TOC, POC and DOC in the Oregon Upwelling Region from Hill (1999). Reprinted from Hill (1999) with permission from J. Hill.

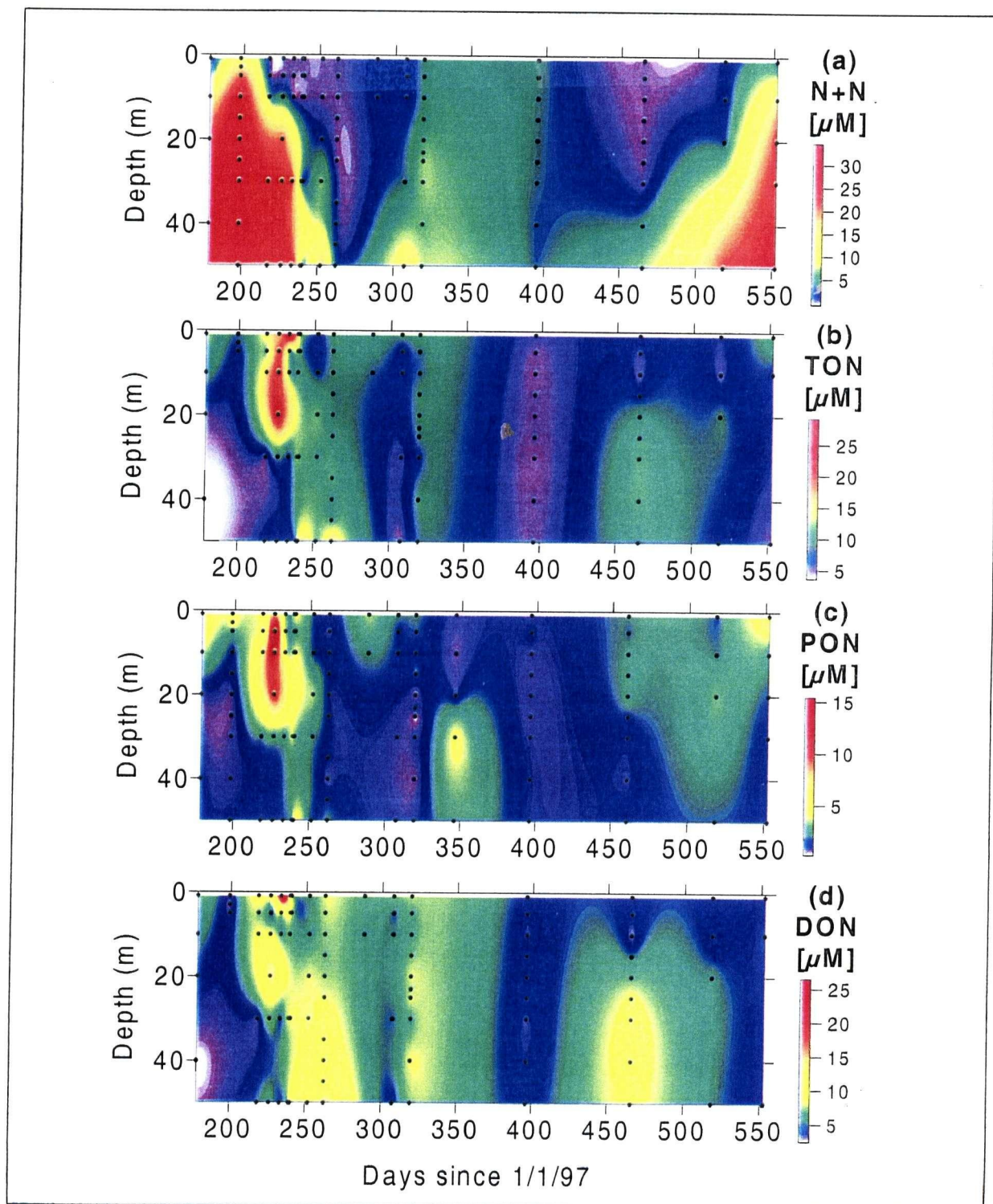


Figure H.2: An annual cycle of DIN, TON, PON and DON in the Oregon Upwelling Region from Hill (1999). Note N+N is nitrate and nitrite. Reprinted from Hill (1999) with permission from J. Hill.

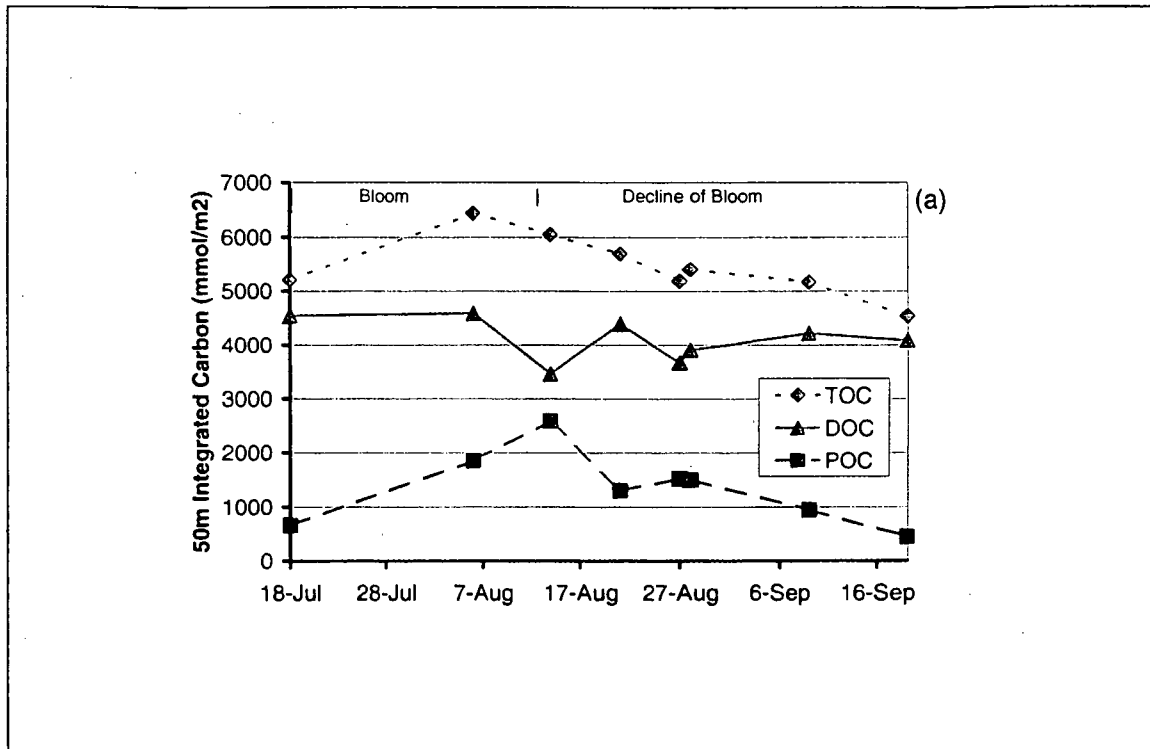


Figure H.3: 50 m Integrated TOC, DOC and POC from the Oregon Upwelling Region from Hill (1999). Reprinted from Hill (1999) with permission from J. Hill.

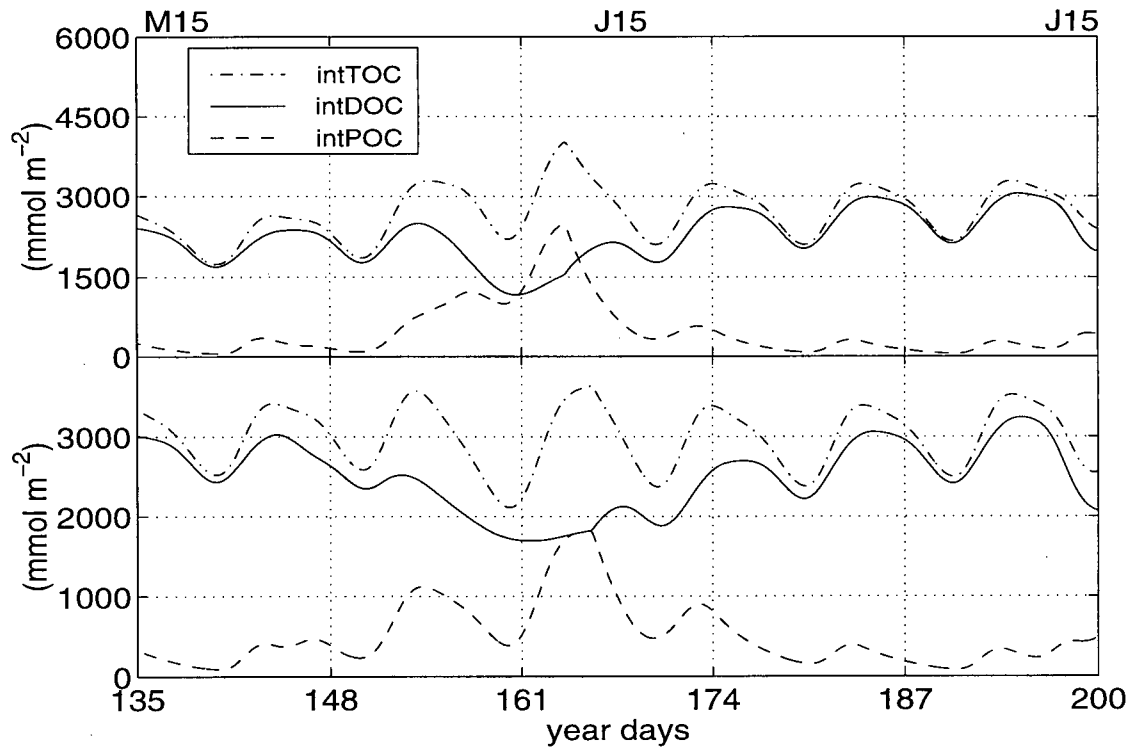


Figure H.4: 50 m Integrated model TOC, POC, and DOC over the shelf (lower panel) and slope (upper panel) for comparison with the Oregon data. The modulation at 10 d periods from storm forcing is enhanced by the integration because the entrained flux into the lower layer is mixed over the entire lower layer box within one time step, appearing as a large 'instant' loss to the upper 50 m.